UNIVERSITY OF SOUTHAMPTON

Nanoparticle Phase Change Functionality for Photonic Switching and Optical Memory

by

Bruno Flávio Nogueira de Sousa Soares

A thesis submitted for the degree of

Doctor of Philosophy

School of Physics and Astronomy

Faculty of Engineering, Science and Mathematics

August 2007

UNIVERSITY OF SOUTHAMPTON

ABSTRACT

FACULTY OF ENGINEERING, SCIENCE AND MATHEMATICS
SCHOOL OF PHYSICS AND ASTRONOMY

Doctor of Philosophy

NANOPARTICLE PHASE CHANGE FUNCTIONALITY FOR PHOTONIC SWITCHING AND OPTICAL MEMORY

by Bruno Flávio Nogueira de Sousa Soares

Nanoscale photonic functionalities based on light-induced structural transitions in nanoparticles have been investigated, and it has been experimentally shown that nanoparticles can act as both low power nanoscale optical switches and as resonator-less optical memory elements.

A system for in-situ growth and characterization of gallium nanoparticles, which combined technologies including atomic-beam deposition, ultra-high vacuum, cryogenics, and sophisticated fibre instrumentation including diode and ultra-fast lasers, has been developed.

Optical switching has been observed in a gallium nanoparticle film on the end of a single mode optical fibre simultaneously in reflection and transmission, and under different regimes of excitation, for the first time. Measurements of the sub-microsecond dynamics of such light-by-light control allowed the first study of the fast kinetics of solid-solid and solid-liquid structural transformations in gallium nanoparticles to be performed.

Single gallium nanoparticles have been grown from an atomic beam in the nanoaperture at the tip of a tapered optical fibre for the first time. Reversible light-induced reflectivity changes associated with a sequence of transformations between different structural forms (both solid-solid and solid-liquid) stimulated by optical excitation at nanowatt power levels, have been observed in such particles for the first time. The complex temperature hysteresis of the nanoparticle's nonlinear response has been observed and it has been discovered that the extent of overcooling can be controlled by varying the optical pumping regime.

The first demonstration of nanoscale all-optical resonator-less memory functionality based on phase transformations has been performed using a film of gallium nanoparticles. It has been shown that single 1 μs optical pulses of a few mW peak power can be used to 'write' information to the memory by converting the particles from a lower energy phase (logic state 0) to a higher energy phase (logic state 1). A high contrast method for 'reading' the state of the particle memory, based on measurements of the reflectivity change induced by a modulated pump beam, has been developed. Both volatile and non-volatile modes of memory operation have been demonstrated.

For the first time, an optical memory element based on a single particle has been demonstrated. It has been shown that an 80 nm gallium nanoparticle can act as a four-level nanoscale optical memory. Information is encoded on the particle by switching it between phases using single optical pulses with energies as low as 1.5 pJ, and by varying the pulse energy different states can be directly accessed from both ground and intermediate states. A closely packed array of such particles could provide a storage density of about 0.2 $\mathrm{Tb/in^2}$.

The experimental work has been underpinned by the development of appropriate qualitative physical models of the processes involved, so as to describe the relationships between excitation controlled phase coexistence in nanoparticles, their optical properties and the demonstrated functionalities.

Contents

Acknowledgements

I would like to thank my supervisor Professor Nikolay Zheludev for his guidance and support throughout my time as a research student.

I would also like to express my gratitude to those with whom I worked in Southampton, namely F. Jonsson, M.V. Bashevoy, S. Birtwell, A.I. Denisyuk, S. Pochon, M. Woodford, V.A. Fedotov, A.V. Krasavin, A.S. Schwanecke, P. Petropoulos, J. Gates, and R.J. Knize (visiting Southampton on sabbatical from the U.S. Air Force Academy, Colorado Springs). Furthermore, I would like to thank the technical and administrative staff at the School of Physics and Astronomy, and at the Optoelectronic Research Centre for all the help and assistance given to me over the years.

I would like to give a very special thank you to Kevin MacDonald for guiding my initial steps as a research student and for providing invaluable support and knowledge throughout my entire time at Southampton, and to Rui Travasso for stimulating my initial interest in Physics, and to both for their friendship. Additionally, I would like to thank all my teachers and professors for their role in my growth both as a person and as a scientist.

I would like to acknowledge the School of Physics and Astronomy for covering my tuition fees and the Portuguese Foundation for Science and Technology for providing my maintenance grant.

I would like to thank once more K.F. MacDonald and S. Birtwell, this time for their assistance in preparing this thesis.

Finally, I would like to thank all my friends for putting up with me and cheering me up during the bad moments, my girlfriend Maria João for her love, wise advice and constant support, and my parents for being there from the start with all their care and help, and especially for teaching me to always strive to achieve my goals.

Chapter 1

Introduction

1.1 Synopsis

This introductory chapter explains the motivation for, and lays the foundations needed to better understand the work presented in the remainder of this thesis.

Section 1.2 describes the motivation to obtain nanoscale photonic devices, gives a brief historical overview of nonlinear optics and other related work, and introduces the idea of using light-induced phase transitions in nanoparticles to obtain nanoscale photonic functionality.

After this general overview, Section 1.3 discusses the optical properties of nanoparticle films through theoretical models. Section 1.4 introduces the basic thermodynamic principles involved in phase transitions, with particular attention being given to what happens during the nucleation and growth of a new phase in a material, and to what changes occur when materials are confined in nanoparticles. Section 1.5 then combines the ideas of the two previous sections to show how it is possible to obtain a nonlinear optical response in nanoparticles undergoing phase transitions. It also describes how such particles allow for optical bistability to be created at the nanoscale. Additionally, the traditional use of optical feedback and a nonlinear material to obtain optical bistability is also described.

Following this, Section 1.6 discusses the general properties that phase change materials need to have, and gives an overview of the most common materials used. The properties of gallium, the material used in the work described in this thesis, are also described. Finally, Section 1.7 concludes this introduction by giving an overview of the remaining chapters in the thesis.

1.2 Introduction

One of the most important goals of nanophotonics is the creation of nanoscale low power nonlinear optical devices that control light with light in highly integrated circuits. The demand for such devices is large, as is the range of potential applications: They could for example control the output of miniature semiconductor lasers, switch signals between elements of three-dimensional photonic band-gap optical routers or serve as high storage-density memories. However, controlling light with light in the nanoscale is an immense challenge. A light signal is controlled when either its intensity or its phase is significantly changed by the presence of another signal, the control signal. In all-optical devices this control is achieved using a control light-wave to change the optical properties of the medium in which the signal light-wave travels.

The first experiment that showed that light could change the optical properties of a material was performed in 1926 by Vavilov and Lewschin of Moscow State University, in Russia [1]. In this experiment the transmission of an uranium-doped glass plate was shown to depend on the intensity of the spark light source used. The reason for this dependence was the saturation of the absorption of the doped glass and Vavilov and Lewschin suggested, in what may be considered the first ever paper on nonlinear optics, that the absorption coefficient should be treated as being intensity dependent. Later, Vavilov would generalize the idea of nonlinear optics writing "An absorption medium must exhibit a nonlinearity not only with respect to absorption. The latter is related to dispersion, and therefore the velocity of light propagation in a medium must generally depend on light power too. For the same reason, other optical properties of a medium - birefringence, dichroism, rotation capacity, and so on - must generally exhibit a dependence on the light power, that is, a violation of the superposition principle." [2]. Unfortunately this was in 1950 and the light powers necessary to observe those effects were not available. Sadly, Vavilov died before the invention of the laser and therefore never saw the dramatic developments brought on by it, not only in the understanding of the physics of nonlinear interactions, but also in the applied field of telecommunications with numerous photonic devices based on the intensity dependence of the refractive index. Nevertheless, the Superposition Principle formulated by Christian Huygens in 1678: "The most remarkable property of light is that light beams traveling in different and even opposite directions pass through one another

without mutual disturbance" was clearly challenged by the Vavilov-Lewschin experiment of 1926 and the rich field of nonlinear optics was born.

The fundamental idea behind nonlinear optics is in itself simple to understand. One can start by considering how the polarization $\mathbf{P}(\mathbf{r},t)$ of a material depends on the strength of the applied field $\mathbf{E}(\mathbf{r},t)$. In the case of traditional optics, there is a linear relation given by:

$$P_\alpha(\mathbf{r},t) = \epsilon_0 \sum_\beta \chi^{(1)}_{\alpha\beta} E_\beta(\mathbf{r},t)$$

Where ϵ_0 is the electric permittivity of free space and $\chi^{(1)}_{\alpha\beta}$ are the components of the linear susceptibility tensor. This relation can be understood by considering that, for low levels of light excitation, that is small amplitudes of the applied field $\mathbf{E}(\mathbf{r},t)$, the charges on the material are displaced proportionally to the amplitude of the applied field and therefore their collective oscillations add up to give a total polarization $\mathbf{P}(\mathbf{r},t)$ linearly proportional to the applied field. However as the amplitude of the field increases, the motion of the charges departs from this linear motion and the above relation no longer holds. One can however generalize the equation by expressing the response as a power series of the field strength:

$$\begin{aligned} P_\alpha(\mathbf{r},t) &= \epsilon_0 \sum_\beta \chi^{(1)}_{\alpha\beta} E_\beta(\mathbf{r},t) \\ &+ \epsilon_0 \sum_{\beta\gamma} \chi^{(2)}_{\alpha\beta\gamma} E_\beta(\mathbf{r},t) E_\gamma(\mathbf{r},t) \\ &+ \epsilon_0 \sum_{\beta\gamma\delta} \chi^{(3)}_{\alpha\beta\gamma\delta} E_\beta(\mathbf{r},t) E_\gamma(\mathbf{r},t) E_\delta(\mathbf{r},t) + \ldots \end{aligned}$$

The tensors $\chi^{(2)}$ and $\chi^{(3)}$ are known as second and third order nonlinear optical susceptibility tensors and relate to the nonlinear optical properties of the material. From this simple idea, the equations that describe the wide range of nonlinear effects detectable in experiments can be derived.

In 1961, soon after the demonstration of the first laser by Mainman in 1960 [3], Franken and co-workers discovered second harmonic generation [4], where a nonlinear material with a non-zero $\chi^{(2)}$ excited by a field of a certain frequency produces a field with twice that frequency. Other nonlinear optical effects based on the second order term were soon observed [5], as were higher order effects [6].

Of particular relevance to our work is the intensity dependence of refractive index, a third order optical nonlinearity that shows itself in a range of effects such as self-focusing, self-diffraction, self-phase modulation and bistability [7]. The fundamentals of various all-optical devices based on this type of nonlinearity have been demonstrated [8, 9] and the search for materials that show larger and faster nonlinearities has been intense [10]. However these devices are normally based on optical resonators and need extended interaction lengths to give nonlinear effects of an adequate size. This presents a serious obstacle to the ever growing need for component miniaturization. Highly integrated micron-scale optical devices are presently available [11], based around passive elements such as mirrors and lenses, but in order to truly move photonics from the micro to the nano world, materials with extremely large nonlinear responses are required. This is a direct consequence of the need to control one beam of light with another in a nanoscale layer of the material.

One can try to estimate the properties of a nonlinear material needed to achieve that kind of nanoscale control by considering a material with a complex refractive index $n + ik$ and denoting by Δn and Δk the nonlinear changes caused by a control beam to the real and imaginary parts of the refractive index. In order to obtain a significant retardation in a signal with a wavelength λ using a layer with a thickness L, the condition $\Delta nL \sim \frac{\lambda}{2}$ should be satisfied. Additionally, to achieve a considerable change in the intensity of the signal the condition $\Delta\alpha L \sim 1$ should also be satisfied. Here $\Delta\alpha$ is the change in the absorption coefficient of the material, which is related to the imaginary part of the refractive index by the equation $\Delta\alpha = \frac{4\pi}{\lambda}\Delta k$. By rearranging these formulae one finds that:

$$L \sim \frac{\lambda}{4\pi\Delta k} = \frac{\lambda}{4\pi}\frac{1}{k}\frac{k}{\Delta k}$$

This expression shows that in order to obtain a low value of L (in the nanoscale), one requires a material not only with a large value of the complex part of the refractive index k, but also in which the induced change Δk is a significant fraction of k. That is, one needs a high refractive index material exhibiting a large change in the index. The materials with the highest values of k are metals, but unfortunately in metals the conventional nonlinearities are very small. This is a direct consequence of the fact that, the traditional

nonlinearities appear as a result of nonlinear components in the restoring force of the electrons displaced by the light's electric field. In metals the optical properties are essentially determined by the response of free electrons and for truly free electrons the restoring force doesn't exist, which means that an ideal bulk metal shouldn't exhibit any nonlinear response. Still electronic nonlinearities are detectable in real metals because of multipole interactions, the dependence of electron mass and relaxation time on energy, and spin-flipping [12], but they are too small to be appropriate for practical applications.

However, there is an alternative way to achieve optical nonlinearities that has recently been given more and more attention [13]. The fundamental idea is extremely simple: Consider a material that has two structural phases with significantly different optical properties. If light could be used to stimulate a transition between these phases, then the materials response could be seen as a nonlinear effect.

However to be of use for most optical data processing applications this transformation must be reversible, that is, when the external excitation is removed the material should quickly return to the initial phase. This could be a potential problem, since in bulk materials phase transitions are usually sharp first-order transitions that frequently present a hysteresis in recovering to the original state. Bulk melting is a good example of this situation: Once the solid material is converted to the liquid state, there is often a need for it to be overcooled before it converts back to solid. Thus, if the melting was caused by laser heating, the original state would not be recovered when the laser excitation was removed.

Nature however provides us with a solution since the sharp and abrupt transformations between phases become dynamic coexistences of structural forms when the material is placed in a confining geometry [14]. A material may be confined, for example, by the formation of an interface with another material or in nanoparticles. Confinement not only blurs the distinction between first and second order phase transitions, making the transition continuous and reversible, but confined materials close to a phase transition also become more sensitive to external stimulation, which provides an increased nonlinearity. So, by confining a material and placing it on the verge of a phase transition, one

may achieve a large optical nonlinearity that can control light with light in a reversible way. Furthermore, the irreversible response described above can still be useful for certain applications (namely in memory applications as will be shown) and can also be obtained in confined geometries.

Another very important advantage of this type of nonlinearity is its energy efficiency. In the traditional type of optical nonlinearity, a single photon can only excite a single atom so at best the maximum effect (obtained when all the atoms in the material are excited) requires a number of photons equal to the number of atoms. On the other hand when using phase transitions as the base of the nonlinearity, one needs only to supply enough energy to obtain the phase transformation. This depends on the difference in enthalpy between the phases involved, and is of the order of a typical phonon energy per atom. The difference between the energy of a phonon and photon means that the new type of phase transition nonlinearity is about three to four orders of magnitude more energy efficient than the conventional nonlinearity.

Thus, the big question is whether a material with a large refractive index can be found that has structural phases with radically different optical properties and which permits light-induced transitions to be excited between these phases. Most metallic elements have similar optical properties that are almost phase independent. However, a material indeed exists that has a high refractive index, multiple structural phases with different optical properties, phase transitions with reasonably accessible temperatures and an ability to undergo light-induced transformations. That material is gallium.

Gallium is an extremely interesting polymorphic material. Despite being an elemental metal, at least nine different structural phases have been discovered [15], with properties ranging from those of the almost semiconductor-like, partially covalent solid $\alpha-$phase [16, 17] to those of the almost ideally metallic liquid phase [18, 19]. Significant optical changes are therefore associated with transitions between some of these phases. Additionally, bulk gallium melting occurs at the convenient temperature of 29.8 ^{o}C. The exploration of gallium's potential began in 1997, when gallium confined at an interface with silica was shown to exhibit a large phase transition based optical nonlinearity when brought to a temperature close to its melting point [20]. Soon after, potential applications of this effect were demonstrated by

applying it to cross-wavelength optical switching [21] and passive Q-switching of fibre lasers [22]. The research continued with the detection of nonlinear effects in gallium nanoparticles subject to laser and electron beam excitation [23, 24]. It is worth pointing out that other materials can also be used to obtain such phase change functionality: for example GST materials (discussed in more detail in Section 1.6) are already commonly used in DVDs to store information.

Nanoparticles are a particularly promising way to achieve nanoscale functionality due to the remarkable changes in optical, electrical and physical properties that can occur when a material is confined on the nanoscale. Indeed, many different ways to obtain various types of functionality with nanoparticles have been proposed. For example, semiconductor nanoparticles have high emission efficiencies [25], so they could act as tunable light-emitting elements in nanoscale circuits, and can be used as labels in chemical and biological applications [26]. Nanoparticles have also proved to be useful tools in improving photodetection processes: The high scattering efficiency of larger nanoparticles and qualitative changes in resonance characteristics are the main physical effects contributing to such detection gains [27]. A related field that has been given particular attention is the use of nanoparticles as sensors. The localized surface plasmon resonance spectra of metallic nanoparticles are extremely sensitive to their size and shape, and the local properties of the surrounding environment. This sensitivity can be exploited to detect a wide range of gases and liquids [28], and may even permit the detection of single molecules [29]. Indeed, RNA and DNA strands can already be detected and identified [30]. It has also been discovered that by attaching DNA molecules to the surfaces of metallic nanoparticles, new hybrid materials with tunable properties can be obtained [31]. In a similar way, covering dielectric nanoparticles with a thin metallic shell also allows for the systematic control of the particle's optical resonance over a wide spectral region extending from the near-UV to the mid-infrared [32]. Both the optical and chemical properties of these type of nanoshell make them ideal for biomedical imaging and therapeutic applications. For example, they can be used as contrast agents for optical coherence tomography or as absorbing elements in NIR thermal therapy of tumors [33]. Finally, the ability of metallic nanoparticles to sustain plasmon oscillations facilitates their use in nanoscale waveguiding: By coupling plasmon nodes between particles in a closely spaced chain one can obtain coherent propagation

of energy along the chain [34]. The development of all these techniques could lead to the creation of nanoscale circuits, in which nanoparticles act as waveguides and as active elements.

The work described on this thesis continues to explore the remarkable properties of gallium nanoparticles and shows for the first time how single gallium nanoparticles can exhibit a variety of useful optical functionalities. In particular, two regimes of excitation will be presented, leading to distinct functionalities. In Chapters 2 and 3 will show how low levels of excitation partially convert the particles to new phases, resulting in reversible transformations that can be used to create low power nanoscale optical switches. If a higher level of optical excitation is applied, the particle is completely transformed to the new phase in an irreversible fashion. Chapter 4 shows how this can be exploited to create nanoscale memory elements. In the remaining of this Chapter the ideas needed to better understand this work are presented in more detail.

1.3 Optical properties of nanoparticles

In the present section, the optical properties of nanoparticle films are analysed through the introduction of suitable theoretical models, following the discussion by Fedotov [35]. The analysis of media consisting of sub-wavelength metal spheres via the use of effective electric constants was first developed by Maxwell-Gaarnett [36] and David [37]. The general idea in these models is that an external electric field polarizes the particles, which in turn generate their own local fields and thus affect the dielectric properties of the host material.

Although these initial models have been used sucessfully for calculating the optical properties of media with a low density of metallic inclusions, they can't be used for the study of higher density volume medium or for planar granular films. To address this type of media Yamaguchi et al. [38] introduced a new model that is described in Section 1.3.1. Although a marked improvement from previous attempts, this model still suffers from some limitations and a further model developed by Fedotov et al. [35] that accurately describes closely packed nanoparticles will be introduced in Section 1.3.2. This model also allows the modelling of nanoparticles consisting of a binary core-shell structure, thus providing a way to interpret the measured optical characteristics of nanoparticles undergoing phase transitions as will be discussed in Section 1.4.3.

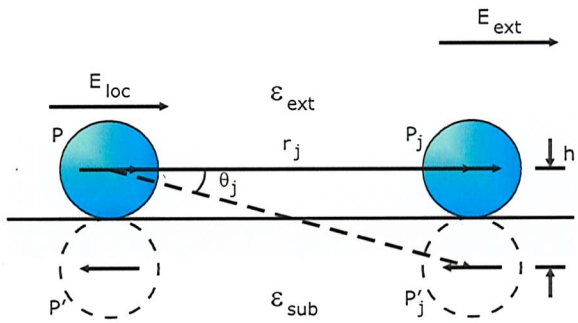

Figure 1.1: Dipole moments P and P' of a particle lying on a substrate surface and of its mirror image. The local field E_{loc} inside the particle is the sum of the applied field E_{ext}, with the field created by the image dipole P' and the field created by the dipoles and their images of all other particles P_j and P'_j. After Fedotov[35].

1.3.1 Disperse nanoparticle films

In order to analyse the properties of discontinous films on a substrate, Yamaguchi, Yoshida and Kinbara developed a model that not only takes into account the diple interaction between nanoparticles and their mirror images on the substrate, but also considers the variety of particle shapes and size effects. For simplicity, this model will be refered to as the YYK model [38].

The model starts by noting that the dipole moment P induced on a nanoparticle on top of a substrate (See 1.1) by the electric field of an incident wave parallel to the substrate is related to that of its mirror image in the substrate by:

$$P' = -\frac{\epsilon_{sub} - \epsilon_{ext}}{\epsilon_{sub} + \epsilon_{ext}} P \tag{1.1}$$

where ϵ_{sub} and ϵ_{ext} are the dielectric constants of the substrate and the exterior media respectively. The film is then seen as a monolayer of such small particles distributed on top of the substrate (See 1.1). For that type of arrangement the local field on each particle E_{loc} is given by the sum of the external field E_{ext}, with the field E_{img} produced by its mirror image, and the field E_{sur} produced by the surrounding particles and their mirror images. One then has:

$$E_{loc} = E_{ext} + E_{img} + E_{sur} \tag{1.2}$$

The contribution from the nanoparticle's mirror image relates to the image's dipole and the particle's height h by:

$$E_{img} = -\frac{1}{4\pi\epsilon_0\epsilon_{ext}h^3}P' \tag{1.3}$$

The expression for P' as a function of P can be replaced in this expression, to yield the E_{img} just as function of the nanoparticle's height and induced dipole.

The next step is to calculate the contribution of the surrounding particles and their mirror images. To achieve this, a spherical system of cordinates is introduced in which the origin of the coordinates is at the nanoparticles centre (See Figure 1.1). Assuming that the distance between neighbour particles r_j is much larger than the particles height h, the dipoles moments P_j and P'_j of the neighbour particle and its image can be approximated by an effective dipole moment P''_j given simply by:

$$P''_j = P_j - P'_j = \frac{2\epsilon_{ext}}{\epsilon_{ext} + \epsilon_{sub}}P_j \tag{1.4}$$

From this it follows that the field E_{sur} can be written as the field produced by the effective dipoles of all the surrounding particles:

$$E_{sur} = -\frac{1}{4\pi\epsilon_0\epsilon_{ext}}\frac{2\epsilon_{ext}}{\epsilon_{ex} + \epsilon_{sub}}\sum_j \frac{1 - 3cos^2\varphi'_j}{r_j^3}P_j \tag{1.5}$$

where φ'_j is the angle between r_j and P''_j.

If the particles are considered to have the same polarizability α and volume V, they will have the same dipole moment and one can obtain the following expression for the local field:

$$E_{loc} = \frac{E_{ext}}{1 + \epsilon_9\epsilon_{ext}\alpha\beta} \tag{1.6}$$

with

$$\beta = -\frac{V}{4\pi\epsilon_0\epsilon_{ext}h^3}\frac{\epsilon_{sub} - \epsilon_{ext}}{\epsilon_{sub} + \epsilon_{ext}} + \frac{1}{\epsilon_0}\frac{2}{\epsilon_{sub} + \epsilon_{ext}}C \tag{1.7}$$

As the shape of the nanoparticles was considered to be that of a rotational oblate (aspect ratio is $\gamma = 2r/h \geq 1$) ellipsoid, the volume may be approximated by:

$$V = \frac{\pi}{6}\gamma^2 h^3 \tag{1.8}$$

One can then numerically calculate the value of C, by assuming that the particles occupy the points of a square lattice with a lattice constant l that is small when compared to the wavelength of light in consideration:

$$C = -0.716\frac{1}{\gamma}(\frac{6}{\pi})^{1/2}q^{3/2} \tag{1.9}$$

where $q = V/l^2h$ is the volume feeling factor of the film.

A monolayer of particles with dielectric constant ϵ_{int}, and the same shape, size and orientation can be described by a plane-paralel film with an effective dielectric constant ϵ_{eff} given by [39]:

$$(\epsilon_{eff} - \epsilon_{ext})E = q\frac{\epsilon_{int} - \epsilon_{ext}}{1 + f(\epsilon_{int} - \epsilon_{ext})/\epsilon_{ext}}E_{loc} \tag{1.10}$$

where E is the macroscopic field inside the film. f is called the geometrical (depolarizing) factor of the particles. If one takes the polarizability α to be of the form [40]:

$$\alpha = \frac{\epsilon_{int} - \epsilon_{ext}}{\epsilon_{ext} + f(\epsilon_{int} - \epsilon_{ext})} \tag{1.11}$$

one can obtain:

$$(\epsilon_{eff} - \epsilon_{ext})E = q\frac{\epsilon_{int} - \epsilon_{ext}}{1 + F(\epsilon_{int} - \epsilon_{ext})/\epsilon_{ext}}E_{ext} \tag{1.12}$$

where F is the effective geometrical factor of the particles

$$F = f + \epsilon_0\epsilon_{ext}\beta \tag{1.13}$$

and the geometrical factor f is given by:

$$f = \frac{\gamma^2}{2\sqrt{(\gamma^2-1)^3}}[\frac{\pi}{2} - \frac{\sqrt{\gamma^2-1}}{\gamma^2} - \arctan(\frac{1}{\sqrt{\gamma^2-1}})] \tag{1.14}$$

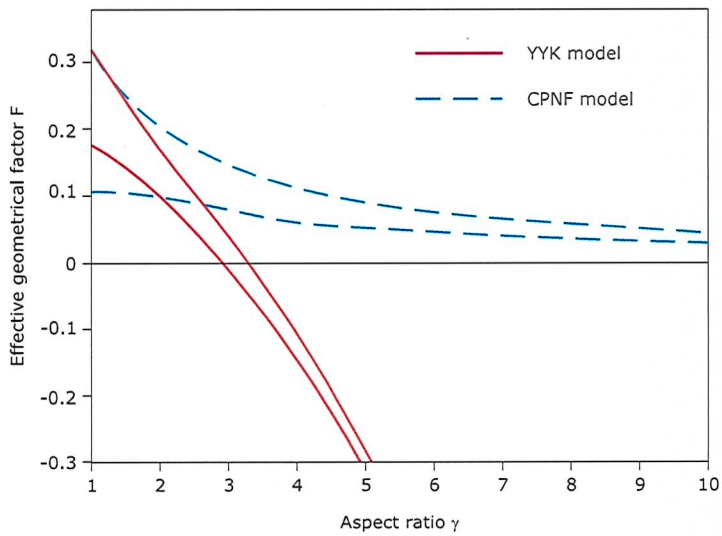

Figure 1.2: Effective geometrical factor of a nanoparticleparticle film as a function of their aspect ratio for filling factors $q = 0.01$ and $q = 0.6$ for both the YYK (red) and the CPNF model (blue). After Fedotov[35].

Finally, one can use the fact that the microscopic electric field inside the film is simply equal to the incident field $E = E_{ext}$, because the tangential part of an electric field is conserved across the interface between two dielectrics, to obtain the effective dielectric constant of the monolayer as:

$$\epsilon_{eff} = \epsilon_{ext}(q\frac{\epsilon_{int} - \epsilon_{ext}}{\epsilon_{ext} + F(\epsilon_{int} - \epsilon_{ext})} + 1) \tag{1.15}$$

These equations have been used to sucessfully analyse a range of experimental data from spectroscopic ellipsometry measurements on discontinuous metalic thin films [41,42]. Nevertheless, it is possible to quickly identify a few limitations of the model just described. The first limitation arises from the fact that the model assumes that the spacing between the particles is larger compared to their size, that is, it is assumed that $q \ll 1$. Moreover, the model is also only valid for monolayers composed of spherical or near spherical particles, that is $\gamma \simeq 1$.

One can more easilly understand where the problem arises by considering the behaviour of the effective geometrical factor as a function of the aspect ratio.

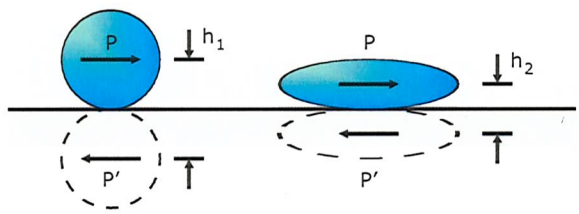

Figure 1.3: As the aspect ratio of a small particles increases, the distance between the point dipole of the particle and of its mirror image also increases, which leads to a discontinuity in the YYK model for disk like particles. After Fedotov[35].

Figure 1.2 shows how, for the parameters used, F becomes negative for $\gamma > 3.25$. This means that for a metal particle which has $\text{Real}(\epsilon_{int}) < 0$ the denominator in equation 1.15 doesn't cancel, meaning that the plasmon resonance shouldn't occur at any frequency. This effect is not observed experimentally. This problem is related to the use of the point dipole approximation to describe the interactions between the particles and their mirror images. This works fine for spherical particles, but when spheroids are considered the approximation is only acceptable for large distances in comparison to the size of the spheroid. Figure 1.3 shows the reason for this: the distance h between the centre of the particle and its mirror image decreases when one moves from a sphere to a spheroid with the same volume. In the YYK model the field produced by the image is proportional to h^{-3} and thus increases rapidly for spheroids, leading to a discontinuity for disk-like particles. In the next section, it will be show how these limitations of the YYK model may be resolved.

1.3.2 Closely packed nanoparticle films

The problems with the YYK model just described mean that it can't be applied in many important situations. For example, the experiments described in Chapter 2 involve closely packed non-spherical particles and, as it was shown, the YYK model can't be applied successfully to that type of film. In order to solve this problem an extension to the YYK model was developed by Fedotov et al. [35]. This model will be referred to as the closely packed nanoparticle film (CPNF) model.

The first improvement of the CPNF model arises from the replacement of the dipole approximation used in the YYK model with a more accurate expression

that takes into account the exact local fields of spheroidal nanoparticles. The expression for the electric potential outside an ellipsoid with semiaxes a, b and c in a uniform applied electric field is [40, 43]:

$$\begin{aligned}\Phi(\xi,\eta,\zeta) &= \Phi_{app}(\xi,\eta,\zeta)+\Delta\Phi(\xi,\eta,\zeta)= \\ &= \Phi_{app}(\xi,\eta,\zeta)[1-\frac{3}{8\pi}V\alpha\int_{\xi}^{\infty}\frac{ds}{\sqrt{(s+a^2)^3(s+b^2)(s+c^2)}}] \quad (1.16)\end{aligned}$$

where $\Delta\Phi$ is the potential generated by the polarized ellipsoid and Φ_{app} is the potential of the electric field applied parallel to the semi-axis a and given by:

$$\Phi(\xi,\eta,\zeta) = -E_{app}\sqrt{\frac{(\xi+a^2)(\eta+a^2)+(\zeta+a^2)}{(b^2-a^2)(c^2-a^2)}} \quad (1.17)$$

In these expressions elliptical coordinates (ξ,η,ζ) were used. Considering particles that are oblate spheroids, that is, $a=b>c$, with $a=r$, the radius of the particles and $c=2h$, the height of the particles, and using a cartesian coordinate system (x',y',z') normalized by the radius of the particle (that is $x'=x/r$, $y'=y/r$ and $z'=z/r$) and with the origin at the centre of the spheroid, the x'-axis parallel to the applied field and the z'-axis the same as the spheroids rotational axis one can obtain the following expressions that describe the exact variation of the x-component of the spheroid's own field in space [35]:

$$E_x(x',y',z') = \alpha E_{app}A(x',y',z') \quad (1.18)$$

$$\begin{aligned}A'(x',y',z') &= -\frac{1}{2(\gamma^2-1)}[\frac{\pi\gamma^2}{2\sqrt{\gamma^2-1}}-\frac{\sqrt{\gamma^2\xi'+1}}{(\xi'+1)}- \quad (1.19)\\ &- \frac{\gamma^2}{\sqrt{\gamma^2-1}}\arctan\sqrt{\frac{\gamma^2\xi'+1}{\gamma^2-1}}+x'\frac{\partial\xi'}{\partial x'}[\frac{\sqrt{\gamma^2\xi'+1}}{(\xi'+1)^2} \quad (1.20)\\ &- \frac{\gamma^2}{\sqrt{\gamma^2\xi'+1}(\xi'+1)}] \quad (1.21)\end{aligned}$$

It is possible to show that only for very large distances ($x',y',z' \gg 1$) do these expressions describe the behaviour of a point dipole. Next, following a

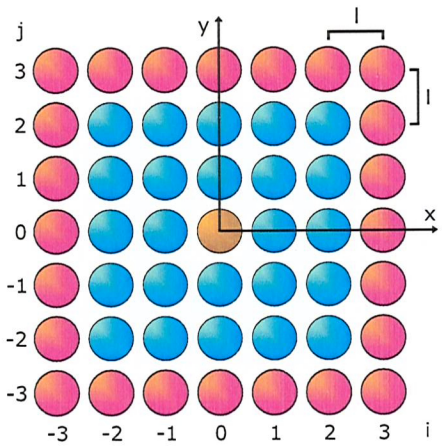

Figure 1.4: Nanoparticles arranged in the square lattice used for the calculations of the modified effective geometrical factor in the CPNF model. The exact fields from the centre particle (brown) and the 23 nearest particles (blue) and their images are taken into account, while the remaining nanoparticles (in pink) and images are taken into account by the dipole approximation. After Fedotov[35].

procedure similar to the YYK model to account for the fields of the images and the neighbours particles, but this time using the above expressions one obtains a new effective geometrical factor:

$$F = f - \sum_{i=-2}^{2}\sum_{j=-2}^{2} A(i\sqrt{\frac{2\pi}{3q}}, j\sqrt{\frac{2\pi}{3q}}, 0) - \tag{1.22}$$

$$- \frac{\epsilon_{ext} - \epsilon_{sub}}{\epsilon_{ext} + \epsilon_{sub}} \sum_{i=-2}^{2}\sum_{j=-2}^{2} A(i\sqrt{\frac{2\pi}{3q}}, j\sqrt{\frac{2\pi}{3q}}, \frac{2}{\gamma}) - \tag{1.23}$$

$$- \frac{2\epsilon_{ext}}{\epsilon_{ext} + \epsilon_{sub}} \frac{0.177}{\gamma}\sqrt{\frac{3q^3}{2\pi}} \tag{1.24}$$

where $A(0,0,0) = 0$. Figure 1.4 shows the 24 nearest neighbours that the second term in the above equation accounts for. The third term in the equation arises from the images of those 24 particles and of the nanoparticle itself. The contribution from the rest of the film is included in the fourth term of the equation and is described as before by using the dipole field approximation.

Figure 1.2 shows how the inclusion of these extra terms makes the CPNF model work for closely packed particles: the effective geometrical factor now approaches zero only at extremelly large γ.

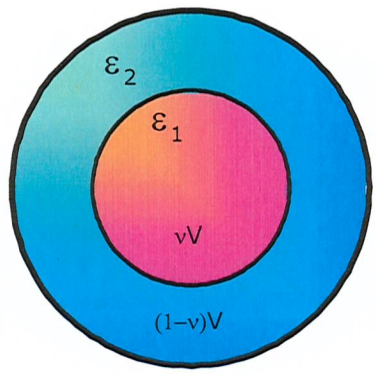

Figure 1.5: Representation of a core-shell spheroid nanoparticle with total volume V. The dielectric constant of the core is ϵ_1 and the core volume is νV, whereas the shell has dielectric constant ϵ_2 and volume $(1-\nu)V$.

1.3.3 Core-shell nanoparticles

A further improvement that is particularly important for the present work is the consideration of nanoparticles consisting of a core and a shell with different dielectric properties [44, 45]. Whereas the YYK model treats only homogeneous particles, these binary particles are considered in the CPNF model by introducing an effective dielectric constant for a homogeneous particle with the same polarizability as the binary nanoshell. It can be shown that the polarizability of a coated spheroid can be written as [40]:

$$\alpha' = \frac{(\epsilon_2 - \epsilon_{ext})[\epsilon_2 + (\epsilon_1 - \epsilon_2)(f_1 - \nu f_2)] + \nu\epsilon_2(\epsilon_1 - \epsilon_2)}{[\epsilon_2 + (\epsilon_1 - \epsilon_2)(f_1 - \nu f_2)][\epsilon_{ext} + (\epsilon_2 - \epsilon_{ext})f_2] + \nu f_2\epsilon_2(\epsilon_1 - \epsilon_2)} \tag{1.25}$$

where ϵ_1 and ϵ_2 are the dielectric constants of the core and the shell, and ν is the fraction of the nanoparticle consisting of the core (See Figure 1.5). f_1 and f_2 are the geometric functions for the core and for the entire nanoparticle.

From this, the effective dielectric constant of an equivalent homogenous particle can be determined by solving the equation $\alpha' = \alpha(\epsilon'_{int})$, where $\alpha(\epsilon'_{int})$ is the polarizability of an homogenous particle given by Equation 1.11. The actual solution is:

$$\epsilon'_{int} = \epsilon_{ext}\frac{\alpha'(f_2 - 1) - 1}{\alpha' f_2 - 1} \tag{1.26}$$

For near-spherical coated particles one has $f_1 = f_2 = 1/3$, in which case

equation 1.25 reduces to:

$$\alpha' = 3\frac{(\epsilon_2 - \epsilon_{ext})(\epsilon_1 + 2\epsilon_2) + (1 - \Delta h/r)^3(\epsilon_1 - \epsilon_2)(\epsilon_{ext} + 2\epsilon_2)}{2(1 - \Delta h/r)^3(\epsilon_2 - \epsilon_{ext})(\epsilon_1 - \epsilon_2)} \tag{1.27}$$

where Δh is the thichness of the coating layer. Additionally for this type of particles equation 1.26 yields:

$$\epsilon'_{int} = \epsilon_{ext}\frac{2\alpha' + 3}{3 - \alpha'} \tag{1.28}$$

Having arrived at the equations for the effective dielectric constant of the closely backed binary nanoparticles in the previous section, one may now treat the nanoparticle film as a plane-parallel film of thickness $h = 2r$. To calculate its reflectance, transmittance and absorption one can then just use the usual thin film formulae REF VAS 13]:

$$R = \frac{A_1 exp(\frac{4\pi h k_2}{\lambda}) + A_2 exp(-\frac{4\pi h k_2}{\lambda}) + 2\sqrt{A_1 A_2}cos(\phi_2 - \phi_1 - \frac{4\pi h n_2}{\lambda})}{exp(\frac{4\pi h k_2}{\lambda}) + A_1 A_2 exp(-\frac{4\pi h k_2}{\lambda}) + 2\sqrt{A_1 A_2}cos(\phi_2 + \phi_1 - \frac{4\pi h n_2}{\lambda})} \tag{1.29}$$

$$T = \frac{n_3}{n_1}\frac{B_1 B_2}{exp(\frac{4\pi h k_2}{\lambda}) + A_1 A_2 exp(-\frac{4\pi h k_2}{\lambda}) + 2\sqrt{A_1 A_2}cos(\phi_2 + \phi_1 - \frac{4\pi h n_2}{\lambda})} \tag{1.30}$$

with $A_{1,2}$, $B_{1,2}$ and $\phi_{1,2}$ given by:

$$A_{1,2} = \frac{(n_{1,2} - n_{2,3})^2 + (k_{1,2} - k_{2,3})^2}{(n_{1,2} + n_{2,3})^2 + (k_{1,2} + k_{2,3})^2} \tag{1.31}$$

$$B_{1,2} = \frac{n_{1,2}^2 + k_{1,2}^2}{(n_{1,2} + n_{2,3})^2 + (k_{1,2} + k_{2,3})^2} \tag{1.32}$$

$$\phi_{1,2} = arctan[2\frac{n_{1,2}k_{2,3} - n_{2,3}k_{1,2}}{n_{1,2}^2 - n_{2,3}^2 + k_{1,2}^2 - k_{2,3}^2}] + C \tag{1.33}$$

where $C = \pi$ if $(n_{1,2}k_{2,3} - n_{2,3}k_{1,2}) \geq 0$ and $[n_{1,2}^2 - n_{2,3}^2 + k_{1,2}^2 - k_{2,3}^2] < 0$; $C = -\pi$ if $(n_{1,2}k_{2,3} - n_{2,3}k_{1,2}) < 0$ and $[n_{1,2}^2 - n_{2,3}^2 + k_{1,2}^2 - k_{2,3}^2] < 0$; and $C = 0$ if $[n_{1,2}^2 - n_{2,3}^2 + k_{1,2}^2 - k_{2,3}^2] \geq 0$.

In the above equations $n_1 - ik_1 = \sqrt{\epsilon_{sub}}$, $n_2 - ik_2 = \sqrt{\epsilon_{eff}}$ and $n_3 - ik_3 = \sqrt{\epsilon_{ext}}$ are the complex refractive indexes of the substrate, the film and the surrounding medium.

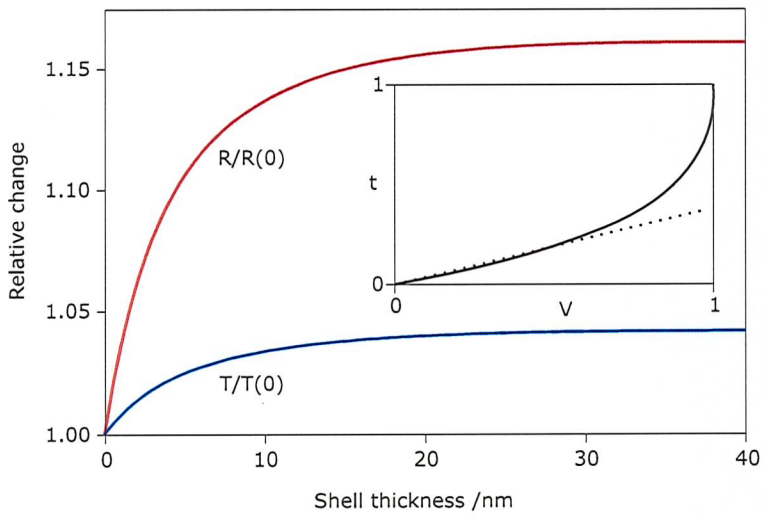

Figure 1.6: Calculated relative changes in the reflectivity (R) and transmission (T) at 1310 nm of a solid-core, liquid-shell gallium nanoparticle film (particle width =80 nm, particle height= 30 nm, particle mean separation= 95 nm) on a silica substrate as a function of shell thickness. The inset is a plot of normalized shell (t) against normalized shell volume (V).

To illustrate the application of the CPNF model, the reflectance and transmittance of a gallium binary nanoshell film have been calculated. For this calculation a probe wavelength of 1310 nm was considered, and the particles were taken to be spheroids with a width of 80 nm and a height of 30 nm distributed on a silica substrate with a mean separation of 95 nm. The solid core of the particles was assumed to have optical properties intermediate between those of the liquid and α phases ($\epsilon_{core}(1310\,\text{nm}) = -25.9 - 39.7i$), and the shell was taken to be in the liquid state ($\epsilon_{shell}(1310\,\text{nm}) = -115.3 - 98.4i$).

Figure 1.6 shows the calculated change in the reflectivity and transmission of the film caused by the presence of the liquid surface layer on the particles (relative to the properties of a film of completely solid particles). Note how a shell just a few nanometres thick produces a significant change in both the reflectivity and the transmission, although the change in the reflectivity is more pronounced. Gallium properties will be further discussed in Section 1.6.3, while in the next section, the details of phase transitions that can lead to this sort of core-shell nanoparticles will be reviewed.

1.4 Phase transitions

1.4.1 Principles

A phase change or phase transition is the process by which at least one new phase appears in a system. The most common examples involve transformations between different matter states, such as the melting of ice to give water, or the reverse process of freezing . Phase changes are however also possible between different phases of the same state of a material. For example, many substances have more than one solid phase, each exibiting a different crystallographic structure. A phase change can then occur during which the solid is converted from one structure to the other. An example of such a transformation is the transformation from orthorhombic solid sulfur to monoclinic solid sulfur. Other examples, of central importance for the work described in this thesis, are the changes between the various gallium crystallographic phases discussed in 1.6.3.

Phase transitions can be classified in different ways, but by far the most common division is the separation between first and second order phase transitions. First order phase transitions are those accompanied by a transfer of heat between the system and the surroundings, that is, there is a latent heat associated with them. A volume change also normally occurs in systems undergoing a first-order phase transition and the heat capacity of the material in the two phases is different. Mixed-phase regimes are yet another characteristic of this type of transformation, as the energy cannot be instantaneously transferred between the system and its environment. Historically, their name comes from the fact that under the Ehrenfest classification scheme these transitions present a discontinuity in the first derivate of the free energy of the system. Many common transitions, such as the transformations between the solid, liquid and gas states, are first-order transitions. Second-order phase transitions are those for which there is no associated latent heat. They are continuous transitions, which in the Ehrenfest classification scheme show a discontinuity only in the second-derivate of the free energy. The transitions between the normal conductivity and the superconductivity states in certain metals are examples of second-order phase transitions.

When analysing phase transitions, a very important parameter is whether a given transition occurs or not in a spontaneous way for a given set of conditions.

Starting from the second law of thermodynamics, consider how one could obtain a way to easily acertain if a transition is spontaneous or not. The second law of thermodynamics says that for a reaction to occur spontaneously it has to increase the entropy of the Universe, that is:

$$\Delta S_{univ} = \Delta S_{sys} + \Delta S_{surr} > 0 \tag{1.34}$$

In order to determine the sign of the change of entropy of the universe however, one must know the change in both the system, ΔS_{sys}, and the surroundings, ΔS_{surr}. Finding the changes in the surroundings is not easy, so one would like to have a thermodynamic function that would express whether a reaction is or not spontaneous by considering only elements of the system itself. One can start by writing the change in entropy in the environment as:

$$\Delta S_{surr} = -\frac{\Delta H_{sys}}{T} \tag{1.35}$$

where ΔH_{sys} is the variation in the system's enthalpy. By substituting this expression into equation 1.34 and multiplying both sides by $-T$ one gets:

$$-T\Delta S_{univ} = -T\Delta S_{sys} + \Delta H_{sys} < 0 \tag{1.36}$$

This expression implies that, at a given temperature T, a reaction is spontaneous if the changes in the enthalpy and the entropy of the system are such that $\Delta H_{sys} - T\Delta S_{sys}$ is less than zero. Having realized this, one may introduce a new thermodynamic function, the Gibbs free energy given by:

$$G = H - TS \tag{1.37}$$

The change of the Gibbs free energy for a process at constant temperature is then given by:

$$\Delta G = \Delta H - T\Delta S \tag{1.38}$$

For $\Delta G < 0$ the reaction is spontaneous, for $\Delta G > 0$ the reaction isn't and for $\Delta G = 0$ the system is in equilibrium. In this context, the Gibbs free energy can be seen as the energy available to make work, or the driving force of a transformation. That is, for a phase change to proceed, the Gibbs free energy G must be reduced by the process.

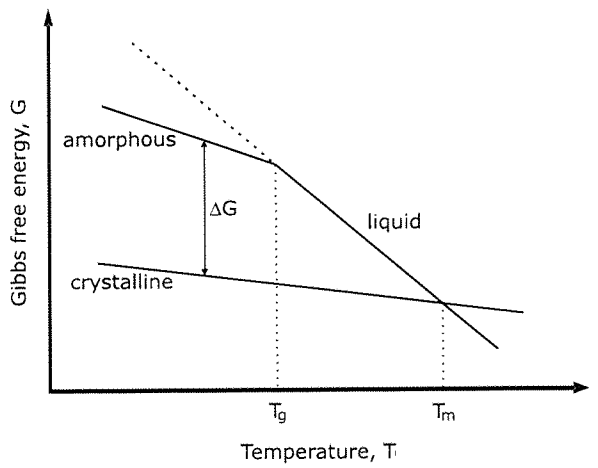

Figure 1.7: Schematic representation of the temperature dependence of the Gibbs free energy for a material with liquid, crystalline and amorphous phases. T_m represents the melting point, and T_G the glass transition temperature. After Waser [47].

1.4.2 Nucleation and growth

Having introduced the concept of Gibbs free energy, consider how it may be applied to the nucleation and growth of a new phase occurring in a material with a liquid, a crystalline and an amorphous phase. As will be described in Section 1.6.1, these types of material are important in many applications, but this section will focus only on the thermodynamic details of the transformation, following the ideas discussed by Waser [47]. If one ignores the temperature dependence of the entropy S and the enthalpy H, then, from equation 1.37, the temperature dependence of the Gibbs free energy for each phase is a straight line with slope $-S$ (See Figure 1.7). There are two important temperatures in this diagram: T_m, the melting point and $T_G$the glass transition temperature, below which the amorphous solid state can exist.

One can then consider how ΔG behaves for the different transitions possible. For the crystalline to liquid transition one has that at the melting point, $\Delta G = 0$, giving $\Delta S = \Delta H/T_m$, where ΔH is the latent heat of the transition. Away from the melting point this leads to a transition driving force:

$$\Delta G = \Delta H \frac{T_m - T}{T_m} \tag{1.39}$$

For the amorphous to crystalline transition two situations are possible. For $T > T_G$one has:

$$\Delta G = \Delta H \frac{T_m - T}{T_m} \tag{1.40}$$

while for $T \leq T_G$ the expression is [48]:

$$\Delta G = \Delta H_{ac}[1 - \frac{T}{T_G}(1 - \frac{\Delta H}{\Delta H_{ac}} \frac{T_m - T_G}{T_m})] \tag{1.41}$$

Here ΔH_{ac} is the exothermic energy of the transition from the amorphous to the cyrstalline state. Note that for low temperatures the transformation proceeds extremelly slowly, which is a good property for memory applications as it assures long term data stability.

Consider now the creation of crystalline regions in a previously amorphous material. The crystallization process consists of a nucleation phase and a growth phase, both being of extreme importance in the optimization of the overall transformation. Considering first the nucleation process: to create a nucleus, one needs to supply not only the energy difference ΔG, but one also needs to overcome the energy necessary to produce an interface boundary ΔG_{IF} and to take into account the elastic energy ΔG_E. However, as the elastic energy term doesn't change the form of the transition, it will be ignored in the following discussion. The total energy change is then given by:

$$\Delta G_{total} = \Delta G + \Delta G_{IF} \tag{1.42}$$

The first term is proportional to the volume V of the nucleus, while the second is proportional to the surface area, A. One can then write:

$$\Delta G_{total} = \Delta G_V V + \gamma A \tag{1.43}$$

where the Gibbs free energy per volume, ΔG_V and the specific interface energy γ were introduced.

One may then proceed by considering the particular case of the formation of a spherical crystalline nucleus in an amorphous medium. If the radius of the nucleus is r one simply has:

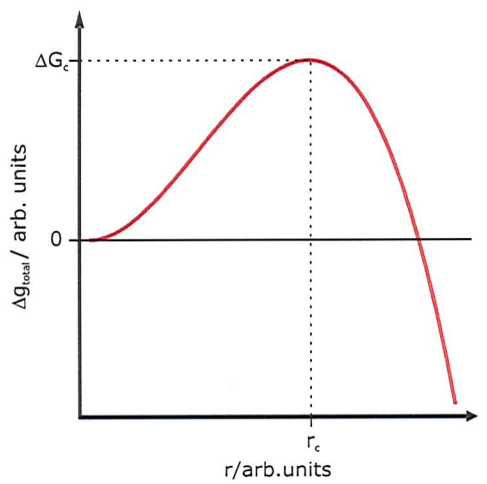

Figure 1.8: Change in the total Gibbs free energy ΔG_{total} necessary to form a nucleus of radius r. After Waser [47].

$$\Delta G_{total} = \Delta G_V \frac{4}{3}\pi r^3 + \gamma \pi r^2 \tag{1.44}$$

Figure 1.8 shows how the total energy required for a nucleus to form changes with its radius r. This energy reaches a maximum ΔG_c for the critical radius $r_c$such that:

$$r_c = -\frac{2\gamma}{\Delta G_V} \tag{1.45}$$

and

$$\Delta G_c = \frac{16}{3}\pi \frac{\gamma^3}{\Delta G_V^2} \tag{1.46}$$

Note that the negative sign in Equation 1.45, arises from the fact that as discussed earlier ΔG_V must be negative for the phase transformation to proceed. Also note, how for $r < r_c$ further nucleus growth is not favourable, while for $r > r_c$ growth is more favourable than decay. Thus, ΔG_c reflects the energy barrier that must be overcome to first create the critical nuclei, and is therefore related to the rate at which these nuclei are created. In fact, by thermal fluctuations new nuclei are constantly forming and decaying. In equilibrium, the number of nuclei with radius r is given by:

$$N(r) = N_0 e^{-\frac{\Delta G_{total}(r)}{k_B T}} \tag{1.47}$$

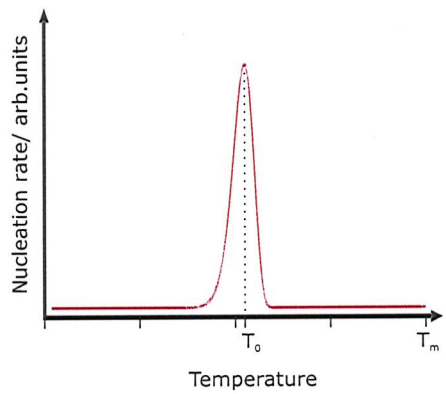

Figure 1.9: Nucleation rate as a function of temperature T. Note the pronounced maximum at T_0at a lower temperature than T_m. After Waser [47].

where N_0 is the total number of possible nucleation sites and k_B the Boltzman constant. The number density of critical nuclei for a given temperature is then given simply by:

$$N_C = e^{-\frac{\Delta G_C}{k_B T}} \tag{1.48}$$

A further atom is needed to convert a critical nucleus into a stable one. The probability of another atom joining the nucleus is proportional to $exp(-W_K/k_BT)$, where W_k is the activation energy barrier to cross the interface between the phases. Thus, the nucleation rate should be proportional to these two parameters. That is, according to the nucleation theory [49, 50] the nucleation rate should be given by:

$$I = \alpha e^{-\frac{W_K + \Delta G_C}{k_B T}} \tag{1.49}$$

where $\alpha$is a proportionallity constant. To a first approximation both α and W_K are independent of the temperature, while ΔG_c decreases as one moves away from T_M. The combination of these factors leads to a significant peak of the nucleation rate centered at a certain temperature and with a certain width, that depends on the melting temperature T_M, the latent heat of melting ΔH, the interface energy γ and the activation energy W_K (See Figure 1.9).

As discussed above, once a stable nucleus has formed there is a two phase coexistance separated by an interface, with the transfer of atoms between the phases governed both by the difference of the Gibbs free energy between the two phases and the activation energy necessary to overcome the interface (See Figure

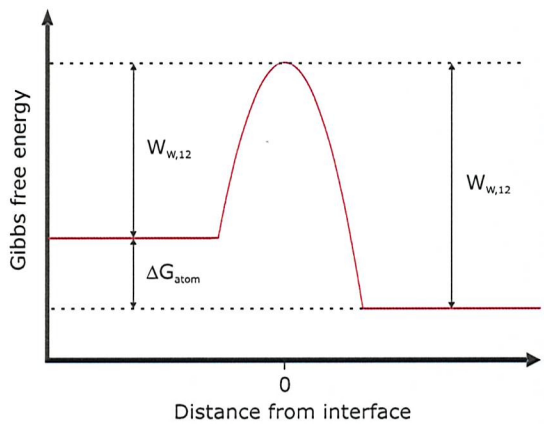

Figure 1.10: Change of the Gibbs free energy of a system undergoing a transition between phases 1 and 2. The activation energy for transition 1 to 2, $W_{W,12}$, differs from the activation energy for the reverse transition, $W_{W,21}$, by ΔG_{atom}, the difference in the Gibbs free energy between the two phases. After Waser [47].

1.10). The growth rate of the nucleus can be shown to be given by [50]:

$$U = \xi n \nu p B V_{atom} e^{-\frac{W_{W21}}{k_B T}} (1 - e^{-\frac{\Delta G_{atom}}{k_B T}}) \tag{1.50}$$

where n is the areal density at the interface. The probability that a site changes to the new phase is p, while B is the probability that it remains in this new phase. The parameter ξ is introduced to take into account the fact that not all areas of the interface can take new atoms, while ν relates to the attempt frequency. Finally ΔG_{atom} is the difference in the Gibbs free energy per atom of the two phases and for the materials normally considered this is much smaller than $W_{W,21}$ or $W_{W,12}$, so they can normally be described only by the activation energy for nucleation W_K. Figure 1.11 shows the growth rate as a function of temperature and a maximum peak is once again present, although this time it is at an higher temperature close to the melting point.

The combination of nucleation and growth can be described by a model by Mehl and Avrami [51, 52], that gives the transformed volume fraction χ as a function of time:

$$\chi(t) = 1 - e^{-(Kt)^{n_A}} \tag{1.51}$$

This equation reflects the fact that experimental data is often of the exponential form. Each transformation can be characterized by two parameters, the rate constant K and the Avrami exponent n_A. This exponent in particular gives very good indication of the nature of the transformation.

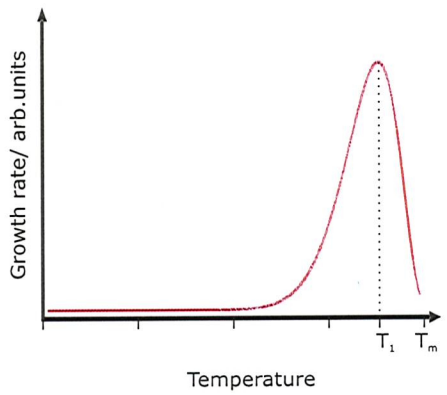

Figure 1.11: Growth rate as a function of temperature. Note how the maximum peak position, T_1 is now at a closer temperature to the melting point T_m. After Waser [47].

To further visualize the time and temperature dependence of isothermal phase transformations, TTT (time - temperature - transformation) diagrams are used. Figure 1.12 shows a shematic of such a diagram, for a typical material. Notice, how at low temperatures the crystallization rate is low despite the driving force being high, because the atomic mobility is low. At high temperatures, close to T_m, the mobility is higher, but now the driving force is low, and one again the crystallization rate is low. In between these two extreme behaviours, the optimum temperature T^* occurs, where suitable driving force and mobility combine to give a fast crystallization, precisely what one wants for memory writting operations.

1.4.3 Phase transitions in nanoparticles

Armed with an understanding of the general characteristics of transitions in phase change media, one can try to identify any changes in these charateristics resulting from the material in question being confined in a nanoparticle.

In nanoparticles the ratio between the surface area and the volume of material is significantly larger, so the surface contribution becomes very important. Atoms on the surface have fewer near-neighbours than internal ones and therefore the surface acts as a boundary at which transformation processes can begin [53-55]. Thus, in nanoparticles transitions from lower-to higher-energy phases are not abrupt, but rather proceed through a dynamic coexistence of

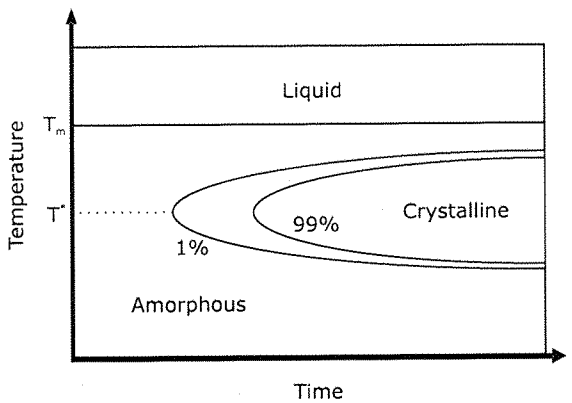

Figure 1.12: Typical TTT diagram for a material with a crystalline, an amorphous an a liquid phase. Each curve shows the volume fraction transformed if the material is held at a particular temperature. After Waser [47].

structural forms across a certain temperature range [56], centered around a nominal transition temperature that depends on the particle size [57].

Within this transition range the particles normally consist of a core in the lower energy phase covered by a shell of the higher energy phase [58]. The thickness of this shell increases with temperature and, if for example the transition is being induced by laser radiation, with light intensity [59] (see Figure 1.13(a)).

Importantly, throughout the temperature range where the two phases coexist, the structural transition is completely reversible. That is, if the temperature or level of optical excitation is reduced before the core is completely converted to the new phase, the surface layer will shrink to an appropriate equilibrium position. This can be seen by considering, as before, the Gibbs free energy changes associated with the process. In this case, one starts with a nanoparticle of radius R and a shell of thickness t of the new phase appears on the surface (See Figure 1.14). The change is the Gibbs energy is thus given by:

$$\Delta G_{np} = \Delta G_{newold}\frac{4}{3}\pi(R^3 - (R-t)^3) - \gamma_{newold}\pi(R-t)^2 \qquad (1.52)$$

where ΔG_{newold} is the change per volume in the Gibbs free energy of the two phases, and γ_{newold} is the surface tension between the two phases. Note how curvature is now in the opposite direction to before, and hence the negative sign in the surface tension term.

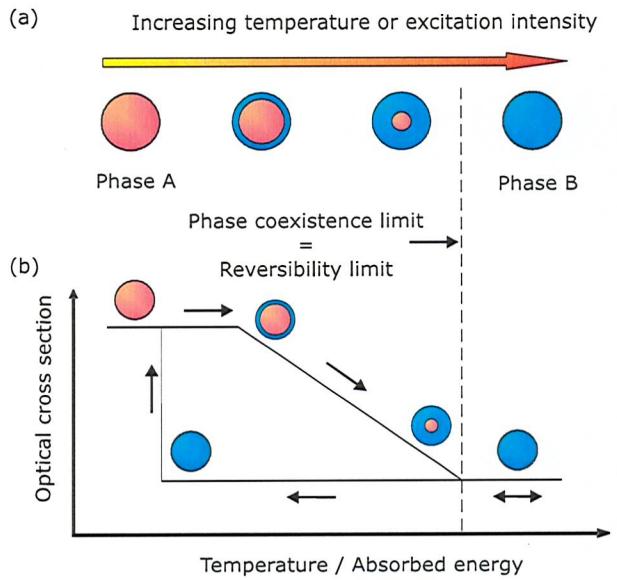

Figure 1.13: (a) Core-shell model of surface-driven phase coexistence for a structural transition in a nanoparticle. (b) Hysteresis with temperature and/or absorbed energy in the optical cross section of a nanoparticle undergoing a structural transition. Reversible excitation-induced changes are possible with increasing temperature/excitation up to the point indicated by the dashed line.

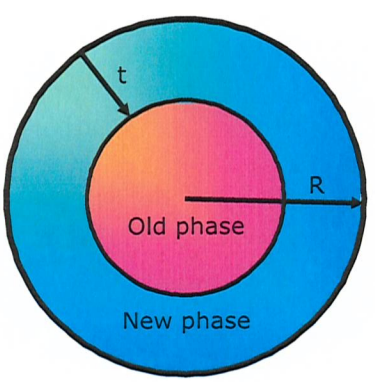

Figure 1.14: Representation of a core-shell nanoparticle structure. A new phase layer of thickness t forms on the surface of a particle with radius R.

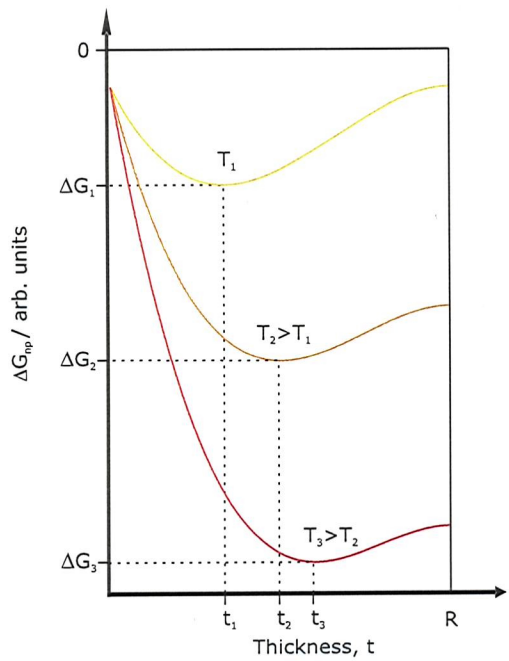

Figure 1.15: Change in the total Gibbs free energy ΔG_{np}as a new shell of thickness t forms on the surface of a nanoparticle with radius R, for increasing temperatures. For each temperature there is an equilibrium shell thichkness t_i corresponding to the minimum in the Gibbs energy change ΔG_i.

Figure 1.15 shows this Gibbs energy change dependence on shell thickness, for different temperatures. For each temperature there is a stable equilibrium position and a corresponding shell thickness. As the temperature is increased this equilibrium thickness progressivelly increases. Changes in temperatures only adjust this equilibrium thickness point, but the overall shape of the curve isn't altered. So, if the temperature change is induced by a laser pulse, the shell will first increase while the particle heats up and once the pulse has passed and the particle cools, it will just revert to the begining equilibration thickness.

On the other hand, when the particle's core is completely consumed by the new phase, a return to an old phase requires the creation of a nucleation centre. As it was shown before this causes the formation of an energier barrier, which means that the nanoparticle becomes stable against such a transition. The reverse transition will now only occur after a certain amount of overcooling and a hysteresis of the nanoparticle's properties appears as a result.

The work described in this thesis focuses on how the existence of such a

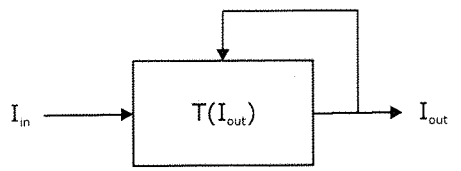

Figure 1.16: Schematic of a generic optical system with feedback. The transmission T is a function of the output I_{out}. After Saleh [60].

hysteresis in the optical properties of the nanoparticles (See Figure 1.13(b)) can be used to achieve optical functionalitly on the nanoscale. The details of the mechanisms by which this becomes possible are discussed in the next section.

1.5 Nonlinear optics via phase transitions

1.5.1 Optical bistability

A bistable or two-state device is a system such that whatever input is applied, the output always takes one of two possible stable values. Bistable devices can be used for various digital operations as switches, memories, registers and flip-flops. They are therefore active elements in fields like communications, signal processing and computing. Presently most of these devices are electronic based, but the use of all-optical devices could bring advantages such as increased speed and lower power consumption. Speed is improved not only because light travels at a faster speed, than signals in electronic circuits, but also because optical bistable devices would also eliminate the need to convert between electric and optical signals, for example in optical communications networks. Power consumption can mainly be reduced because of the lower energy dissipation characteristics of optical circuits. Another advantage is that optical devices normally scale very well, and they can be operated at a wider range of frequencies. Of course, there are also difficulties with all-optical devices. One of the main obstacles is the creation of sufficiently small devices, that are able to compete with the present level of miniaturization of electronic devices. Therefore obtaining nanoscale all-optical bistable devices is seen as decisive step forward in this important field.

Let's first take a look at how bistability can be achieved in a system following the ideas outlined by Saleh [60]. For a system to be bistable, it normally has to

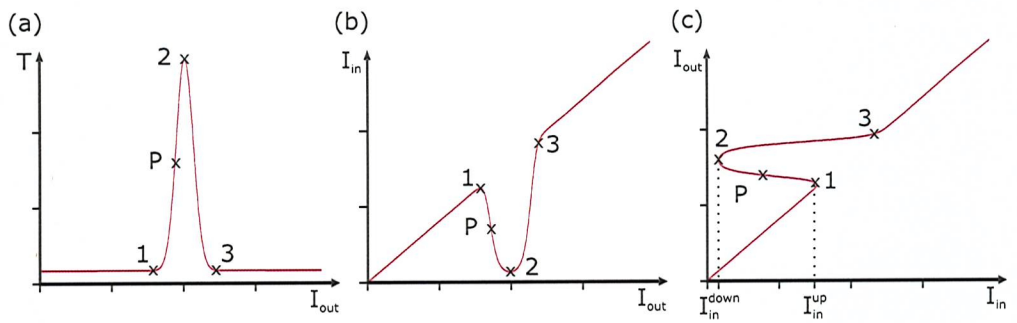

Figure 1.17: Response curves of a generic optical system with feedback: (a) Transmittance T as a function of the output I_{out}; (b) Input I_{in} as a function of the output I_{out}; and (c) Output I_{out} as a function of the input I_{in}.
After Saleh [60].

exhibit two features: nonlinearity and feedback. In optics this bistability is usually obtained by using mirrors to feed back the output of a nonlinear optical element and control the transmission of light through the element. Figure 1.16 shows a generic optical system where the output intensity I_{out} controls the transmittance T of the system, T being therefore a nonlinear function of I_{out}. As $I_{out} = TI_{in}$ one has:

$$I_{in} = \frac{I_{out}}{T(I_{out})} \tag{1.53}$$

If $T(I_{out})$ is a nonmonotonic function like the one shown in Figure 1.17a), then $I_{in} = I_{out}/T(I_{out})$ is also a nonmonotonic function of I_{out} (See Figure 1.17b)). This means that I_{out} must be a multivalued function of I_{in} as can bee seen in Figure 1.17c).

For small inputs such that $I_{in} < I_{in}^{down}$, and for large inputs such that $I_{in} > I_{in}^{up}$, a given input only has a single corresponding output value, but for inputs such that $I_{in}^{down} < I_{in} < I_{in}^{up}$ there are three possible output values corresponding to each input. The intermediate region however, that is, the line joining points 1 and 2, is unstable. Therefore such a system exhibits bistable behaviour. One can see this is so by considering a point P in the intermediate region (See Figure 1.17). For such a point, a small increase in the output I_{out}, will result in a large increase in the transmittance, which, due to the feedback, will further increase the output, and so on. The overall result is that as one passes the threshold level I_{in}^{up} there is a transition from the lower to the higher branch, without passing through the intermediate region. A similar situation occurs as

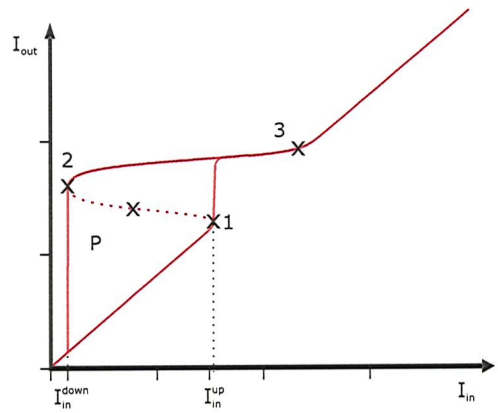

Figure 1.18: Output as a function of the input for a typical optical bistable device. Input powers thresholds of I_{in}^{up} and I_{in}^{down} delimitate the bistable region. Point P represents an unstable state that will quickly fall into one of the stable regions. After Saleh [60].

the input is decreased and the ouput follows the higher branch until the value I_i^{down}, at which point the output jumps to the lower section of the curve. The curve just described is plotted in Figure 1.18.

A device with this type of response can be used as an optical switch by fixing the input at a bias level I_b, for which the two stable points L_1 and L_2 are possible. The system can then be forced into the higher state with a pulse of light so that the total input exceeds I_{in}^{up}, and switched to the lower state by momentarily blocking the input beam. The same idea can be used to store information in the system by associating logic states with the low and high levels of the device. Finally, one should note that there are several other nonlinear functions that lead to bistable and even to multistable systems, that is systems with more than two stable outputs for a given input: the bell shape curve was used only for illustrative purposes.

There are two main ways by which the optical bistability idea just described can be implemented in a system: using dispersive or dissipative nonlinear elements (See Figure 1.19). In dispersive nonlinear systems the refractive index of the material is a function of the optical intensity, whereas in dissipative nonlinear systems it is the absorption coefficient α that is a function of optical intensity.

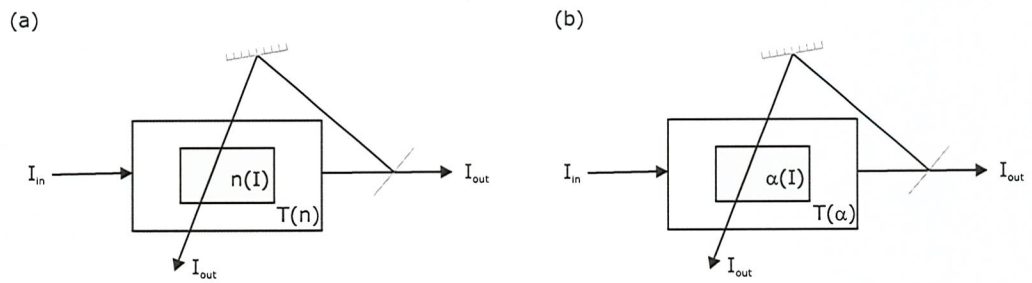

Figure 1.19: Different types of nonlinear elements for optical bistable devices. (a) dispersive system, where the transmittance T is a function of the refractive index, that varies with the output intensity I_{out}; (b) dissipative system, where the transmittance T is a function of the absorption coefficient α, that varies with the output intensity I_{out}. After Saleh [60].

Consider now the details of the operation of a dispersive nonlinear system: For such a system the refractive index of the medium changes with the intensity I as:

$$n = n_0 + n_2 I \tag{1.54}$$

where n_0 and n_2 are constants. Here it will be assumed that materials for which this occurs exist, while in Sections 1.5.2 and 1.5.3 the way that such a dependence may arise is discussed in more detail. A medium with such a dependence is then placed inside an interferometer, for example in one of the branches of a Mach-Zender interferometer (See Figure 1.20(a)). Taking into account equation 1.54 the transmittance through the system is given by [60]:

$$T(I_{out}) = \frac{1}{2} + \frac{1}{2} cos(2\pi \frac{d}{\lambda_0} n_2 I_{out} + 2\pi \frac{d}{\lambda_0} n_0 + \phi) \tag{1.55}$$

where λ_0 is the vacuum wavelength for light, d is the length of the nonlinear medium and ϕ is a constant. By plotting this transmittance as a function of I_{out} (See Figure 1.20(b)), one can see how it is a periodic repetition of a nonmonotic function of the type that previously was shown to lead to optical bistability. Therefore a Mach-Zender interferometer with a medium for which the refractive index follows equation 1.54 in one of its branches, can be operated as an optical switch or as an optical memory. Note that the entire system is limited in the minimum size it can take, by the need of the interferometer feedback. A more

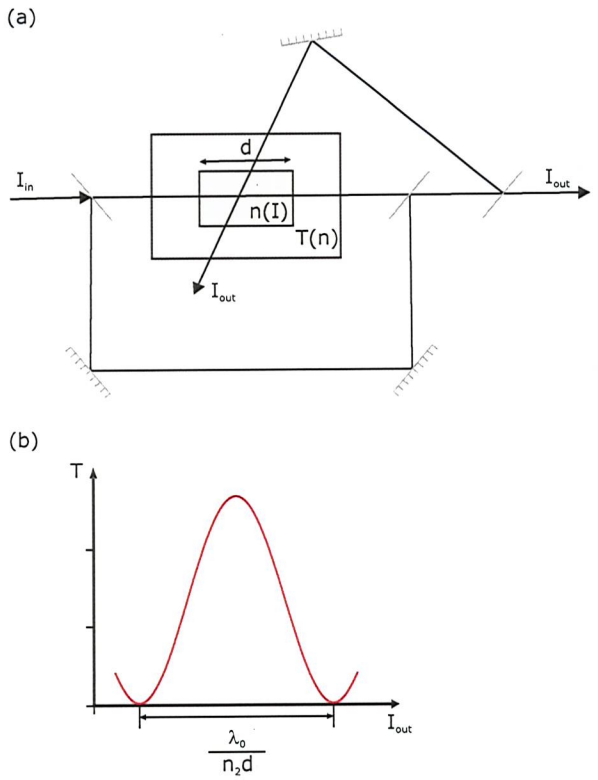

Figure 1.20: Bistable optical device based on a Mach-Zehnder interferometer. (a) A nonlinear material with a refractive index determined by the intensity is placed inside one of the arms of the interferometer. This creates the response curve for the transmission as a function of the output intensity shown in (b). In the text it is shown that such a curve leads to bistable behaviour of the overall system. After Saleh [60].

detailed discussion of this and other types of optical bistable devices can be found in [61].

1.5.2 Conventional nonlinearity: intensity dependent refractive index

In the Introduction, the concept of nonlinear materials was presented by introducing the second and third order nonlinear optical susceptibility tensors, $\chi^{(2)}_{\alpha\beta\gamma}$ and $\chi^{(3)}_{\alpha\beta\gamma\delta}$. In this section, a simple argument will be given that shows how in materials with a significant third order nonlinearity, the refractive index exhibits a dependence to light intensity given by equation 1.54. For a more detailed discussion see for example [61].

Consider a simple applied monochromatic field given by:

$$E(t) = E_0 cos(wt) \tag{1.56}$$

Then the contribution to the third order nonlinear polarization, which is of the form:

$$P^{(3)}(t) = \chi^{(3)} E(t)^3 \tag{1.57}$$

is given by:

$$P^{(3)}(t) = \frac{1}{4}\chi^{(3)} E_0^3 cos(3wt) + \frac{3}{4}\chi^{(3)} E_0^3 cos(wt) \tag{1.58}$$

where the trignometric identity $cos^3(x) = \frac{1}{4}cos(3x) + \frac{3}{4}cos(wt)$ was used. The first term of this equation describes the process of third harmonic generation [7], that is a response at a frequency $3w$ caused by the applied field at frequency w. On the other hand, the second term of equation 1.58 describes a nonlinear contribution to the polarization at the same frequency w of the applied field. It can be shown [61] that the precise contribution of this extra term leads to a total polarization at frequency w given by:

$$P^{total}(w) = \chi^{(1)} E(w) + 3\chi^{(3)} |E(w)|^2 = \chi_{eff} E(w) \tag{1.59}$$

The introduction of a new effective first order optical susceptibility χ_{eff}, that depends on the applied electric field, means that the material behaves like the refractive index is actually changing with power. One can then write the changes in the refractive index as:

$$n = n_0 + n_2 I \tag{1.60}$$

where n_2 is the nonlinear refractive index and I is the time-averaged intensity of the optical field:

$$I = \frac{n_0 c}{2\pi} |E(w)|^2 \tag{1.61}$$

This change of refractive index with intensity is called the optical Kerr effect, by comparison with the electroptic Kerr effect, where the refractive index of the material changes with the applied static electric field. Electronic polarization and molecular orientation are examples of physical processes that can lead to this type of nonlinear change. The third order nonlinear optical susceptibilty of

a material $\chi^{(3)}$ can be related to the nonlinear refractive n_2 by using the following identity:

$$n^2 = 1 + 4\pi\chi_{eff} \tag{1.62}$$

Substituting expression 1.60 in this equation and considering only terms up to $|E(w)|^2$ finally leads to:

$$n_2 = \frac{12\pi^2}{n_o c}\chi^{(3)} \tag{1.63}$$

A typical value of the magnitude of the coefficent n_2 of 10^{-14} means that a laser beam with an intensity of $1\,MW/cm^2$ can only produce a change of the order of $\sim 10^{-8}$ in the refractive index. So, this type of nonlinearity usually needs high energies and long interaction lengths to obtain a considerable response. In the next section, an alternative process to obtain optical nonlinearity will be introduced that relaxes these requirements.

1.5.3 Phase change nonlinearity

This section describes an alternative mechanism for an optical nonlinearity based on the use of light to stimulate transitions between material phases with different optical properties.

Section 1.3 discussed how nanoparticles consisting of different structural phases of a material can exhibit significant contrast in their optical properties. In particular, Figure 1.6 showed how the transmission and reflection of a film of nanoparticles, consisting of a core and a shell of different materials, changed continuously as the thickness of the shell increased. Then, Section 1.4.3 described how this type of core-shell is precisely how phase transitions occur in nanoparticles. As the phase transition temperature is approached, a shell of the new material is created and as the temperature increases it progressively consumes the old phase. The changes are totally reversible as long as there is still some of the old phase remaining.

This means that, if light is used to increase the temperature of the system, to a point before the full conversion temperature, any changes will be reversed when the light excitation is withdrawn. Inside this reversible region, that is between levels Q_1 and Q_2 in Figure 1.21, higher intensities will convert a thicker layer and cause a larger optical change, and so the system shows a nonlinear response

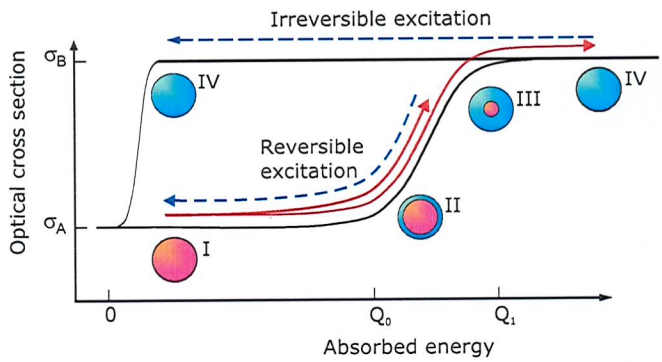

Figure 1.21: Optical nonlinearity through phase transitions in nanoparticles. For energy levels between Q_0 and Q_1 the nanoparticle is a mixed phase state and all transformation are fully reversible. If the excitation exceeds Q_1 then the particle remains in the upper level even after the excitation is withdrawn and overcooling is necessary to bring the particle back to the initial state.

to light intensity. The energy required to obtain this type of nonlinearity depends on the energy difference between the material phases, which is of the order of a phonon per atom. This results in a power requirement about three or four orders of magnitude lower than that of a traditional nonlinear media to observe similar responses. Chapters 2 and 3 show how this idea can be experimentally demonstrated first with a gallium nanoparticle film and then with a single gallium nanoparticle.

These elements could in principle be introduced in the type of interferometer devices described in Section 1.5.1 to obtain bistable systems with lower switching energies than those using traditional optical nonlinearities. However this considerable energy gain is not the only advantage of using phase transitions in nanoparticles to obtain nonlinear effects: Optical bistability can also be achieved in nanoparticles without using any feedback mechanisms. Such bistability occurs when the system is operated at light intensities that are sufficient to fully convert the nanoparticle. The full conversion means that to recover to initial configuration a nucleus would have to be created, which as discussed in Section 1.4 creates an energy barrier against the return. Thus, to return to the initial state the particles now have to be significantly overcooled, meaning that a large hysteresis is present in the nanoparticles optical properties. This bistability can, as before, be used to store information but, as

feedback is no longer required, much higher storage densities are now possible. In fact, more than one bit of information can be stored in individual particles if there are more than two phases available. Chapter 4 discusses in more detail the processes involved in using nanoparticles as optical memory elements.

1.6 Phase change materials

1.6.1 General requirements

For a material to be of use for the phase change applications just described, it has to possess a very particular set of characteristics. These are directly related to the demands of the type of functionality that one is trying to achieve. In this section, the main requirements that these types of materials need to satisfy are described following the general ideas discussed by Waser [47].

The first task that needs to be executed to store information in a medium is the writing of that information. In the materials commonly used today in comercial optical data storage systems such as DVD's, this writability demand means that the material must be an easy glass former, with a relatively low melting point of around 500 °C. A layered design is normally used, both to improve the absorption of light on the phase change film and to assist the conversion of the power absorbed into heat. Furthermore, the active layer is normally surrounded by dielectrics with very low thermal conductivity in order to increase the sensitivity and to create devices for which less that $5\,\mathrm{mW}/\mu\mathrm{m}^2$ is sufficient write single bits.

Once information is stored in a medium, a further requirement comes into play: Data needs to remain available for a long period of time, with typical accepted values of at least 10 years at room temperature. This means that information has to be stored in a stable phase, with a relatively large activation energy, on the order of or higher than 1 eV/atom.

On the other hand, information also has to be erased quickly by using high local temperatures. For materials storing information in armophous/crystalline phases, speed improvements are related to a better understanding of the recrystalization process. Very short times of around 10 ns per bit are normally regarded as ideal, because of the demands of applications such as the recording

of high definition TV signals and computer mass data storage, that require high rates of data transfer.

Furthermore, the stored data has to be accessed easilly, which means that there should be a large signal-to-noise ratio. To improve this ratio the contrast between the properties of the phases involved should be as large as possible, while the structure should be designed to yeld a noise level as low as possible.

The final requirement is that of cyclability: the material has to resist a large number of read and write cycles if it is going to be used in commercial applications. The commonly regarded target to achieve is 10^7 cycles. Attempts to improve this parameter are normally centered around increasing the stability of the layer design, as the main problems arise from the stresses caused by the volume changes during the phase transformation.

1.6.2 Commonly used materials

The following describes some of the materials being currently used or researched for phase change applications. In the 1970s research began on the use of tellurium compounds for optical data storage. The interest in tellurium compounds arose from the fact that Te is an easy glass former. Over the years different materials were studied with particular interest in Ge-Te compounds. However, these compounds required very precise preparation as, for compositions other than $Ge_{50}Te_{50}$, phase separation occurs on melting which leads to very long recrystallization times [62].

A family of compounds where moving away from the ideal composition doesn't cause a significant decrease in the quality of the properties is the ternary $GeSbTe$ system (See Figure 1.22). The best properties are found along the $GeTe - Sb_2Te_3$ line [63]. Currently this type of material is the most commonly used in phase change applications, being present in all DVD/DVR disks. As discussed, data recording is achieved by switching between amorphous and crystalline phases with appropriate laser pulses, while reading is also done optically by measuring the differences in reflectivity between the two phases. This type of memory has seen its latest development in Blu-ray DVD/DVR disks with a data storage density of $0.015\,\mathrm{Tb/in^2}$.

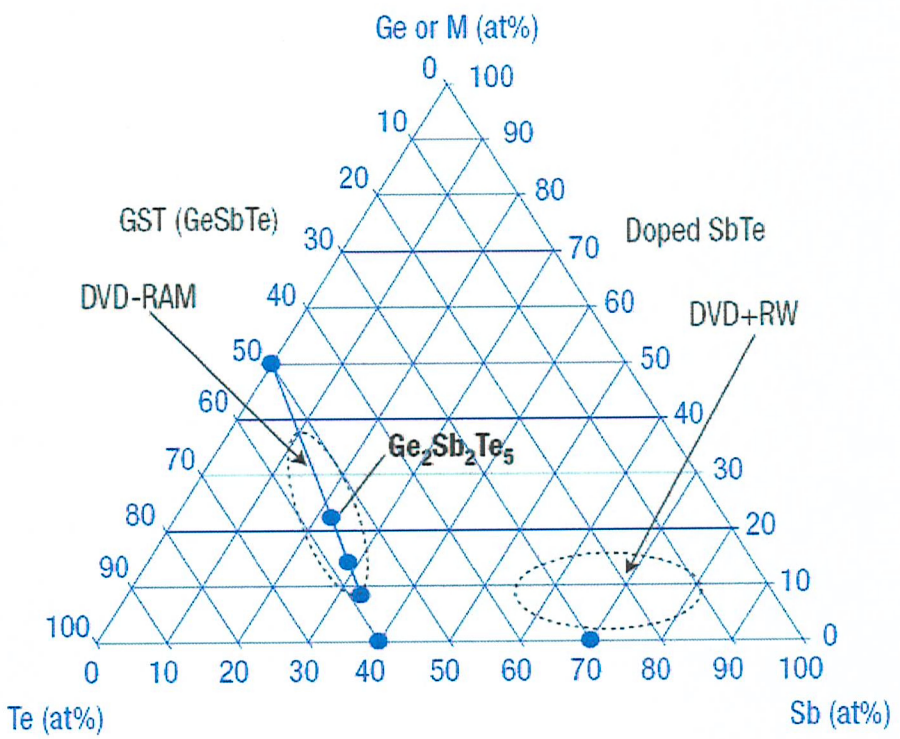

Figure 1.22: Different compounds of the *GeSbTe* family used in phase-change optical and electronic memory. After Lankhorst[64].

The differences between the amorphous and crystalline phases express themselves not only as contrasting optical properties, but also mean that there is a significant change on the resistivity between the phases. This fact is exploited in so called ovonic unified memory [63]. Recent changes to the type of cell used have shown great improvement in the potential of this type of memory [64]. A different configuration employing shorter lines, which lead to lower switching voltages, means that doped-SbTe materials are now seen as the most suitable type for this kind of application. Cell sizes smaller than 100 nm and writing speeds of the order of 50 ns have already been demonstrated.

A further way to explore phase change materials is through all-thermal memory systems [66]. In these devices a nanoheater, based around an AFM probe, is used to write spots with dimensions of less than 50 nm. Reading is achieved by using a low current to measure the resistance that depends on the phase of the film spot. Storage density of up to 3.3 Tb/inch^2 were demonstrated, with writing times as shorts as 10 ns.

Recently, another type of ultra-high density data storage medium has been proposed, based on a diode created by growing a InSe/GaSe phase-change bilayer on silicon [67]. Bits are recorded as amorphous regions in the InSe layer, while reading is done by the current induced in the diode by a scanning electron beam. It has been demonstrated that bits can be stored in 150 nm regions and that there is a strong constrast in the measured current. The long term stability also looks promising, but further research is still needed to better understand the full potential of these devices.

Finally, another very interesting development has been the demonstration of dislocation switching in $SrTiO_3$ [68]. Dislocations are defects or irregularities inside a crystal structure. In these experiments, the applied electric field controls oxygen transport along the dislocations, which in turn determines the conductivity. With densities of up to 10^{12} cm^{-2}, if individual dislocations can be reliably addressed, data densities as high as a terabit per cm^2 are possible.

1.6.3 Gallium

In the previous section, the most common materials used for different types of phase change functionalities were introduced, while in this section, attention is focused on the material employed in the work described in this thesis: gallium.

In 1871, Mendeleev predicted the existence of an unknown element whose properties should be similar to those of aluminium. Four years later, in 1875, gallium was identified spectroscopically by Paul-Emile Lecoq de Boisbaudran. In the same year he also succeeded in isolating the soft silvery-grey metal by electrolysis of a solution of the hydroxide $Ga(OH)_3$ in KOH.

Nowadays gallium is normally obtained as byproduct of the aluminium industry. When bauxite is purified by the Bayer process, the alkaline solution has a aluminium: gallium ratio from 5000 to 300. After that, electrolysis using a mercury electrode gives an improved concentration and further electrolysis using a stainless steel cathode results in liquid gallium. If very pure gallium is required, a series of further processes are necessary.

Although gallium is used in a variety of applications, the most important one presently is in the semiconductor industry, normally in the form of the well studied compound of gallium arsenide. The present work however concerns the properties of gallium when it is on its elemental form.

Gallium has atomic number 31, an atomic weight of $69.723(1)\,\mathrm{g.mol^{-1}}$ and its electronic configuration is $3d^{10}4d^{10}4p^1$. At atmospheric pressure gallium melts at a temperature of $29.8\,^{\circ}C$ and has a very high boiling point of $2403\,^{\circ}C$, making it the metal with the longest temperature range in the liquid state. Another interesting property of bulk gallium is that it is easily supercooled, that is, it remains in the liquid state a few degrees below the melting point, before solidifying.

Even more interesting is the fact that solid gallium can exist as a number of different crystalline forms. At standard conditions gallium crystallizes on the stable $\alpha-$phase, but when pressure increases two other phases become stable, *Ga II* and *Ga III*. There is also a number of metastable phases known as β, γ, δ and ϵ [69]. Figure 1.23 shows the phase diagram for bulk gallium obtained by Bosio [70]. By using a diamond anvil cell capable of reaching pressures up to 3 GPa in the temperature range $170 - 370\,\mathrm{K}$, he was able to study the x-ray diffraction patterns of single crystals as the conditions changed and identify the crystalographic structures involved.

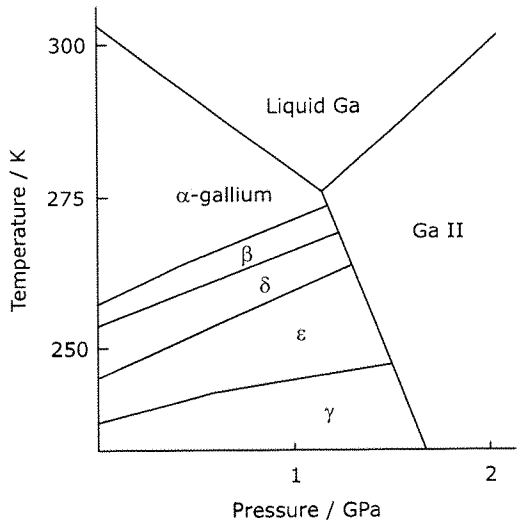

Figure 1.23: Phase diagram for (bulk) gallium. After Bosio [70].

Although Bosio was particularly interested in the high-pressure phases, Ga-II and Ga-III (not shown in Figure 1.23), at lower pressures he also observed various meta-stable phases occuring in the 80 μm diameter droplets used in the experiment.

In the present work, it is the properties of these lower pressure phases, β, γ, δ and ϵ, that are of particular importance. Their structural characteristics and thermodynamic properties have been reviewed in the past by Defrain [69] and are summarized in Figures 1.24 to 1.28.

Unfortunately, optical data for all the different phases are not available in the literature. Nevertheless, the dielectric constants for two of the phases are well-know: Figure 1.29 shows the spectral dependence of the real and imaginary parts of the dielectric constant for both $\alpha-$gallium (a-axis) and the liquid phase [71].

Phase name	α
Melting Point, T_m at P=0 (K)	302.92
Latent heat of fusion, L at T_m at P=0 (J/mol)	5560
Heat capacity C_p at constant pressure (J/K.mol)	26.6 at 303K
Energy difference to the α-phase $\Delta Gx10^4$ (atomic units)	0
Electrical resistivity, ρ at P=0 (μΩcm)	15.05 at 20°C
Density, d at P=0 (g/cm^3)	5.904 at 29.78°C
Crystallographic system	Orthorhombic
Spatial Group	Cmca
Atoms per celll	8
Parameters at P=0 (angstrons)	a=4.5186 b=7.6570 c=4.528 at $T=T_m$

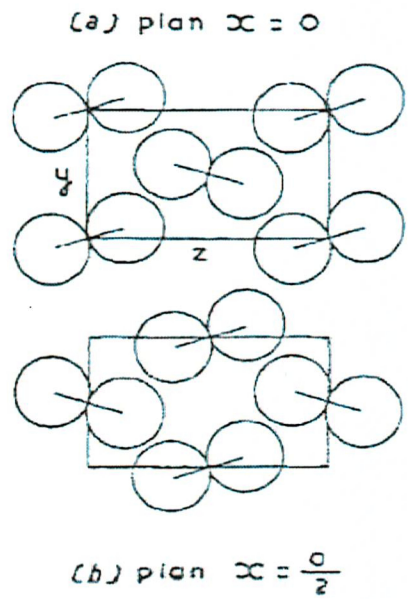

Figure 1.24: Left: summary of $\alpha-$gallium properties. Right: arrangement of gallium atoms in the $x = 0$ and $x = a/2$ planes. After Defrain [69]

Phase name	β
Melting Point, T_m at P=0 (K)	256.85
Latent heat of fusion, L at T_m at P=0 (J/mol)	2650
Heat capacity C_p at constant pressure (J/K.mol)	28.0 at 256K
Energy difference to the α-phase $\Delta Gx10^4$ (atomic units)	8.19
Electrical resistivity, ρ at P=0 (μΩcm)	8.3 to 11.3 at -17°C
Density, d at P=0 (g/cm^3)	5.904 at 29.78°C
Crystallographic system	Monoclinic
Spatial Group	C2/c
Atoms per celll	4
Parameters at P=0 (angstrons)	a=2.7713 b=8.0606 c=3.3314 β=91.574°

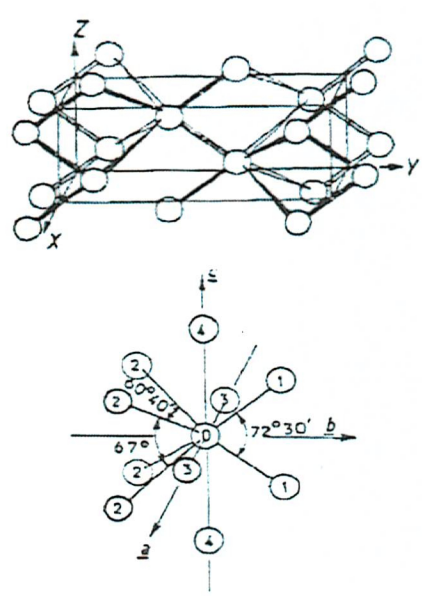

Figure 1.25: Left: summary of $\beta-$gallium properties. Right: atomic arrangement of gallium atoms in the crystallographic cell. After Defrain [69].

Phase name	γ
Melting Point, T_m at P=0 (K)	237.6
Latent heat of fusion, L at T_m at P=0 (J/mol)	2440
Heat capacity C_p at constant pressure (J/K.mol)	26.8 at 237K
Energy difference to the α-phase $\Delta Gx10^4$ (atomic units)	8.94
Electrical resistivity, ρ at P=0 (μΩcm)	
Density, d at P=0 (g/cm^3)	6.20 at -35.6°C
Crystallographic system	Orthorhombic
Spatial Group	Cmcm
Atoms per celll	40
Parameters at P=0 (angstrons)	a=10.593 b=13.523 c=5.203°

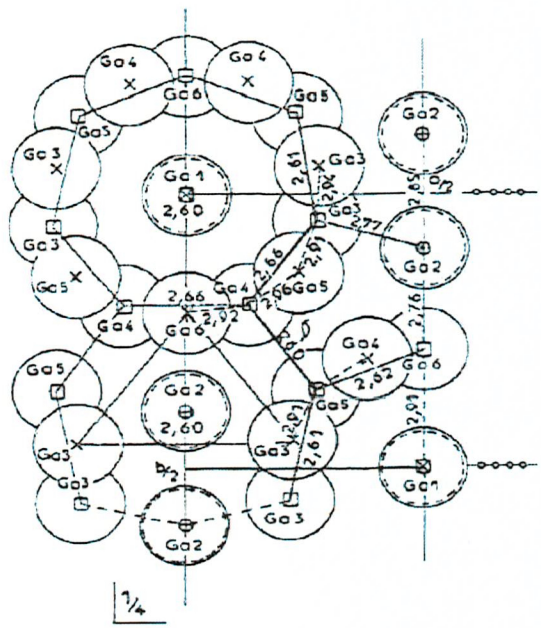

Figure 1.26: Left: summary of $\gamma-$gallium properties. Right: projection on the (001) plane of $\gamma-$gallium structure. After Defrain [69].

Phase name	δ
Melting Point, T_m at P=0 (K)	253.8
Latent heat of fusion, L at T_m at P=0 (J/mol)	2580
Heat capacity C_p at constant pressure (J/K.mol)	
Energy difference to the α-phase $\Delta Gx10^4$ (atomic units)	8.30
Electrical resistivity, ρ at P=0 (μΩcm)	
Density, d at P=0 (g/cm^3)	6.21 at -19.4°C
Crystallographic system	Rhombic
Spatial Group	R3m
Atoms per celll	22
Parameters at P=0 (angstrons)	a=7.729 α=91.574°

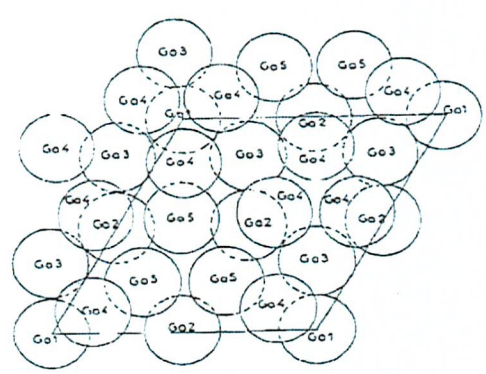

Figure 1.27: Left: summary of $\delta-$gallium properties. Right: arrangement of gallium atoms between 0 and 1/6 of the hexagonal lattice. After Defrain [69].

Phase name	ε	liquid
Melting Point, T_m at P=0 (K)	244.6	
Latent heat of fusion, L at T_m at P=0 (J/mol)	2520	
Heat capacity C_p at constant pressure (J/K.mol)		28.0 at 300K
Energy difference to the α-phase $\Delta Gx10^4$ (atomic units)		
Electrical resistivity, ρ at P=0 (μΩcm)		25.8 at 30°C
Density, d at P=0 (g/cm^3)		6.095 at 30°C

Figure 1.28: Summary of $\delta-$and liquid gallium properties. After Defrain [69].

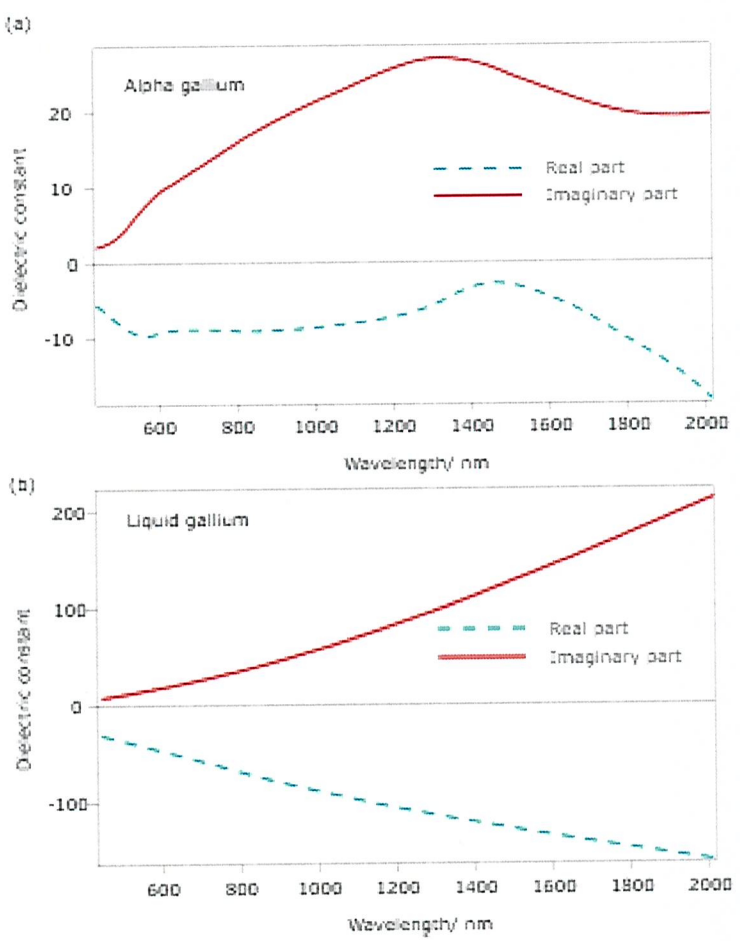

Figure 1.29: Dielectric constants for (a) $\alpha-$gallium a-axis and (b) liquid gallium. After Kofman [71].

1.7 Thesis plan

Following this introductory chapter, this thesis is divided into four other chapters:

Chapter 2 describes how light-induced structural transformations in gallium nanoparticle films grown from atomic beam at the tip of an optical fibre were studied using low-power diode lasers. The data presented show that these transformations can be used to reversibly control the optical properties of metallic nanoparticles and therefore provide a paradigm for controlling light with light.

Chapter 3 reports on how this type of nonlinearity was used to control the optical properties of a single gallium nanoparticle. Studying a single particle as opposed to a nanoparticle film allowed the detection of a more complex sequence of reversible transitions between several of the different gallium structural forms.

Chapter 4 focuses on the idea of using nanoparticles undergoing light-induced structural transformations as optical memory elements. In particular, it details experiments that demonstrated that a film of gallium nanoparticles can act as a two level rewritable all-optical memory and that a single gallium nanoparticle can act as an all-optical quaternary memory element.

Chapter 5 concludes the thesis with a summary of the results reported in previous chapters and a discussion of ongoing and potential research work.

The work reported in this thesis was carried out while the author was registered as a postgraduate student in the School of Physics and Astronomy at the University of Southampton, United Kingdom. It is, unless otherwise indicated, the original work of the author.

1.8 References

[1] S.J. Vavilov, and W.L. Lewschin *Zeitschrift für Physik* **35**: 920 (1926).

[2] S.J. Vavilov *Microstructura Sveta (Microstructure of Light)* USSR Academy of Sciences Publishing, Moscow (1950).

[3] T.H. Maiman *Nature* **187**: 493 (1960).

[4] P.A. Franken, A.E. Hill, C.W. Peters, and G. Weinreich *Physical Review Letters* **7**(4): 118 (1961).

[5] M. Bass, P.A. Franken, A.E. Hill, C.W. Peters, and G. Weinreich *Physical Review Letters* **8**(1): 18 (1962).

[6] R.W. Terhune, P.D. Maker, and C.M. Savage *Physical Review Letters* **8**(10): 404 (1962).

[7] H.M. Gibbs, S.L. McCall, and T.N.C. Venkatesan *Physical Review Letters* **36**(19): 1135 (1976).

[8] H.M. Gibbs, S.L. McCall, T.N.C. Venkatesan, A.C. Gossard, A.Passner, and W.Wiegmann *Applied Physics Letters* **35**(6): 451 (1979).

[9] D.A.B. Miller, S.D. Smith, and A. Johnston *Applied Physics Letters* **35**(9): 658 (1979).

[10] *Handbook of Advanced Electronic and Photonic Materials: Nonlinear Optical Materials, Volume 9* Academic Press, San Diego (2001).

[11] M. Roukes *Physics World* **14**: 25 (2001).

[12] N.I. Zheludev, P.J. Bennett, H. Loh, S.V. Popov, I.R. Shatwell, Y.P. Svirko, V.E. Gusev, V.F. Kamalov, and E.V. Slobodchikov *Optics Letters* **20**(12): 1368 (1995).

[13] N.I. Zheludev *Contemporary Physics* **43**(5): 365 (2002).

[14] R.S. Berry, and B.M. Smirnov *Journal of Chemical Physics* **113**(2): 728 (2000).

[15] R.D. Heyding, W. Keeney, and S.L. Segel *Journal of Physics and Chemistry of Solids* **34**(1): 133 (1973).

[16] M. Bernasconi, G.L. Chiarotti, and E. Tosatti *Physical Review B* **52**(14): 9988 (1995).

[17] R. Kofman, P. Cheyssac, and J. Richard *Physical Review B* **16**(12): 5216 (1977).

[18] N.R. Comins *Philosophical Magazine* **25**(4): 817 (1972).

[19] O. Hunderi, and R. Ryberg *Journal of Physics F-Metal Physics* **4**(11): 2096 (1974).

[20] S. Dhanjal, I.R. Shatwell, Y.P. Svirko, and N.I. Zheludev *Quantum Electronic and Laser Science 1997*, Optical Society of America, Washington DC (1997).

[21] P.J. Bennett, S. Dhanjal, P. Petropoulos, D.J. Richardson, N.I. Zheludev, and V.I. Emelyanov *Applied Physics Letters* **73**(13): 1787 (1998).

[22] P. Petropoulos, H.L. Offerhaus, D.J. Richardson, S. Dhanjal, and N.I. Zheludev *Applied Physics Letters* **74**(24): 3619 (1999).

[23] K.F. MacDonald, V.A. Fedotov, and N.I. Zheludev *Applied Physics Letters* **82**(7): 1087 (2003).

[24] S. Pochon, K.F. MacDonald, R.J. Knize, and N.I. Zheludev *Physical Review Letters* **92**(14): 145702 (2004).

[25] Y. Kanemitsu, and A. Ishizumi, *Journal of Luminescence* **119-120**: 161(2006).

[26] F. Wang, W.B. Tan, Y. Zhang, X. Fan, and M. Wang *Nanotechnology* **17**: R11 (2006).

[27] H.R. Stuart, and D.G. Hall *Applied Physics Letters* **73**(26): 3815 (1998).

[28] J.H. Amanda, and P.V.D. Richard *Analytical and Bioanalytical Chemistry* **379**(7): 920 (2004).

[29] J.C. Riboh, A.J. Haes, A.D. McFarland, C.R. Yonzon, and R.P.V. Duyne *Journal of Physical Chemistry B* **107**(8): 1772 (2003).

[30] L. Olofsson, T. Rindzevicius, I. Pfeiffer, M. Kall, F. Hook *Langmuir* **19**(24): 10414 (2003).

[31] J. Zhang, Y. Liu, Y. Ke, H. Yan *Nano Letters* **6**(2): 248 (2006).

[32] S.J. Oldenburg, R.D. Averitt, S.L. Westcott, and N.J. Halas *Chemical Physics Letters* **288**(2-4): 243 (1998).

[33] C. Loo, A. Lin, L. Hirsch, M. Lee, J. Barton, N. Halas, J. West, R. Drezek *Technology in Cancer Research and Treatment* **3**: 33 (2004).

[34] S.A. Maier, P.G. Kik, H.A. Atwater, S. Meltzer, E. Harel, B.E. Koel, A.A.G. Requicha *Nature Materials* **2**(4): 229 (2003).

[35] V. A. Fedotov, V. I. Emel'yanov, K. F. MacDonald, and N. I. Zheludev *Journal of Optics A-Pure and Applied Optics* **6**(2): 155 (2004).

[36] J.C. Maxwell-Garnett *Philosophical Transactions of the Royal Society* **203**: 885 (1904).

[37] E. David *Zeitschrift für Physik* **114**: 389 (1939).

[38] T. Yamaguchi, S. Yoshida, and A. Kinbara *Thin Solid Films* **21**: 173 (1974).

[39] T. Yamaguchi, S. Yoshida, and A. Kinbara *Thin Solid Films* **18**: 63 (1973).

[40] A.F. Bohren, and D.R. Huffman *Absorption and Scattering of Light by Small Particles* Wiley, New York (1983).

[41] P. Tognini, M. Geddo, A. Stella, P. Cheyssac, and R. Kofman *Journal of Applied Physics* **79:** 1032 (1996).

[42] H.V. Nguyen, and R.W. Collins *Journal of the Optical Society of America A* **10**: 515 (1993).

[43] L.D. Landau, and E.M. Lifshitz *Electrodynamics of Continuous Media* Pergamon, Oxford (1984).

[44] E. Prodan, P. Nordlander, and N.J. Halas *Chemical Physics Letters* **368**: 94 (2003).

[45] S.L. Westcott, J.B. Jackson, C. Radloff, and N.J. Halas *Physical Review Letters B* **66**: 155431 (2002).

[46] O.S. Heavens *Optical Properties of Thin Solid Films* Butterworths Scientific Publications, London (1955).

[47] R. Waser *Nanoelectronics and Information Technology* Wiley-VCH, Weinheim (2005).

[48] C. Peng, L. Cheng, and M. Mansuripur, *Journal of Applied Physics* **82**: 4183 (1997).

[49] M. Vollmer, and A. Weber *Zeitschrift für Physikalische Chemie* **119**: 277 (1925).

[50] R. Becker, and W. Döring *Annals of Physics* **24**:719 (1935).

[51] W.A. Johnson, and R.F mehl, *Trans. A.I.M.E.* **135**: 416 (1939).

[52] M. Avrami *Journal of Chemical Physics* **7**: 1103 (1939).

[53] R. Garrigos, P. Cheyssac, and R. Kofman *Zeitschrift Fur Physik D-Atoms Molecules and Clusters* **12**(1-4): 497 (1989).

[54] K. F. Peters, Y. W. Chung, and J. B. Cohen *Applied Physics Letters* **71**(16): 2391 (1997).

[55] G. B. Parravicini, A. Stella, P. Tognini, P. G. Merli, A. Migliori, P. Cheyssac, and R. Kofman *Applied Physics Letters* **82**(9): 1461 (2003).

[56] R. S. Berry, and B. M. Smirnov *Journal of Chemical Physics* **113**(2): 728 (2000).

[57] P. Buffat, and J. P. Borel *Physical Review A* **13**(6): 2287 (1976).

[58] A. S. Shirinyan, and M. Wautelet *Nanotechnology* **15**: 1720 (2004).

[59] M. Wautelet *Journal of Physics-Condensed Matter* **16**(12): 163 (2004).

[60] B.E.A. Saleh, and M.C Teich *Fundamentals of Photonics* John Wiley and Sons, New York (1991).

[61] R. W. Boyd *Nonlinear Optics* Academic Press, San Diego (2003).

[62] M. Libera, and M. Chen *MRS Bulletin* **40** (1990).

[63] N. Yamada *MRS Bulletin* **48** (1996).

[64] M. H. R. Lankhorst, B. W. S. M. M. Ketelaars, and R. A. M. Wolters *Nature Materials* **4**(4): 347 (2005).

[65] M. Gill, T. Lowrey, and J. Park, *2002 IEEE International Solid-State Circuits Conference Digest Technical Papers* San Francisco **1**: 202 (2002).

[66] H. F. Hamann, M. O'Boyle, Y. C. Martin, M. Rooks, and K. Wickramasinghe *Nature Materials* **5**(5): 383 (2006).

[67] G. A. Gibson, A. Chaiken, K. Nauka, C. C. Yang, R. Davidson, A. Holden, R. Bicknell, B. S. Yeh, J. Chen, H. Liao, S. Subramanian, D. Schut, J. Jasinski, and Z. Liliental-Weber *Applied Physics Letters* **86**(5): 051902 (2005).

[68] K. Szot, W. Speier, G. Bihlmayer, R. Waser *Nature Materials* **5**: 312 (2006).

[69] A. Defrain *Journal De Chimie Physique Et De Physico-Chimie Biologique* **74**(7-8): 851 (1977).

[70] L. Bosio *Journal of Chemical Physics* **68**(3): 1221 (1978).

[71] R. Kofman, P. Cheyssac, and J.T. Richard, *Physical Review B* **16**: 5216 (1977).

Chapter 2

Controlling light with light via structural transformations in gallium nanoparticle films

2.1 Synopsis

Light-induced structural transformations in gallium nanoparticles grown from atomic beam at the tip of an optical fibre have been studied using low-power diode lasers operating at telecommunication wavelengths. The study, in transmission and reflection, of the nonlinear response characteristics of the nanoparticles indicates the occurrence of both solid-solid and solid-liquid transitions. The megahertz dynamics of light-by-light control in the particle film provide an insight into the kinetics of structural transformations in nanoparticles and are consistent with an effective medium model for the optical properties of closely packed nanoparticle films.

In Section 2.3 the growth of gallium nanoparticle films is described in detail: the ultra high vacuum (UHV) system that serves as a base for the experiments, the optical setup necessary for the light-assisted deposition, and the actual deposition process are presented. Then, in Section 2.4 the temperature and power dependences of the transmission and reflection properties of gallium nanoparticle films are discussed. The high-frequency response characteristics of the gallium films are analyzed in Section 2.5, and in Section 2.6 the study of second harmonic generation in a gallium nanoparticles film is described.

2.2 Introduction

The growing interest in materials for highly integrated photonic devices has fueled the search for ways to control light with light in a nanoscale layer of material. Obtaining significant changes in the intensity or in the phase of a probe signal with a pump beam in such a small region, preferably at reduced power levels and at high speeds is no simple task. In this respect, nanoparticles have huge potential to provide an answer to those problems due to the modifications that occur in the properties of materials when they are confined in an extremely small three dimensional region. In fact, the remarkable properties of nanoparticles may provide solutions for a wide range of fields such as spectroscopy [1], photodetection [2], selective catalysis [3], manipulation of light waves through the control of surface plasmons oscillations [4], and data storage [5]. Nanoparticle investigation is thus an extremely interesting and active field of research.

The linear and nonlinear optical properties of clusters and nanoparticles have been studied extensively [6], with special attention being given to the dynamics of ultra fast laser excitation [7-10]. Nanoparticles and clusters are very interesting media for nonlinear studies, as their strong local field enhancement at the surface [11], normally leads to a strong enhancement of second-harmonic conversion efficiency [12, 13]. Furthermore, even if the nanoparticle material is centrosymmetric, second-harmonic generation (SHG) is still supported, because the inversion symmetry is locally broken at the interface. SHG from films of metallic nanoparticles has also be shown to allow for the determination of the nanoparticle size distribution [14]. This last point is extremely important, because nanoparticle properties are extremely sensitive to size and shape changes [15-17] and this imposes significant demands on manufacturing processes. In fact, many different methods have been proposed to produce nanoparticles, such as patterning and etching [18], lithography [19], chemical synthesis leading to colloidal solutions [20] and evaporation-condensation in ultra high vacuum [21-23]. Various self-assembly techniques [2, 24, 25] have been given particular attention, because of their potential to provide simpler and cheaper production processes. However, these methods suffer from the problem that they normally produce nanoparticles with a wide range of sizes. This causes difficulties not only for the study of the size-dependent effects, but more importantly it raises serious difficulties in applications that require

particles with a very specific size. Some of the proposed solutions to this problem involve the use of high-power lasers to manipulate the nanoparticles' shapes and sizes distribution [26-31]. Recently however, it has been shown that using lower power lasers during slow atomic beam deposition in UHV leads to the creation of particle films with a relatively narrow size distribution [32]. The material used in these last experiments was gallium.

Prior to these experiments, gallium had already been found to exhibit very interesting optical properties. For example, gallium-dielectric interfaces show a strong optical nonlinearity based on a reversible light-induced phase transformation in nanoscale layers of material [33-34]. The importance of this effect for practical applications was also proved with the demonstration of cross-wavelength optical switching [35], photoelectric light detection [36], and passive Q-switching [37]. Following this work, a similar transition-based nonlinearity was observed in gallium nanoparticles [38-39], indicating their potential to act as active elements in low energy nanophotonic and plasmonic devices. The conventional optical nonlinearities of gallium nanoparticles have also been studied. For example, second-harmonic generation by gallium nanoparticles embedded in a SiO_2 matrix has previously been analysed as a function of particle radius and temperature [40].

In this Chapter, the experimental study of the reflective and transmissive nonlinear response of a gallium nanoparticle film to low-power near-infrared optical excitation modulated at frequencies up to 1 MHz is described. Furthermore, second-harmonic generation by a free-standing film grown at the tip of an optical fibre is compared with previous studies of embedded particles [40]. The characteristics of the transition-based response observed are consistent with an effective medium model for the optical properties of closely packed nanoparticle films [41], are functions of the particles' size distribution, and indicate that the particles undergo both solid-solid and solid-liquid transitions.

2.3 Light-controlled growth of gallium nanoparticles

The gallium nanoparticle films used in this work were prepared by the light-assisted self-assembly technique [32, 42] in a dedicated UHV system

originally assembled by K.F. MacDonald [43] (pictured in Figure 2.1 and shown schematically in Figure 2.2).

The main chamber was a fourteen-port "spherical square" vacuum chamber from Kimball Physics Inc., with the vacuum created by a turbomolecular pump backed by a rotary pump, in a typical ultra-high vacuum pumping combination. A combined Pirani and ion pressure gauge attached to one of the ports, and capable of measuring pressures in the range from atmospheric to 5×10^{-10} mbar, monitored the pressure in the chamber. Under normal operation the system achieved a typical pressure of about 10^{-8} mbar.

The atomic beam source was based upon the system developed by Ross [44], with the gallium evaporated from an open top graphite crucible, heated by a pair of molybdenum wire elements wrapped around the base of the crucible and near the nozzle. Two chromel-alumel thermocouples monitored the base and nozzle temperatures of the cell. When changes had to be made in the main chamber, a gate valve isolated the gallium source from the atmosphere. On the chamber side of this valve, a 5 mm diaphragm collimated the gallium beam, and a mechanical shutter allowed for the sample exposition to the atomic beam to be easily controlled. In a typical deposition experiment the temperatures at the nozzle and at the base were increased to about 1010 °C and 1000 °C respectively by running ~ 6.8 A and 3.8 A currents from an external power supply through the nozzle and base heating elements. This temperature allows a vapor pressure of about 5×10^{-3} mbar to be achieved [45], giving a deposition rate of $\sim 0.3\,\mathrm{nm.min^{-1}}$ (measured with a quartz crystal microbalance). During the deposition process, the pressure inside the chamber increased to $\sim 5 \times 10^{-6}$ mbar.

The cleaved end of a standard telecommunications optical fibre was chosen as a substrate because fibres are not only vacuum-safe, but also make the coupling of light signals (used to both probe and act on the nanoparticles) simpler. Subsequent manipulation and imaging procedures are also made easy by the use of a fibre substrate and finally, as it is such a widespread technology, costs are minimal. This last point is particularly important in this type of research as it

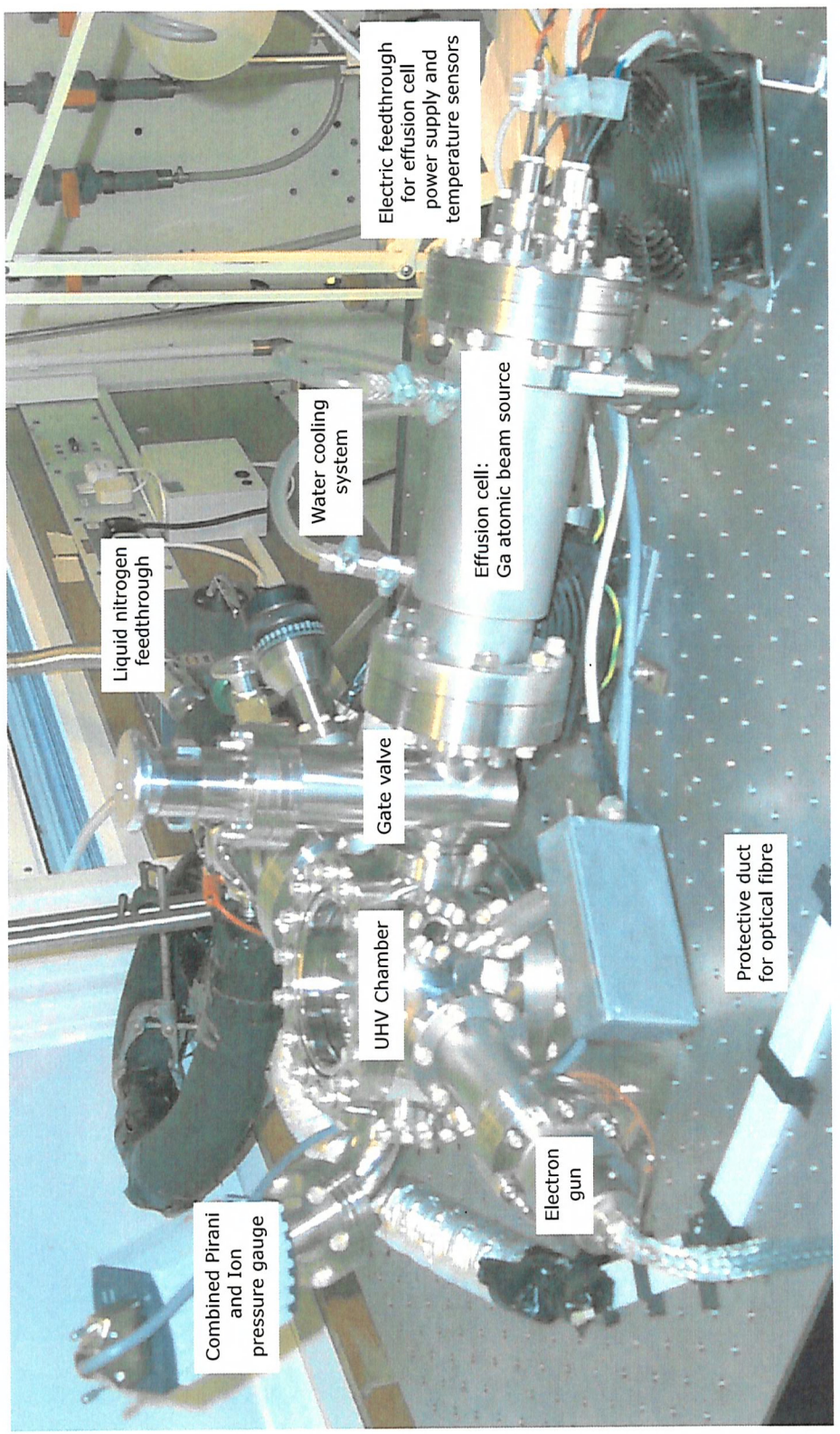

Figure 2.1: The UHV system used for the creation and study of the gallium nanoparticles.

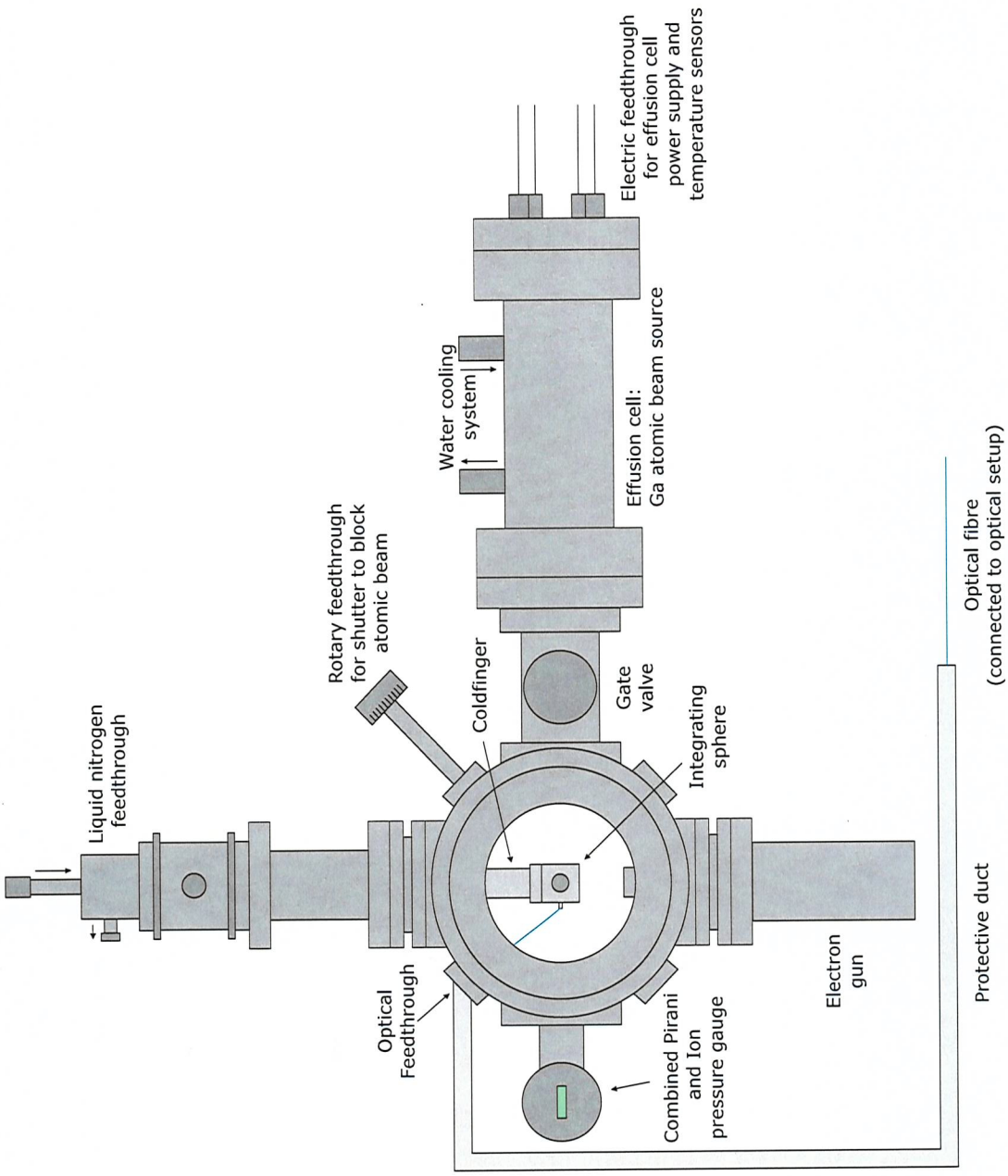

Figure 2.2: Schematic top view of the UHV gallium deposition system.

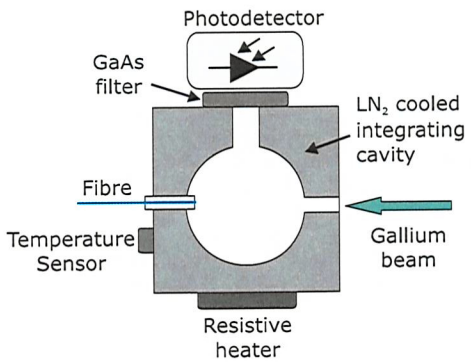

Figure 2.3: Schematic of the integrating sphere used to hold the fibre inside the vacuum chamber. Light collected by the cavity passes through a GaAs filter and is detected by an InGaAs photodiode. A second opening allows gallium to be deposited on the fibre. The temperature can be increased via a resistive heater and is monitored with a silicon diode sensor.

allows for an extensive study to be carried out with limited resources. The fibres used were single-mode at both 1310 nm and 1550 nm, with core and cladding diameters of 9 μm and 125 μm respectively. They were fed into the vacuum chamber via a feedthrough sealed with vacuum-safe glue. The vacuum end of the fibre was cleaved and mounted inside a custom-built integrating sphere (see Figure 2.3). This acted as an optical trap and integrator for light transmitted by the nanoparticle film and scattered within the cavity, helping its detection by a temperature-stabilized InGaAs photodiode (with built-in amplifier) attached to the outer surface of the cavity. For efficient cooling of the tip to occur, the fibre had to extend by less than 1 mm from the two semi-cylindrical aluminium pieces gripping it.

The sample holder was attached to the end of a cold-finger cooled by liquid nitrogen. This, together with a resistive heater, allowed the temperature to be controlled in the range between 80 K and 300 K. A silicon diode sensor, located on the outer surface of the cavity as close as possible to the fibre entry point, measured the sample temperature.

The main components of the optical setup used in the experiment were outside the vacuum chamber. This made it a very versatile and efficient system, because when a new experiment was devised it could be put into practice quickly without breaking the vacuum in the chamber.

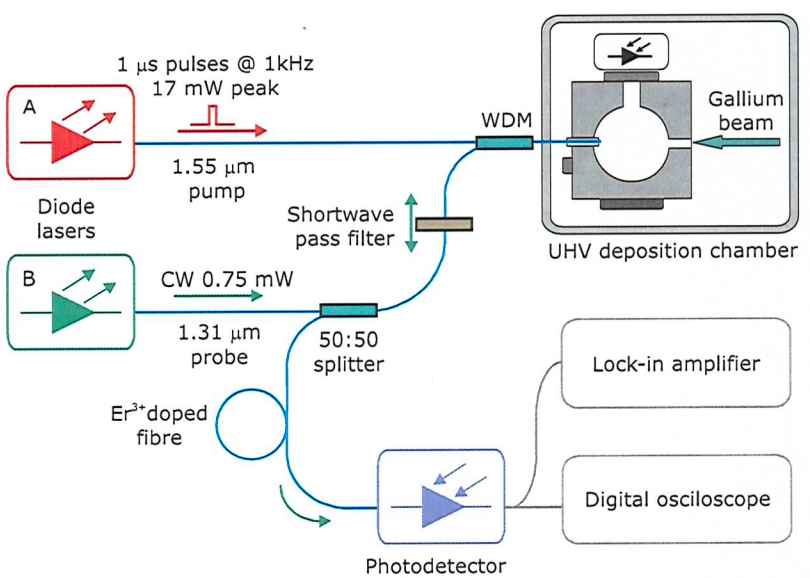

Figure 2.4: Optical setup for the light-assisted deposition of gallium nanoparticle films and simultaneous interrogation of their optical properties. The WDM (Wavelength-Division Multiplexer) combines/splits signals at different wavelengths, while the shortwave-pass filter and the erbium-doped fibre stop reflected pump light from reaching the detector. The reflected probe signal is recorded with an oscilloscope and a lock-in amplifier.

The optical setup used for deposition is presented schematically in Figure 2.4. A continuous wave diode laser operating at 1310 nm, with a power of 0.75 mW, probed the fibre tip's reflectivity. A second diode laser, operating at 1550 nm and producing 1 μs pulses with a peak power of 17 mW and a repetition rate of 1 kHz was also used. This second laser was the main element of the light-assisted self-assembly technique [32] used to prepare the nanoparticle films. Two nonthermal growth control mechanisms, light-enhanced desorption, and light-suppressed adsorption, work together to narrow the size distribution of the particle film during the growth process [42].

A low-noise DC-coupled photodetector with a bandwidth of 125 MHz collected the reflected 1310 nm light, while the 1550 nm component was blocked by a combination of a shortwave-pass filter and a length of erbium-doped fibre. The detected signal was recorded with a lock-in amplifier and a digital oscilloscope connected to a computer and controlled by purpose-written HP-VEE (Hewlett-Packard Visual Engineering Environment) software.

Gallium nanoparticle films were created by taking the following steps :

1. The fibre end was cleaved and attached to the integrating sphere mount.
2. The chamber was closed and pumped down to $\sim 10^{-8}$ mbar.
3. The fibre end was cooled to ~ 80 K.
4. The fibre was exposed to the gallium atomic beam source for ~ 90 min.
5. The fibre was returned to room temperature.

During the gallium source exposure period, the reflectivity changed from 3.3 % (a value used for calibration purposes and assumed to be the reflectivity of a clean fibre end in vacuum) to about 7.0 % (see Figure 2.5), indicating the deposition of gallium on the end of the fibre. To reveal the structure of the film and the size of the particles present, the fibre was removed from the chamber and imaged in a scanning electron microscope. The nanoparticles on the core of the fibre are closely packed with a typical average diameter of ~ 50 nm (see Figure 2.6).

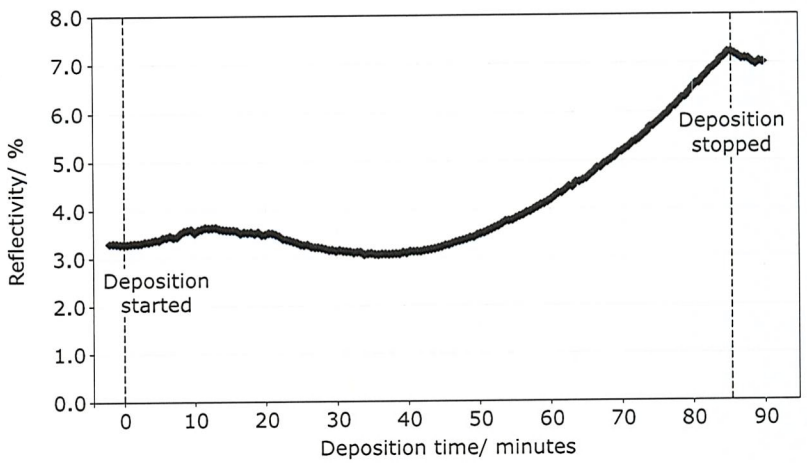

Figure 2.5: Reflectivity as a function of time for a ninety minute period of gallium deposition at a rate of $\sim 0.3\,\mathrm{nm.min^{-1}}$ on a fibre cooled to $\sim 80\,\mathrm{K}$ under a $\sim 10^{-6}\,\mathrm{mbar}$ vacuum.

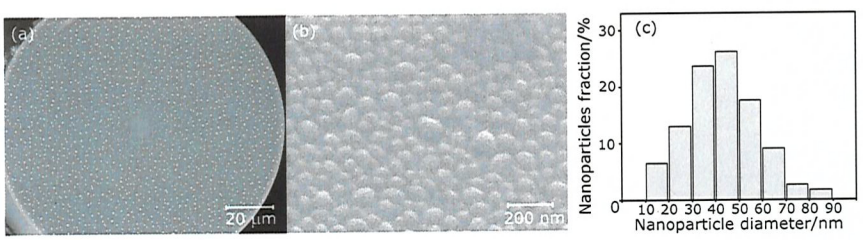

Figure 2.6: (a) SEM image of the end face of an optical fibre after light-assisted gallium deposition. Note the clear difference between the core area where light was present and the area around the core. (b) SEM image of the core region of the optical fibre. (c) Nanoparticle size distribution from (b) obtained by Andrey Denisyuk and shown here for illustrative purposes. The nanoparticles have an average diameter of $\sim 50\,\mathrm{nm}$.

Once this relation between the change in reflectivity and the formation of a nanoparticle film was established, the samples were kept under vacuum after deposition and a more detailed study of their optical properties was performed, as described in the next section.

2.4 Pump-probe study of optical transmission and reflection properties of gallium nanoparticle films

Previous work [38, 46] has illustrated that reflective pump-probe techniques are extremely powerful tools for the study of nanoparticle films, providing information not only about the optical properties of the particles, but also about their phase constitution and transition processes. This section describes how this very useful technique can be expanded, by extending it to the transmission mode of detection, while the next section will focus on measuring the response in reflection for high pump modulation frequencies.

In the first set of experiments, the reflectivity and transmission of the nanoparticle film were probed with the fibre-optic arrangement shown in Figure 2.7, using a low power (0.48 mW) continuous wave 1550 nm diode laser. A second diode laser operating at 980 nm acted as a pump laser, inducing structural changes in the nanoparticles. It was modulated at 234 Hz (square wave, 50 % duty cycle) with a peak power of up to 2.8 mW. The low modulation frequency was necessary because of the limited bandwidth of the transmission detector.

The magnitude of pump-induced changes in reflectivity and transmission were recorded by using digital lock-in amplifiers to detect variations in the 1550 nm probe signals at the pump modulation frequency. The reflected pump light was blocked by a wavelength-division multiplexer and a cut-off filter in the fibre-optic arrangement outside the vacuum chamber. Inside the chamber, the transmitted light was collected by a detector situated on top of the integrating sphere (see Figure 2.3 in Section 2.3). The light integrated by the cavity passed through a semiconductor filter that prevented the majority of transmitted pump light from reaching the detector. However it was found that leakage from the pump was still present in the detected signal, so a computer controlled optical shutter was placed in the probe path (outside the chamber), so that the genuine transmitted signal level could be determined by comparing the levels recorded in the presence and absence of the probe beam.

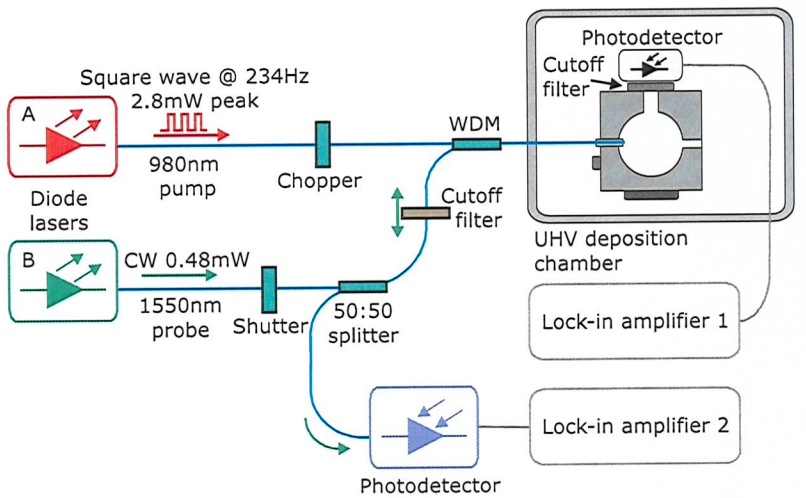

Figure 2.7: Optical setup for pump-probe experiments on gallium nanoparticles' films. The induced change caused by a pump laser is measured on transmission and reflection with the help of two lock-in amplifiers. The pump signal is almost completely prevented from reaching the detectors by GaAs filters, however an additional computer controlled chopper was included to solve pump leakage problems on the transmission detector.

Using this setup, pump-induced changes in the reflection and transmission of the nanoparticle film were recorded as a function of temperature at a range of pump power levels. Any changes induced by the presence of the continuous probe beam were ignored because this study was only concerned with the existence and characteristic features of an effect, rather than in its absolute magnitude.

A representative data set is shown in Figure 2.8. The main features of these graphs are the positive peaks detected in the increasing temperature sections of both the reflection and transmission signals. It has been shown previously that such peaks in the reflective response of gallium (bulk or nanoparticle) are associated with transitions between phases having different optical properties [47]. For example, a transition between the stable bulk solid phase α-gallium and liquid gallium would generate a positive peak in the pump-probe signal because liquid gallium is considerably more metallic than α-gallium [48, 49]. In the confined geometry of a nanoparticle however, the metastable phases β-, γ-, δ-, and ϵ-gallium, which have optical properties between those of the liquid and the α-phases [49], exist in preference to the α-form [50]. The detected peaks must relate to transitions between some of these phases and ultimately (at high temperature) the liquid state.

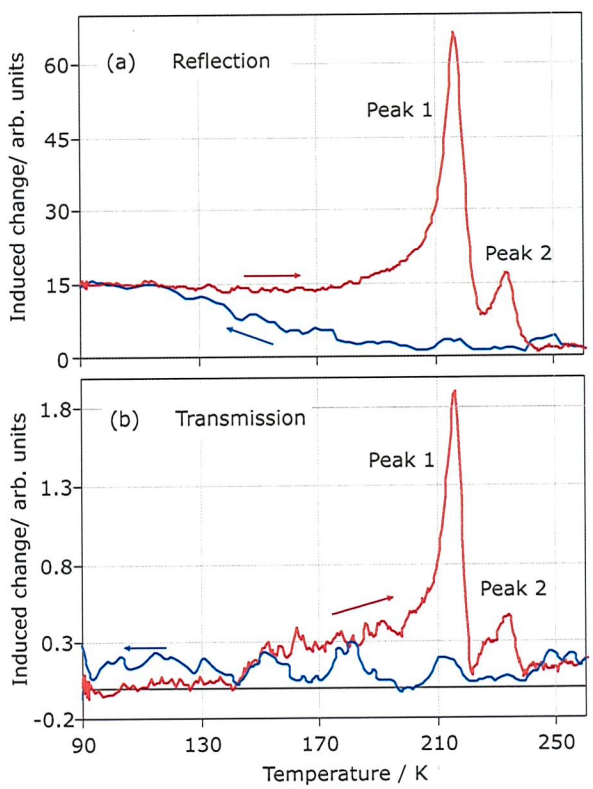

Figure 2.8: Magnitude of pump-induced changes (980 nm pump peak power = 1.4 mW) in (a) the reflection and (b) the transmission of probe light (1550 nm cw probe power = 0.48 mW) by a gallium nanoparticle film as a function of temperature. The red curves show the response for the heating part of the cycle, while the blue curves illustrate the cooling part.

The presence of two peaks indicates that two structural phase transitions occur, but there are two scenarios in which this is possible. In the first, the nanoparticles undergo a sequential transition from one solid phase to another and then from that phase to the liquid, whereas in the second two solid phases coexist at low temperatures and undergo separate parallel transitions to the liquid state at different temperatures.

The height, position, and width of the peaks shown in Figure 2.8 are functions of pump power. This power dependence was analyzed to try to identify the phases involved. The results of this study are shown in Figure 2.9. As the heights of the transmission and reflection peaks remain in constant proportion across the range of pump powers used, the corresponding results were scaled for presentation so that a single trend line could be drawn.

The height of the peaks increases with power, but the increase is more rapid at low powers. This is consistent with the idea that transitions begin at the particles' surface and propagate inwards to a depth determined by the temperature and the level of external excitation (see Section 1.4 of Chapter 1). In fact, the optical properties of gallium nanoparticles are essentially determined by the nature of the material within a few nanometers of the surface. Indeed, as was discussed in Section 1.3 of Chapter 1, effective-medium modeling of a gallium nanoparticle film on silica [36] indicates that a liquid layer just 5 nm thick on the surface of 50 nm solid particles produces $\sim 75\,\%$ of the maximum possible change in the reflectivity and transmission of the film. This model also predicts dependences of induced reflectivity and transmission change on surface layer thickness (see Figure 1.6) similar to the experimental plot of induced change against pump power shown in Figure 2.9(a). Assuming that a structural transition occurs in a volume of gallium directly proportional to the pump power applied, this similarity can be expected, as the thickness of the surface layer is (for thicknesses up to 70 % of the particle radius) almost directly proportional to pump power (see inset to Figure 1.6).

Figure 2.9(b) shows how the peak positions (which correspond to the phase transition temperatures) depend linearly on pump power. Extrapolating to zero-pump the positions $T_1 = 229\,\mathrm{K}$ and $T_2 = 244\,\mathrm{K}$ are obtained. A similar plot of peak position against probe power reveals that the probe-induced

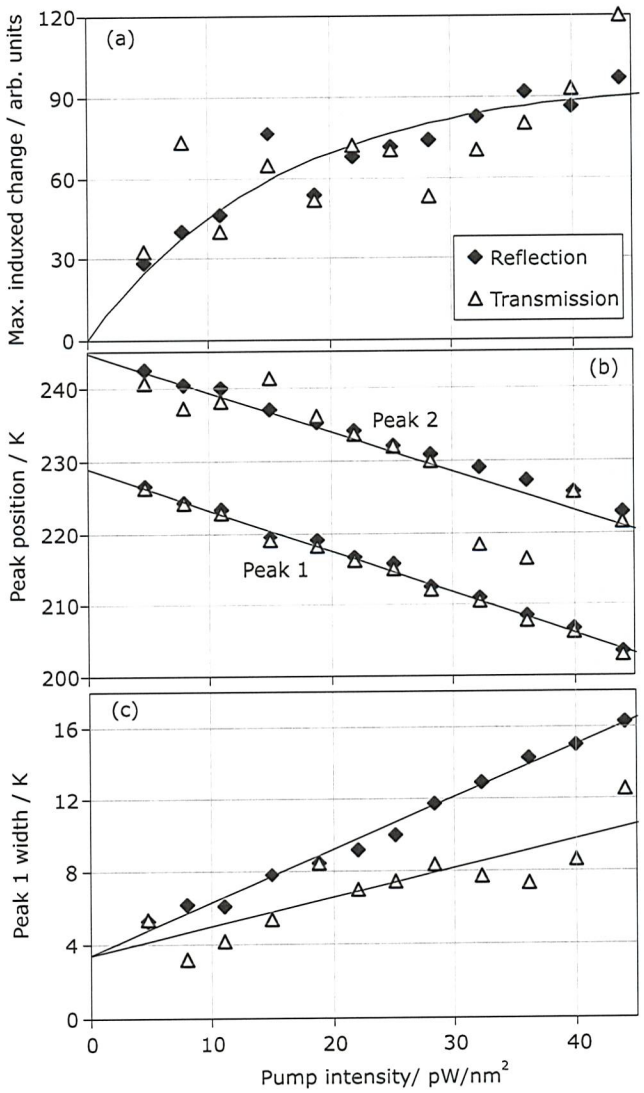

Figure 2.9: Characteristics of the reflection and transmission response peaks: Dependence on pump intensity of (a) the maximum pump-induced changes, i.e., the height of peak 1 (note that the transmission data is scaled to allow the fitting of a single trend-line); (b) the positions of peaks 1 and 2, and (c) the width of peak 1 (full-width half-maximum).

positional shift is $\sim 3\,\mathrm{K}$, so in the absence of any laser radiation, the transitions would occur at $T_1' = 232\,\mathrm{K}$ and $T_2' = 247\,\mathrm{K}$. Furthermore, in nanoparticles, the transition temperature is known to be a function of particle size: The melting point decreases with particle size, because smaller particles have a higher proportion of loosely bound surface atoms, according (for spherical particles) to the Gibbs-Thompson equation:

$$4\Delta T \sigma \nu_0 T_m / Ld = k/d$$

Where d is the particle diameter, σ is the surface tension of the solid, L is the latent heat of fusion, T_m is the bulk melting temperature, and ν_0 is the molar volume of the solid. The constant k is experimentally found to be ~ 600 for β-gallium nanoparticles in an opal matrix [51] and the available data [52] indicate that the other crystalline phases should have similar values. Thus, in gallium nanoparticles with a diameter of 50 nm this effect will suppress melting points by $\sim 12\,\mathrm{K}$. This means that the transitions observed would occur in bulk gallium at $T_1'' = 244\,\mathrm{K}$ and $T_2'' = 259\,\mathrm{K}$.

The melting points of gallium's phases are $T_\beta = 257\,\mathrm{K}$, $T_\delta = 254\,\mathrm{K}$, $T_\epsilon = 245\,\mathrm{K}$ and $T_\gamma = 238\,\mathrm{K}$ [52]. As these values are very close together, it is difficult to associate the response peaks with specific transitions, but one may reasonably conclude that the second peak is associated with the melting of β-gallium. Further evidence to strength this claim comes from studies of gallium micro- and nanoparticles that have found β-gallium to be the most stable solid form of the metal after the bulk α- phase [50, 52]. The 2 K difference between T_β and T_2'' could be attributed to an instrumental discrepancy between the measured temperature and the actual fibre-tip temperature or to an error in the assumed particle diameter.

With this in mind, if a 2 K downward correction is applied to T_1'', it falls roughly halfway between T_ϵ and T_γ. However, it should be noted that if the first peak corresponds to a solid-solid transition there is no reason why its (bulk equivalent) position should match any of the known melting points. The fact that the γ-phase is the next most stable after β-gallium (with ϵ-gallium being the least stable of the four crystalline structures available [50, 52]), suggests that it is the most likely to constitute the low-temperature phase of the

nanoparticles. However, in the sequential solid-solid-liquid scenario this would imply that peak 1 is associated with a forbidden γ-to-β transition (a free-energy analysis indicates that the only allowed sequence of solid-solid transitions is $\gamma \rightarrow \epsilon \rightarrow \delta \rightarrow \beta$ [52]). There is of course the possibility that given the close energetic spacing of the phases (e.g., the difference between the δ and β forms is only 0.3 meV/atom), that all of these transitions are present but not resolved as individual peaks in the current experiment. This is in fact the most likely situation: In Chapter 3 it will be shown that by studying a single gallium particle, the resolution can be improved to allow peaks corresponding to other transitions to be observed.

Finally, the peak width W depends linearly on pump power as shown in Figure 2.9(c) (the effect of the probe is negligible). The transmission and reflection peaks both have a zero-excitation width W_0 of ~ 3.3 K. This width is determined by a combination of the peak width for a single 'average' particle and the range of transition temperatures presented by particles of different sizes. Experiments described in Chapter 3 show that in the low-power limit, the peak width for a single particle is a small fraction of a degree, and so it may be concluded that the 3 K width seen here is predominantly a reflection of the particles' size distribution.

2.5 Light-induced high frequency reflectivity changes in gallium nanoparticle films

In a separate experiment, the high-frequency response characteristics of another gallium nanoparticle film were studied. These measurements were conducted only in reflection because of the limited bandwidth of the transmission detector. A 1550 nm distributed-feedback (DFB) laser and an electrooptic modulator were used to generate 100 ns pump pulses with a peak power of ~ 6 mW at a frequency of 1 MHz. A 1310 nm diode laser (~ 0.5 mW cw) was used as the probe source.

The temperature dependence of the magnitude of the pump-induced reflectivity change (upper part of Figure 2.10) was somewhat different from that detected at lower frequencies. However, two peaks corresponding to two phase transitions are still present. More importantly, at this higher modulation frequency, the

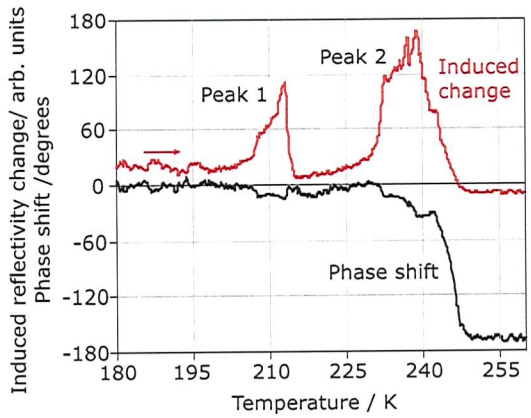

Figure 2.10: Red trace: Temperature dependence of the magnitude of the change induced in the reflectivity of a gallium nanoparticle film by 1550 nm, 100 ns pump pulses with a peak power of 6 mW and repetition rate of 1 MHz (1310 μm cw probe power < 0.5 mW). Black trace: The corresponding temporal phase shift between the pump and reflected probe modulations. Note that the temperature scale has been adjusted (on the basis of average pump power) to compensate for additional pump induced heating of the film in this experiment as compared to those conducted using the 234 Hz chopped pump laser.

temporal phase data obtained from the lock-in amplifier (lower part of Figure 2.10) provides some insight into the dynamics of the excitation-induced transitions in the nanoparticles. These temporal phase data are related to the retardation between pump and probe modulations (see Appendix A).

The fact that there is a large phase shift associated with peak 2 but almost none associated with peak 1 indicates that the dynamics of the corresponding structural transitions are different. From entropic arguments [53] it follows that a solid-to-liquid (i.e., order-to-disorder) transition should occur faster than liquid-to-solid (disorder-to-order) and solid-to-solid (order-to-order) transitions. The increase in pump-probe retardation indicated by the phase shift at peak 2 can then be assumed to relate to the time taken for the liquid to recrystallize following withdrawal of the optical excitation. This asymmetry in the dynamics of the melting and freezing processes has been observed previously in silicon and is understood to result from the fact that the speed of the melting process is only collision limited while that of the freezing process is entropy limited [53].

In contrast, the absence of a significant phase shift around peak 1 indicates that both the forward and reverse transition times are small compared to the period

of the excitation cycle (1 μs). This lends support to the hypothesis that it corresponds to a transition between two of gallium's crystalline forms, because as previously described one may reasonably expect that the response and relaxation dynamics of such a transition (a solid-to-solid transformation in both directions with only a small entropic difference between the states) would be similar to each other and faster than those of a liquid-to-solid transition.

Thus, the results of this high-frequency experiment support the idea that the transitions in gallium nanoparticle films occur as a sequential transition from one solid phase to another and then from that phase to the liquid.

2.6 Second-Harmonic generation in gallium nanoparticle films

The study of gallium nanoparticles' optical properties described in the previous sections was centered around optical nonlinearities based on phase change mechanisms. However, an alternative way to probe the properties of a material is to study their conventional nonlinear optical properties. In this Section, the use of second harmonic generation to study the optical characteristics of gallium nanoparticle films is discussed.

For this experiment, gallium nanoparticles were grown to an average diameter of $\sim$ 80 nm at the end of an optical fibre using the light-assisted deposition technique described previously (see Section 2.3). The nanoparticles were then optically excited using a 250 fs pulsed laser with a wavelength of 1064 nm and a repetition rate of 50 MHz. The transmitted second harmonic signal from the nanoparticles was measured through a cut-off filter using a photo-multiplier (see Figure 2.11). In order to reduce problems caused by fluctuations in pump laser power, it was modulated with a chopper, and a beamsplitter was used to direct part of the beam to a Potassium Titanium Oxide Phosphate ($KTiOPO_4$), or KTP crystal. A lock-in amplifier was used to record the second-harmonic signal generated by the crystal thus providing a normalization level to enable fluctuations in laser power to be accounted for in the second harmonic signal from the nanoparticles.

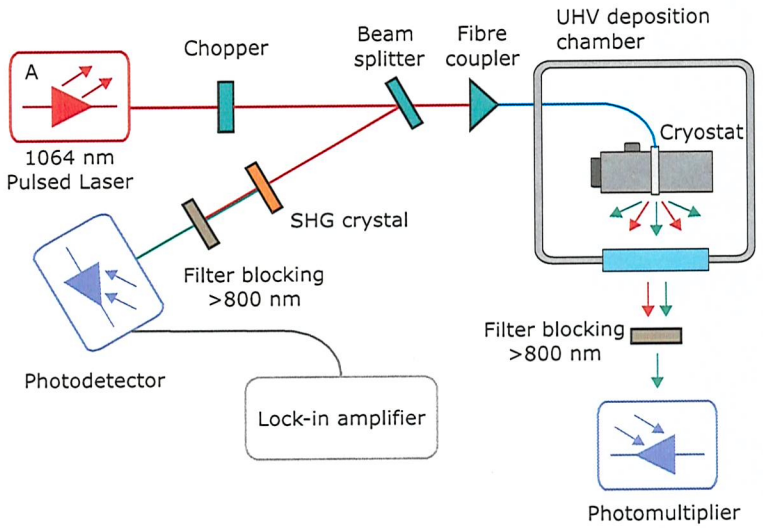

Figure 2.11: Optical setup for probing gallium nanoparticle films via second-harmonic generation. A 1064 nm femtosecond pulsed pump laser excites the nanoparticle film and the generated second-harmonic is detected in transmission by a photomultiplier. A beamsplitter directs part of the pump beam to a KTP crystal which generates a transmitted second-harmonic that is used to to monitor power fluctuations in the pump laser and improve the signal-to-noise ratio in the experiment.

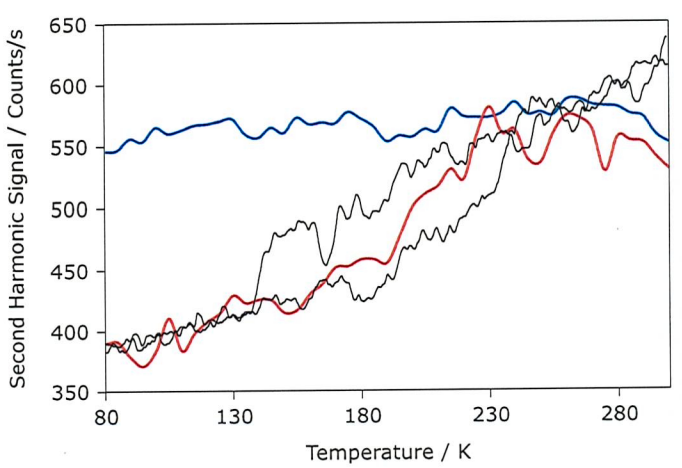

Figure 2.12: Temperature scans showing the second harmonic signal at a wavelength of 532 nm, collected in transmission through the nanoparticle film during heating (red curve) and cooling (blue curve). The black curves show the scaled second harmonic signal of gallium nanoparticles embedded in a SiO_x matrix as reported in [40].

Figure 2.12 shows the detected second-harmonic signal as a function of nanoparticle film temperature. The signal clearly increases with increasing temperature. The ratio between the high- and low-temperature signal levels is $I_{2\omega}^{High}/I_{2\omega}^{\mathrm{Low}} = 1.5$. This should be compared with the undetectable change in linear transmission of the film at the second harmonic wavelength: A 532 nm cw beam was coupled into the fibre and the power adjusted to a level that produced the same number of low temperature counts as detected in the second harmonic generation experiment. A temperature scan was then performed, but it was found that any changes in the linear transmission signal were below the noise level of the experiment. The second harmonic generation properties of a gallium nanoparticle film are clearly more sensitive to the phase of the particles than the linear transmission properties.

The ratio between the high- and low-temperature levels reported here is consistent with previous reports of second harmonic generation in gallium nanoparticles embedded in a SiO_x matrix [40]. However, the present study reveals a much wider hysteresis: The nanoparticles remain in the higher energy state even as the sample is cooled down to the low temperature starting point of the scan (80 K). In order to convert the nanoparticles to the ground state the pump laser must be switched off so that the nanoparticles are further cooled. When the laser is turned back on the low-temperature signal is recovered and subsequent scans reproduce this behaviour. This gives a lower limit for the width of the hysteresis of $\sim$ 150 K, as compared to the previously reported value of $\sim$ 95 K. The wider hysteresis in the present experiments could be related to the fact that the gallium nanoparticles are more densely packed and are only supported on a silica substrate in vacuum, with only a limited contact area with the fibre substrate, whereas the results reported previously relate to nanoparticles fully embedded in a silica matrix.

The second harmonic generation process is a second-order process and so the dependence of the second harmonic signal on incident intensity should be quadratic [54]. This is indeed the case: the second harmonic signal for the nanoparticle film clearly shows a quadratic dependence on the intensity of the incident light, both at low ($T = 80$ K) and high ($T = 300$ K) temperatures (see Figure 2.13) .

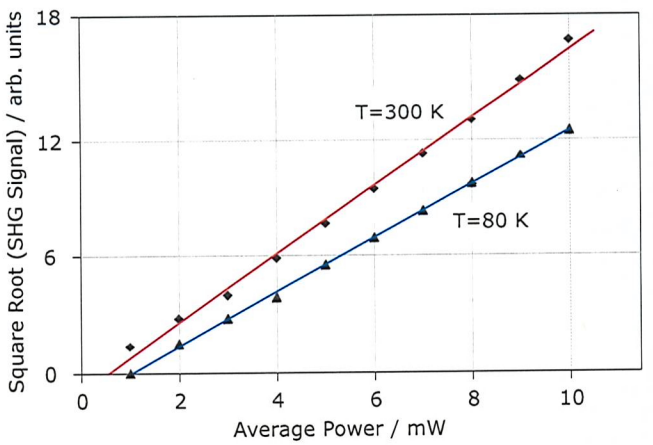

Figure 2.13: Square root of the transmitted second harmonic signal as function of optical power of the exciting beam, measured at temperatures of $T = 80\,\mathrm{K}$ and $T = 300\,\mathrm{K}$. The lines show fits of linear functions to the experimental data, indicating the expected quadratic dependence of the second harmonic generation signal on the incident optical intensity.

As discussed in Section 2.4, solid gallium nanoparticles are most likely to be found in the β phase. This has a monoclinic crystallographic structure and belongs to a centrosymmetric point-symmetry group. For such structures the second-order nonlinear susceptibility vanishes, so any change in second harmonic signal associated with the phase transition to the liquid state (which is isotropic and therefore also has a zero second-order nonlinear susceptibility) is entirely due to interface effects resulting from changes in the dielectric coefficient and possibly shape changes. One can try to compare the experimental results with theory by considering changes in the dielectric properties as the particles change from the $\beta-$gallium phase to the liquid state. Mie scattering theory has been successfully applied to predict the reflection and transmission properties of a sparsely distributed film of spherical metallic nanoparticles [40, 55]. However, in the present experiment the nanoparticles are densely packed and, as will be discussed in the next section, in order to properly assess the local field-enhancement factors a modified theory must be applied [41, 56]. Important parameters in this model are the ratio between the mean particle separation and the diameter of the particles, and obviously the dielectric properties of the nanoparticles and of the substrate on which they are deposited.

The field enhancement factor, $q(\omega) = E_{\mathrm{loc}}(\omega)/E_{\mathrm{ext}}(\omega)$, relating the externally applied electric field $E_{\mathrm{ext}}(\omega)$ to the local field $E_{\mathrm{loc}}(\omega)$ plays a fundamental role

in the calculation of the expected second harmonic signal. The intensity of the second harmonic signal is related to the incident intensity I_ω by $I_{2\omega} \sim q^2(\omega)q(2\omega)I_\omega^2$.

Hence, at a constant intensity the change in the second harmonic signal as the medium undergoes a solid-to-liquid phase transition is:

$$I_{2\omega}^{(\mathrm{liq})}/I_{2\omega}^{(\mathrm{sol})} = \frac{q_{\mathrm{liq}}^2(\omega)q_{\mathrm{liq}}(2\omega)}{q_{sol}^2(\omega)q_{sol}(2\omega)}$$

By applying the modified Yamaguchi model [41] to calculate the local field enhancement factors for gallium nanoparticles (80 nm wide, 30 nm high, and 95 nm separation) on a silica substrate in vacuum, a theoretical prediction for the ratio $I_{2\omega}^{(\mathrm{liq})}/I_{2\omega}^{(\mathrm{sol})}$ can be obtained. Taking the high-energy phase to be liquid gallium ($\epsilon(1064\,\mathrm{nm}) = -84.94 + 68.02\mathrm{i}$) and the low-energy phase to have properties between the α and the liquid phases ($\epsilon(1064\,\mathrm{nm}) = -36.96 + 38.30i$) one obtains $I_{2\omega}^{(\mathrm{liq})}/I_{2\omega}^{(\mathrm{sol})} = 1.72$. This should be compared with the experimental value of 1.5 and with the corresponding theoretical ratio for the linear transmission of only $I_\omega^{(\mathrm{liq})}/I_\omega^{(\mathrm{sol})} = 1.17$. The increase in second harmonic signal is thus found theoretically to be significantly larger than the increase in the transmission of the nanoparticle film, in agreement with the experimental observations. Although this seems to indicate that second harmonic generation would be ideally suited to the study of the optical properties of gallium nanoparticles and even to potential applications, in practice the problems associated with higher intensity beams and with higher noise levels, mean that the pump-probe setup discussed in Section 2.4 is still the most viable way to conduct these studies.

2.7 Summary and conclusions

An optical system was developed to study the properties of gallium nanoparticles grown on the end of an optical fibre by light-assisted deposition. The data obtained in both transmission and reflection show that light-induced surface-driven structural transitions can be used to reversibly control the optical properties of metallic nanoparticles and thereby provide a paradigm for controlling light with light.

In particular, it was demonstrated that gallium nanoparticles exhibit reflective and transmissive transition-based nonlinear responses to low-power near-infrared excitation modulated at frequencies up to 1 MHz. It was also shown that using a femtosecond pulsed laser, second harmonic generation in the nanoparticle film was possible and a larger contrast between the optical properties of the low and high temperature phases was obtained as compared to linear transmission at the same wavelength.

The results indicate that the particles pass through at least two of gallium's metastable crystalline phases and the liquid phase as their temperature is cycled across the range from 80 to 300 K. The observed excitation-induced increases in the transmission and reflectivity of a gallium nanoparticle film are consistent with an effective medium model for the optical properties of closely packed nanoparticle films, and the characteristics of the nonlinear response peaks are functions of the particles' size distribution.

The response dynamics imply that the kinetics of solid-solid transitions are faster and more symmetrical than those of the solid-liquid transition, where the recrystallization time is much longer than the melting time.

The low energy required to achieve this kind of transition based nonlinearity in nanoparticles suggests that they could be used as active elements in nanophotonic devices operating at extremely low power levels. For example, they may be incorporated into particle-chain waveguides [64], used as scattering centers in photonic-bandgap or plasmon-polariton waveguides, employed as optical circuit elements [65], placed in optical nanoapertures (see Chapter 3), or act as all-optical memory elements (see Chapter 4).

2.8 References

[1] S. M. Nie, and S. R. Emery *Science* **275**: 1102 (1997).

[2] H. R. Stuart, and D. G. Hall *Applied Physics Letters* **69**(16): 2327 (1996).

[3] M. Haruta *Catalysis Today* **36**(1): 153 (1997).

[4] J. R. Krenn, M. Salerno, N. Felidj, B. Lamprecht, G. Schider, A. Leitner, F. R. Aussenegg, J. C. Weeber, A. Dereux, and J. P. Goudonnet *Journal of Microscopy* **202**(1): 122 (2001).

[5] H. Ditlbacher, J. R. Krenn, B. Lamprecht, A. Leitner, and F. R. Aussenegg *Optics Letters* **25**(8): 563 (2000).

[6] U. Kreibig, and M. Vollmer *Optical Properties of Metal Clusters* Springer-Verlag, Berlin (1995).

[7] K. Puech, and W. J. Blau *Journal of Nanoparticle Research* **3**(1): 13 (2001).

[8] M. Nisoli, S. Stagira, S. De Silvestri, A. Stella, P. Tognini, P. Cheyssac, and R. Kofman *Physical Review Letters* **78**(18): 3575 (1997).

[9] F. Stietz, J. Bosbach, T. Wenzel, T. Vartanyan, A. Goldmann, and F. Trager *Physical Review Letters* **84**(24): 5644 (2000).

[10] M. Perner, S. Gresillon, J. Marz, G. von Plessen, J. Feldmann, J. Porstendorfer, K. J. Berg, and G. Berg. *Physical Review Letters* **85**(4): 792 (2000).

[11] D. Ricard, P. Roussignol, and C. Flytzanis *Optics Letters* **10**(10): 511 (1985).

[12] T. F. Heinz, C. K. Chen, D. Ricard, and Y. R. Shen *Physical Review Letters* **48**(7): 478 (1982).

[13] C. K. Chen, T. F. Heinz, D. Ricard, and Y. R. Shen *Physical Review B* **27**(4): 1965 (1983)

[14] V. M. Akulin, E. Borsella, and A. A. Nesterenko *Physical Review Letters* **73**(9): 1231 (1994).

[15] T. V. Shahbazyan, I. E. Perakis, and J. Y. Bigot *Physical Review Letters* **81**(15): 3120 (1998).

[16] B. Lamprecht, J. R. Krenn, A. Leitner, and F. R. Aussenegg *Physical Review Letters* **83**(21): 4421 (1999).

[17] C. Voisin, D. Christofilos, N. D. Fatti, F. Vallee, B. Prevel, E. Cottancin, J. Lerme, M. Pellarin, and M. Broyer *Physical Review Letters* **85**(10): 2200 (2000).

[18] D. Heitmann, and J. P. Kotthaus *Physics Today* **46**(6): 56 (1993).

[19] P. Grambow, T. Demel, D. Heitmann, M. Kohl, R. Schule, and K. Ploog *Microelectronic Engineering* **9**(1-4): 357 (1989).

[20] V. L. Colvin, A. N. Goldstein, and A. P. Alivisatos *Journal of the American Chemical Society* **114**(13): 5221 (1992).

[21] E. Sondergard, R. Kofman, P. Cheyssac, and A. Stella *Surface Science* **364**(3): 467 (1996).

[22] V. A. Shchukin, and D. Bimberg *Reviews of Modern Physics* **71**(4): 1125 (1999).

[23] H. Brune *Surface Science Reports* **31**(4-6): 121 (1998).

[24] A. Taleb, V. Russier, A. Courty, and M. P. Pileni *Physical Review B* **59**(20): 13350 (1999).

[25] M. M. R. Evans and J. Nogami. *Physical Review B* **59**(11): 7644 (1999).

[26] F. Gonella, G. Mattei, P. Mazzoldi, E. Cattaruzza, G.W. Arnold, G. Battaglin, P. Calvelli, R. Polloni, R. Bertoncello, and R. F. Haglund *Applied Physics Letters* **69**(20): 3101 (1996).

[27] H. Kurita, A. Takami, and S. Koda *Applied Physics Letters* **72**(7): 789 (1998).

[28] S. Y. Park, T. Isobe, M. Senna, R. A. Weeks, and R. A. Zuhr. *Applied Physics Letters* **73**(18): 2687 (1998).

[29] A. L. Stepanov, D. E. Hole, A. A. Bukharaev, P. D. Townsend, and N. I. Nurgazizov *Applied Surface Science* **136**(4): 298 (1998).

[30] J. Bosbach, D. Martin, F. Stietz, T. Wenzel, and F. Trager *Applied Physics Letters* **74**(18): 2605 (1999).

[31] T. Wenzel, J. Bosbach, A. Goldmann, F. Stietz, and F. Trager *Applied Physics B-Lasers and Optics* **69**(5-6): 513 (1999).

[32] K. F. MacDonald, V. A. Fedotov, S. Pochon, K. J. Ross, G. C. Stevens, N. I. Zheludev, W. S. Brocklesby, and V. I. Emel'yanov *Applied Physics Letters* **80**(9): 1643 (2002).

[33] P. J. Bennett, S. Dhanjal, P. Petropoulos, D. J. Richardson, N. I. Zheludev, and V. I. Emel'yanov *Applied Physics Letters* **73**(13): 1787 (1998).

[34] K. F. MacDonald, V. A. Fedotov, N. I. Zheludev, B. V. Zhdanov, and R. J. Knize *Applied Physics Letters* **79**(15): 2375 (2001).

[35] V. Albanis, S. Dhanjal, N. I. Zheludev, P. Petropoulos, and D. J. Richardson *Optics Express* **5**(8): 157 (1999).

[36] V. A. Fedotov, M. Woodford, I. Jean, and N. I. Zheludev *Applied Physics Letters* **80**(7): 1297 (2002).

[37] P. Petropoulos, H. L. Offerhaus, D. J. Richardson, S. Dhanjal, and N. I. Zheludev *Applied Physics Letters* **74**(24): 3619 (1999).

[38] K. F. MacDonald, V. A. Fedotov, and N. I. Zheludev *Applied Physics Letters* **82**(7): 1087 (2003).

[39] S. Pochon, K. F. MacDonald, R. J. Knize, and N. I. Zheludev *Physical Review Letters* **92**(14) (2004).

[40] A. Stella, S. Achilli, M. Allione, A. M. Malvezzi, M. Patrini, and R. Kofman *Microelectronics Journal* **34**: 619 (2003).

[41] V. A. Fedotov, V. I. Emel'yanov, K. F. MacDonald, and N. I. Zheludev *Journal of Optics A-Pure and Applied Optics* **6**(2): 155 (2004).

[42] V. A. Fedotov, K. F. MacDonald, N. I. Zheludev, and V. I. Emel'yanov *Journal of Applied Physics* **93**(6): 3540 (2003).

[43] K.F. MacDonald *Ph.D. thesis* University of Southampton (2002).

[44] K. J. Ross *Vacuum* **44**(8): 863 (1993).

[45] *CRC Handbook of Chemistry and Physics* CRC Press Inc., Boca Raton, 73rd edition edition (1992).

[46] K. F. MacDonald, V. A. Fedotov, S. Pochon, G. Stevens, F. V. Kusmartsev, V. I. Emel'yanov, and N. I. Zheludev *Europhysics Letters* **67**(4): 614 (2004).

[47] K. F. MacDonald, V. A. Fedotov, R. W. Eason, N. I. Zheludev, A. V. Rode, B. Luther-Davies, and V. I. Emel'yanov *Journal of the Optical Society of America B-Optical Physics* **18**(3): 331 (2001).

[48] N. R. Comins *Philosophical Magazine* **25**(4): 817 (1972).

[49] M. Bernasconi, G. L. Chiarotti, and E. Tosatti *Physical Review B* **52**(14): 9988 (1995).

[50] A. Di Cicco *Physical Review Letters* **81**(14): 2942 (1998).

[51] E. V. Charnaya, C. Tien, K. J. Lin, and Y. A. Kumzerov *Journal of Physics-Condensed Matter* **10**(32): 7273 (1998).

[52] A. Defrain *Journal De Chimie Physique Et De Physico-Chimie Biologique* **74**(7-8): 851 (1977).

[53] J. Y. Tsao, M. J. Aziz, M. O. Thompson, and P. S. Peercy *Physical Review Letters* **56**(25): 2712 (1986).

[54] R. W. Boyd *Nonlinear Optics* Academic Press, San Diego (2003).

[55] T. Müller, P. H. Vaccaro, F. Balzer, and H. G. Rubahn *Optics Communications* 135: 103 (1997).

[56] T.Yamaguchi, S. Yoshida, and A. Kinbara *Thin Solid Films* **21**(1): 173 (1974).

[57] R. Garrigos, P. Cheyssac, and R. Kofman *Zeitschrift Fur Physik D-Atoms Molecules and Clusters* **12**(1-4): 497 (1989).

[58] K. F. Peters, Y. W. Chung, and J. B. Cohen *Applied Physics Letters* **71**(16): 2391 (1997).

[59] G. B. Parravicini, A. Stella, P. Tognini, P. G. Merli, A. Migliori, P. Cheyssac, and R. Kofman *Applied Physics Letters* **82**(9): 1461 (2003).

[60] R. S. Berry, and B. M. Smirnov *Journal of Chemical Physics* **113**(2): 728 (2000).

[61] P. Buffat, and J. P. Borel *Physical Review A* **13**(6): 2287 (1976).

[62] A. S. Shirinyan, and M. Wautelet *Nanotechnology* **15**: 1720 (2004).

[63] M. Wautelet *Journal of Physics-Condensed Matter* **16**(12): 163 (2004).

[64] S.A. Maier, P.G. Kik, H.A. Atwater, S. Meltzer, E. Harel, B.E. Koel, A.A.G. Requicha *Nature Materials* **2**(4): 229 (2003).

[65] N. Engheta, A. Salandrino, and A. Alu *Physical Review Letters* **95**(9): 095504 (2005).

Chapter 3

Light-induced structural transformations in a single gallium nanoparticle

3.1 Synopsis

In a single gallium nanoparticle self-assembled from an atomic beam in a nanoaperture at the end of a tapered optical fibre, reversible light-induced reflectivity changes stimulated by optical excitation at nanowatt power levels were observed. These are associated with a sequence of transformations between a number of structural forms with different optical properties. It was also found that the large overcooling present when the particle is excited with a modulated cw pump beam is dramatically reduced when using a nanosecond pulsed laser. The ability to control the optical properties of a single nanoparticle using structural transformations provides a new mechanism for photonic functionality on the nanoscale.

In Section 3.3 the process of growing a single nanoparticle at the end of a tapered optical fibre is described. The results of studies of the optical response of the single nanoparticle to modulated cw excitation are presented in Section 3.4. Finally Section 3.5 describes what happens when this cw excitation is replaced by a nanosecond pulsed pump.

3.2 Introduction

In the previous chapter it was shown that a film of gallium nanoparticles could be used to control light with light at the nanoscale using low powers. The demand for this type of functionality is high as it is expected to play a very significant role in the development of a wide range of nanophotonic devices. So, understanding well the phase transitions behind this type of optical nonlinearity is of crucial importance.

However, there is a significant obstacle to achieving this clearer view of phase transitions in a film of nanoparticles. In nanoparticles, phase transition temperatures and optical absorption cross-sections depend strongly on particle size. If the entire film was made of identical nanoparticles, then there would be no difficulty. Unfortunately, even when the light-assisted deposition process described in Section 2.3 is used, there is still a significant inhomogeneous broadening due to the nanoparticles' size distribution. This increases the width of the signal peaks associated with the transitions and this not only makes it more difficult to identify the exact details of the process, but may even hide certain transitions.

With such techniques as confocal microscopy, optical tweezers, and scanning near-field imaging, it is now possible to detect photoluminescence and Raman spectra and perform sophisticated transient spectroscopic measurements on single nanoparticles [1-4]. This essentially removes the inhomogeneous broadening characteristic of nanoparticle film spectroscopy. Studying transitions in a single nanoparticle, as opposed to a nanoparticle film, should lead to advantages similar to those obtained in the optical spectroscopy of single particles.

From a more practical point of view it would also be a lot more useful (for example in terms of miniaturization potential) if one could control an individual nanoparticle, instead of an entire film of particles. Single particles could then be integrated with other nanostructures and used as individual functional elements.

In this Chapter experimental evidence is presented, indicating a sequence of transformations involving several different structural forms in a single gallium nanoparticle. The results are consistent with the fact that phase transitions in nanovolumes of material are achieved through continuous and reversible

surface-driven coexistences of different forms [5, 6] and demonstrate that such transformations can be stimulated and controlled by extremely low power optical excitation. It has been possible to induce and monitor transitions between phases that differ in free energy by only a fraction of a meV per atom and it has been found that the nanoparticle's response to optical excitation settles within a few tens of microseconds. It has also been observed that while a nanoparticle probed with low intensity modulated cw laser light overcools by more than 90 K before it returns to the low-temperature phase, when the nanoparticle is excited with a higher intensity nanosecond pulsed laser this substantial overcooling can be reduced to less than 5 K.

3.3 Single nanoparticle growth

As described in Chapter 2, using optical fibres as substrates for the growth and monitoring of the optical properties of nanoparticle films is an extremely successfully technique. Therefore, to study the properties of a single nanoparticle, a similar setup was employed. The main change from the previous work was the replacement of the standard telecommunications fibre with a tapered optical fibre normally used in scanning-near field optical microscopy (SNOM). SNOM makes optical imaging systems with resolutions better than the traditional diffraction limit possible, by utilizing a nanoscale opening at the end of a metal-coated tapered optical fibre [7]. Commercially available fibres can have apertures smaller than 100 nm, presenting an ideal site to grow a single nanoparticle and monitor its optical properties. In the experiments described below gold-coated silica single-mode fibres tapered to apertures ranging from 30 to 100 nm produced by Jasco Corporation were used (see Figure 3.1).

As in the case of a particle film, growing the nanoparticle on the end of a fibre allows for the precise coupling to the nanoparticle of optical excitations to stimulate phase transformations, and also for the collection of the probe signal reflected by the nanoparticle, to monitor its state. However, it should be noted that care must be taken when choosing the power level of the lasers. The throughput of a tapered fibre is normally around 1000 to 10000 times smaller than that of a standard fibre, making the signal available for detection much

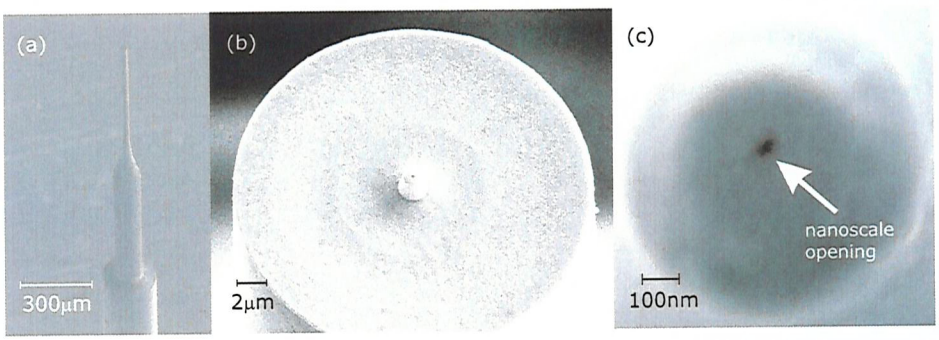

Figure 3.1: Scanning electron microscope images of the Jasco Corporation scanning near field optical microscopy optical fibre probes used in the study of a single gallium nanoparticle. The nanoscale aperture where the nanoparticle is formed can be seen in (c).

smaller for a given laser power. In addition, the available power is concentrated in a much smaller area thus increasing the energy per unit area incident on the gallium, and making it possible to eject any gallium deposited in the aperture by applying too much power. Furthermore the SNOM tips themselves have a damage threshold of only a few mW [8]. All of this means that the detection of simple 'linear' reflectivity changes in the end of the SNOM tip is extremely difficult and is only possible during the process of deposition. However, as the next section will describe, the nonlinear induced reflectivity change signal is strong enough, even at very low powers, to be used as the probing mechanism.

The SNOM fibre tip was attached to a liquid nitrogen cryostat coldfinger at 80 K inside a vacuum chamber evacuated to 10^{-6} mbar. To grow a single nanoparticle, a gallium atomic beam with a mass flux of $f = 0.3$ nm/min was directed at the end of the fibre for between 30 and 60 min (see Figure 3.2). During deposition the other end of the fibre was connected to the optical setup shown in Figure 3.5. The details of this system are described in Section 3.4, but in short it allows for the measurement of the linear reflectivity of the fibre tip as well as the detection of any reflectivity changes induced by a pump laser. During deposition, the accumulation of gallium in the nanoaperture was indicated by changes in both signals as shown in Figure 3.3 for a 30 min deposition on a fibre with a 30 nm aperture.

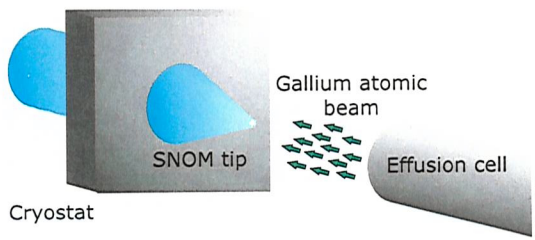

Figure 3.2: Schematic of the deposition configuration for the formation of a gallium nanoparticle on a SNOM fibre tip.

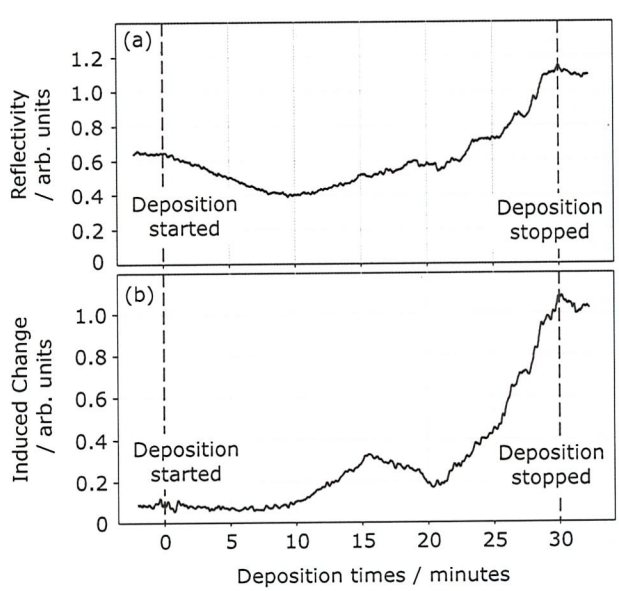

Figure 3.3: Reflectivity (a) and Induced Reflectivity Change (b) as a function of time for a thirty minute deposition of gallium at a rate of $\sim 0.3\,\mathrm{nm/min}$ on a SNOM tip cooled to 80 K under a 10^{-6} mbar vacuum.

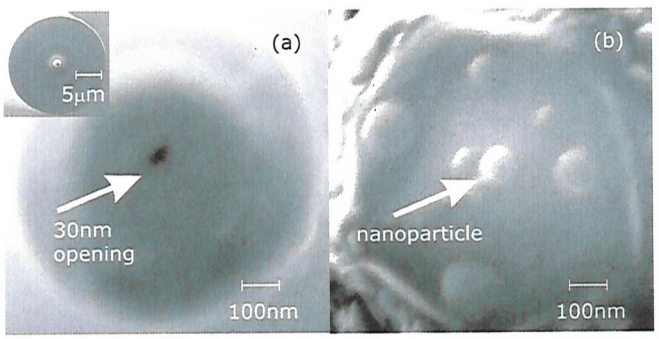

Figure 3.4: Scanning electron microscope images of the aperture at the tip of a SNOM fibre before (a) and after (b) growth of a gallium nanoparticle. In this case, the nanoparticle has a diameter of $\sim 80\,\text{nm}$.

Scanning electron microscope images of the fibre tip before and after deposition clearly show that a nanoparticle is formed in the aperture (see Figure 3.4). In this particular case, the nanoparticle has a diameter of $\sim 80\,\text{nm}$.

3.4 Optical properties of a single gallium nanoparticle undergoing structural transformations

To study the optical properties of single gallium nanoparticles, an extremely sensitive pump-probe setup was used (see Figure 3.5). A cw diode laser operating at 1310 nm was used as a probe and another at 1550 nm, typically modulated at $f = 2.3\,k\text{Hz}$, was used as the pump. The reflected probe signal was monitored using an InGaAs photodetector. A wavelength-division multiplexer (WDM) and band-pass filter prevented reflected pump light from reaching the photodetector.

Structural transformations were observed by monitoring pump-beam induced changes in the reflectivity of individual nanoparticles as a function of temperature between 80 and 300 K. The temperature was varied at a rate of 2 K/min. The results presented in this section were obtained for a nanoparticle grown at the end of a SNOM fibre with a 100 nm aperture using pump and probe powers of ~ 30 and $\sim 20\,\text{nW}$ respectively at the nanoaperture. Using an oscilloscope, it was observed in real time that with each pump pulse

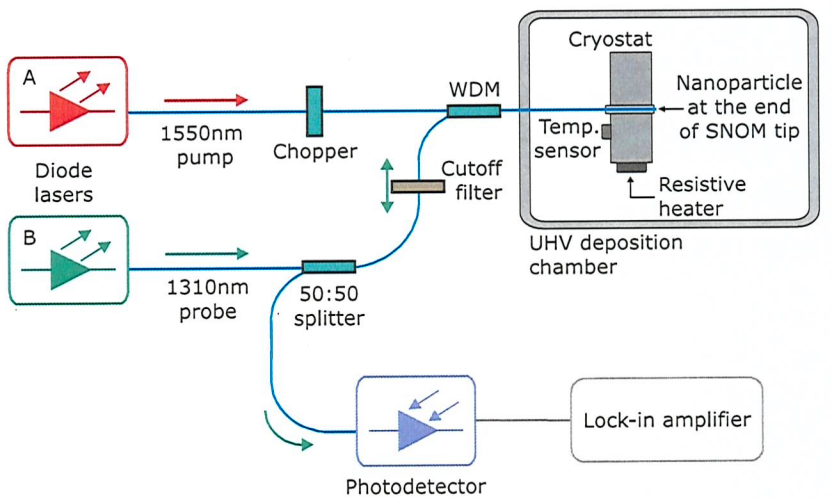

Figure 3.5: Fibre-optic arrangement for reflective pump-probe measurements with on a single gallium nanoparticle.

the nanoparticle reflectivity changed in response to the pulse and recovered after the pulse in a reversible fashion (see Figure 3.6).

The magnitude of this modulation was recorded as a function of temperature using a lock-in amplifier referenced to the pump modulation frequency f. This method doesn't record any reflectivity change induced by the cw probe beam, but this may be ignored as the study is concerned only with the existence of an effect rather than with its absolute magnitude. With increasing temperature, several narrow peaks in the induced reflectivity change signal are observed at temperatures between 200 and 250 K (see Figure 3.7(a)). No features are observed outside the temperature range shown. The positive and negative peaks correspond to pump-induced increases and decreases respectively in the nanoparticle's reflectivity. When the heating cycle is repeated, the peaks appear at the same positions, but their relative heights can vary.

Substantial changes in the optical properties of a single nanoparticle may occur when it undergoes a transition between two phases or geometrical forms. Such changes are typically much more dramatic than temperature-dependent variations occurring within a single phase and the peaks observed in the pump-induced reflectivity change signal are characteristic of such transitions.

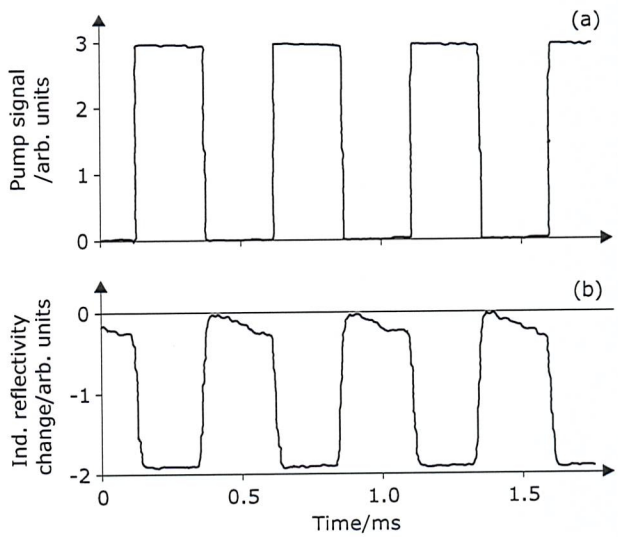

Figure 3.6: Induced change on the reflectivity of a single gallium nanoparticle (b) by a modulated pump (a) for $T = 235\,\mathrm{K}$.

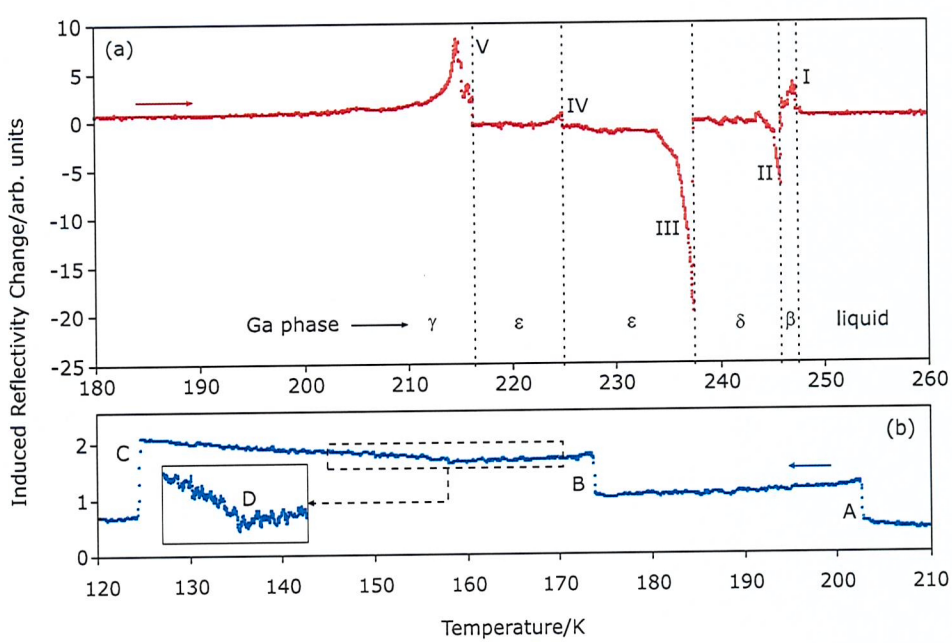

Figure 3.7: Pump-induced reflectivity change for a single gallium nanoparticle as a function of (a) increasing and (b) decreasing temperature. The cw probe power at the 100 nm aperture was $\sim 20\,\mathrm{nW}$, while the peak pump power was $\sim 30\,\mathrm{nW}$. Note that the plotted temperature is that recorded by the coldfinger and is therefore somewhat lower than the actual temperature of the gallium nanoparticle due to localized laser heating.

Indeed, this type of asymmetric peaked optical response has been observed previously at gallium/dielectric interfaces [9] and in gallium nanoparticle films (see Chapter 2), though these experiments did not resolve the fine detail of sequential transitions through several structural forms. As described in Chapter 1, the differences between the electronic density of states of gallium's various phases [10] lead to significant differences between their dielectric coefficients. A phase change in a gallium nanoparticle thus affects its optical absorption cross-section [11] and in the present case will change the reflectivity of the nanoaperture. The fact that in confined solids phase transformations take the form of a dynamic phase coexistence extending across a certain temperature interval (as opposed to an abrupt transition at a specific temperature) [5, 6], with the surface (where atoms have less nearest neighbours than internal atoms) acting as a boundary at which transformations start [12, 13], has also been explained previously (see Section 1.4 of Chapter 1). At temperatures within or just below the transitional range, the phase equilibrium can be influenced by external excitations [14].

In the current experiment, absorption of periodically modulated pump light leads to a periodic excitation of gallium's electronic structure and a periodic modulation of its temperature (at the pump modulation frequency f), which affects the phase equilibrium in the nanoparticle and therefore its reflectivity. As explained in Chapter 1, this process can be further analyzed by considering a nanoparticle (at a fixed temperature) consisting of a core in one phase covered by a thin shell of a different phase [6]. The thickness of the shell layer will increase with the level of external excitation and the optical properties of the particle will change continuously from those of the core phase to those of the surface phase. If the excitation level is reduced before the transformation to the new phase is complete, the changes will be reversed, that is the skin layer will shrink to an appropriate equilibrium position and the reflectivity will return to its original level. However, if the core is fully consumed by the surface phase the particle becomes stable against a return to the original phase, because this would require the creation of a nucleation center and any applied excitation ceases to induce any significant change in the particle's optical properties, until the temperature approaches the next phase transition point.

The pump-induced reflectivity change signal observed during the cooling of the nanoparticle (see Figure 3.7(b)) is very different from that observed during

heating. It is smaller, always positive and shows abrupt step changes (instead of sharp peaks) in the signal. The temperatures at which this steps occur are also different from those of any of the peaks. These temperature differences and the continuously low signal level are results of overcooling: With decreasing temperature the nanoparticle remains in a given phase until its temperature is somewhat lower than the equilibrium transition temperature, and in these conditions pump excitation produces very little signal. When the overcooled particle transforms abruptly into a lower energy form, the pump-induced probe modulation remains small because this change happens at a temperature far below the increasing-temperature signal peak for that phase. If the last peak, I, and the last step, A, are associated with transitions into and out of the highest temperature phase, and the first peak, V, and first step, C, are in turn associated with transitions into and out of the lowest temperature phase, this implies the presence of overcooling of 45 and 90 K respectively.

While five peaks are identified in the heating part of the curve (see Figure 3.7(a)), there are only four features in the cooling part of the temperature cycle (see Figure 3.7(b)): Three distinct steps (A, B, and C) and a gradient change D (which is more clearly seen in the inset on an enlarged y-axis). This may be because features are harder to resolve at the reduced signal level recorded during cooling (e.g., with heating, peaks I and II are very closely spaced - their cooling counterparts may overlap), or perhaps because the sequence of transitions undertaken by the particle with decreasing temperature is not simply the reverse of the increasing temperature sequence. Such nonreciprocity in the sequence could result from the fact that the transition mechanisms for heating and cooling are very different: With increasing temperature transitions are continuous and surface-driven, but with decreasing temperature they occur more abruptly following the formation of a nucleation center within the particle. However, it is possible that the reason for the presence of one less feature in the cooling curve may be that one of the peaks in the heating curve is associated with a shape (rather than phase) change in the particle. If that is indeed the case, the reverse change may not be observable when the nanoparticle is cooled. Another difference between the heating and cooling curves is that the pump-induced reflectivity change is always positive with decreasing temperature, while switching between positive and negative with increasing temperature. This may result from the

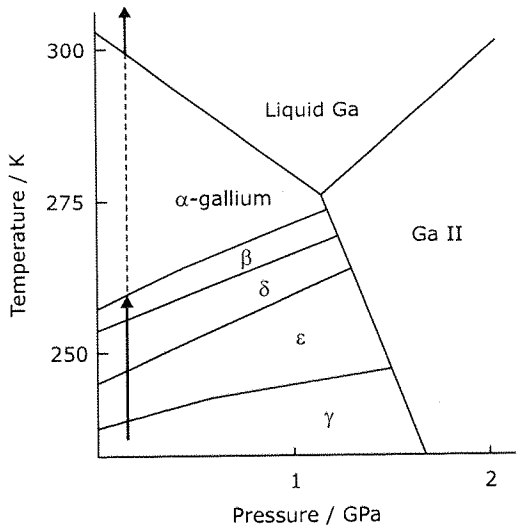

Figure 3.8: Phase diagram for (bulk) gallium after Bosio [15] showing the sequence of phase transitions expected in a gallium nanoparticle undergoing adiabatic heating from 180 to 300 K. The dotted line indicates that the β phase transforms directly to liquid as the α phase is not found in nanostructures.

nonreciprocity mentioned above, or may be an indication that there are two components to the response of the nanoparticle: One that gives a small positive background signal with a magnitude that depends on the phase of the metal but not on temperature, and another that produces a larger positive/negative component in the vicinity of the transition points.

Using gallium's phase diagram (introduced in Section 1.6.3 of Chapter 1 and shown again in Figure 3.8) and the available information on the relative stability of its crystalline forms, one may attempt to assign specific phase transitions to the peaks in Figure 3.7(a). One may reasonably assume that peak I is associated with a transition from a solid state to the liquid. An X-ray diffraction study of gallium nanoparticles found that α-gallium, the stable solid state of bulk gallium, is completely absent in small particles [16]. This being the case, it then follows from Defrain's analysis of the free energies of gallium's metastable phases [17] that the only possible sequence of phase transformations in gallium nanostructures is $\gamma \rightarrow \epsilon \rightarrow \delta \rightarrow \beta \rightarrow$ liquid (with γ, ϵ, δ and β all crystalline phases). This progression is in agreement with the established phase diagram for gallium shown in Figure 3.8: The pressure inside a particle may be

estimated using the Laplace-Young equation:

$$P = \frac{4}{3}\rho(\frac{2}{d} + \frac{1}{h})$$

Where ρ is the surface tension ($0.7\,\mathrm{Jm}^{-2}$ for liquid gallium), $d \sim 100\,\mathrm{nm}$ is the particle diameter, and $h \approx ft = 18\,\mathrm{nm}$ is its height, giving $P = 0.1\,\mathrm{GPa}$. The sequence is then obtained moving up in temperature at this pressure as indicated by the arrow in Figure 3.8.

According to this sequence, peak I in Figure 3.7(a) (at $T_I = 248\,\mathrm{K}$) would correspond to a transition from the monoclinic $\beta-$gallium phase to the liquid. The bulk melting point of $\beta-$gallium is 257 K [17], but as explained in Chapter 2 transition temperatures are reduced in nanoparticles [18].

If one assumes, in accordance with the above sequence and with its strong presence in gallium nanoparticle X-ray spectra [16], that the γ phase is the ground state, that is, the lowest temperature phase, then one is left with three phase transitions remaining ($\gamma \rightarrow \epsilon \rightarrow \delta \rightarrow \beta$) and four peaks ($II$, III, IV and V), suggesting that one of the peaks is associated with something other than a phase change. A shape change, for example, may give such a response. Peak IV differs from the others in a number of ways and is therefore the most likely candidate to be associated with a shape change: It is the smallest peak and the only one that crosses the zero level on the low temperature side of the peak. Furthermore, and perhaps more importantly, the change in the retardation between pump and probe modulations associated with peak IV is at least an order of magnitude larger than for any other peak.

If peak IV relates to a shape change, then peak V can be associated with the $\gamma \rightarrow \epsilon$ gallium transition, peak III with $\epsilon \rightarrow \delta$ and peak II with $\delta \rightarrow \beta$. Unfortunately, the absence of any data on the dielectric constants of gallium's metastable crystalline phases, makes it impossible to obtain more information on the phase transition sequence from the signs or relative magnitudes of the peaks in Figure 3.7(a).

The light-induced reflectivity changes described above are observed at very low levels of optical excitation. Figure 3.9 shows the power dependence of the height of peak V. Notice how the signal saturates at pump powers higher than

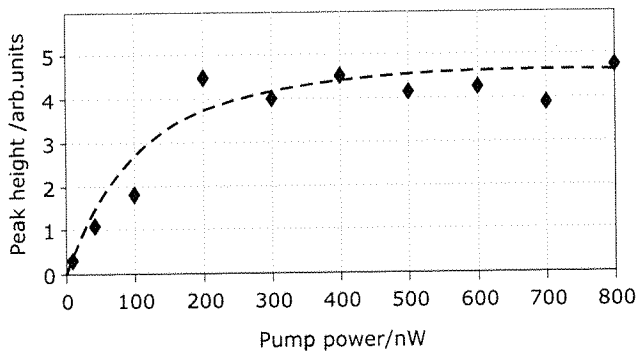

Figure 3.9: Dependence on pump power at the nanoparticle of the pump-induced change, measured as the height of peak V of Figure 3.7 (probe power = 20 nW).

$\sim$ 200 nW, and can be observed with as little as 10 nW. These low levels can be used because the differences ΔG between the free energies of some of the metastable phases involved are very small: For example, $\Delta G_{\delta\to\beta} = 0.3\,\text{meV/atom}$ and $\Delta G_{\gamma\to\delta} = 1.7\,\text{meV/atom}$ [17]. Thus, the absorption of a pump quantum with an energy of 1 eV should be sufficient to convert about 3300 atoms from the δ phase to the β phase, and about 600 atoms from the γ phase to the δ phase. Finally, it should also be noted that the light-induced transitions are likely to be driven primarily by thermal excitation (i.e. laser induced heating) but there may also be a contribution from a temperature-independent, nonthermal mechanism whereby the phase change is caused by band-structure collapse and lattice instability resulting from electronic excitation [14].

3.5 Reduction of overcooling under nanosecond excitation

In the last section it was shown that the pump-induced reflectivity change signal observed during the heating of the nanoparticle (see Figure 3.7(a)) is very different from the signal observed during cooling (see Figure 3.7(b)). In particular, the cooling signal is smaller, always positive and shows abrupt step changes at temperatures different from those of any of the sharp peaks present in the heating curve. These results illustrated that under the conditions used (1550 nm cw pump excitation modulated at 2.5 kHz) the particle is subject to overcooling of between 45 and 90 K.

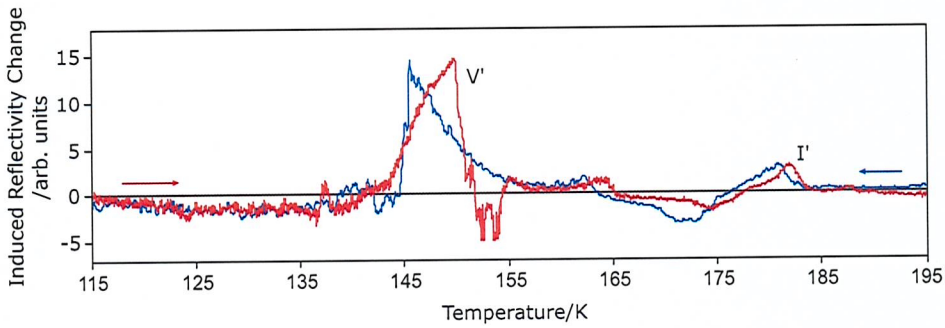

Figure 3.10: Pump-induced reflectivity change for a single gallium nanoparticle excited with 3 ns pulses at a repetition rate of 30 kHz and with a peak power of 0.1 mW at the nanoaperture as a function of increasing (red line) and decreasing (blue line) temperature.

Figure 3.10 shows the pump-induced reflectivity change signal obtained when the modulated cw beam is replaced with one at the same wavelength but giving 3 ns pulses at a repetition rate of 30 kHz with a peak power of 0.1 mW at the nanoaperture (i.e. an average power of the same order as previously).

Under this regime of pulsed excitation, the response of the particles is dramatically changed. With increasing temperature, peaks I and V (of Figure 3.7) are still clearly visible (now labeled I' and V'), however the intermediate peaks are replaced by smoother, broader features. Most importantly, with pulsed excitation the response patterns in both directions of temperature are very similar: With increasing and decreasing temperature, the same major peaks are seen with overcooling of only $\sim 2\,\mathrm{K}$ for peak I' and $\sim 5\,\mathrm{K}$ for peak V'. Note that the peak positions are shifted by around 65 K as compared to the modulated cw regime because of greater laser-induced heating by the short pulses: Thermodynamic calculations confirm that the energy absorbed by the particle cannot dissipate during the pulse and therefore rapidly increases its temperature.

It has already been explained that in nanoparticles, transitions from lower to higher energy states occur through a dynamic coexistence of structural forms over a certain temperature range, and that while transitions are reversible within the temperature range, the particle becomes stable against a return to the old phase once it is fully converted to the new phase, because this would

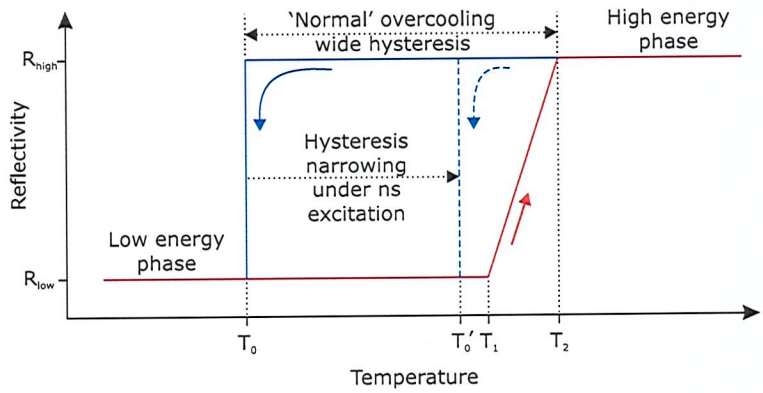

Figure 3.11: Using light to control the hysteresis properties of two level nanoparticles. Solid line: schematic of the hysteresis in the optical properties of gallium nanoparticles under modulated cw excitation. The $T_2 - T_0$ hysteresis results from the extensive overcooling of the high energy phase that is normally required before a transition to the low energy phase occurs. Dashed line: The use of nanosecond pulsed excitation considerably narrows the hysteresis to $T_2 - T_0'$.

involve the creation of a nucleation center. Thus, a transition from a high to a low energy phase normally only occurs after a certain amount of overcooling creating a hysteresis in the nanoparticle's optical properties as seen with the modulated cw pump (see Figure 3.7).

However, the results for nanosecond pulsed pump excitation presented in Figure 3.10 show that overcooling is practically eliminated under these conditions and the signal structure in both directions of the temperature scan is very similar. This near-total disappearance of overcooling may result from the fact that a short, intense pulse can provide the energy required for a slightly overcooled nanoparticle to overcome the potential barrier between the phases and transform from a higher temperature phase to a lower temperature phase. A similar effect is observed in the 'explosive crystallization' of thin metal films, where a localized energy input stimulates an abrupt transition from an overcooled liquid state to the solid state [19].

This ability to use short, intense optical excitation pulses to greatly reduce the overcooling in nanoparticles (see Figure 3.11) may be of great importance for future applications. For example, as Chapter 4 will explain, the presence of overcooling leads to a form of optical bistability that enables gallium nanoparticles to act as memory elements. In this type of memory, the different

structural states represent different logical memory states and microsecond optical pulses can be used to write information to the nanoparticles, that is, to switch them from a low energy state to a higher one. Reading the memory state is also achieved optically by probing the reflective properties of the nanoparticle, but to erase information one needs to substantially cool the particles. However, the results presented here demonstrate that short, high intensity, low energy light pulses may significantly reduce the extent of overcooling in gallium nanoparticles and may thus be used to convert a particle from a higher state to a lower state. This means that all memory functions, i.e. reading, writing and erasing, might be performed optically at a fixed temperature.

3.6 Summary and conclusions

Systems have been developed to grow and study the properties of individual gallium nanoparticles was developed. The single nanoparticles are formed by atomic beam deposition at the nanoaperture of a tapered gold-coated optical fibre. Reversible light-induced transformations in a single gallium nanoparticle have been investigated for the first time. It has been found that the energy required to excite these transitions is very low and that the extent of overcooling shown by the particle depends on the type of excitation being used. The ability to use such low power optical signals to control the optical properties of a single nanoparticle is an important step forward in developing nanoscale photonic functionality.

The results indicate that with increasing temperature a gallium nanoparticle goes through the following sequence of phase
transitions: $\gamma \rightarrow \epsilon \rightarrow \delta \rightarrow \beta \rightarrow$ liquid. These have sharp peaks in the induced reflectivity change signal associated with them. Evidence also indicates that one of the peaks could be related to a shape change in the nanoparticle. Transitions have been observed using incident pump powers of as little as 10 nW.

Significant overcooling of up to 90 K is observed when the particles are excited with a modulated cw pump, but under nanosecond pulsed excitation at the same wavelength this overcooling is all but eliminated.

The low energy requirements for the observation of optically induced phase transitions in nanoparticles, accompanied by changes in the reflection and

transmission properties, the phase stability on overcooling, and the ability to optically control this overcooling, suggest that nanoparticles can provide a way to create key logical and memory elements for nanophotonic devices operating at extremely low power levels.

3.7 References

[1] J. Prikulis, F. Svedberg, M. Kall, J. Enger, K. Ramser, M. Goksor, and D. Hanstorp *Nano Letters* **4**(1): 115 (2004).

[2] K. Lindfors, T. Kalkbrenner, P. Stoller, and V. Sandoghdar *Physical Review Letters* **93**(3): 037401 (2004).

[3] L.A. Peyser, A.E. Vinson, A.P. Bartko, and R.M. Dickson *Science* **291**(5501): 103 (2001).

[4] W.E. Doering, and S. Nie *Journal of Physical Chemistry B* **106**(2): 311 (2002).

[5] R.S. Berry, and B.M. Smirnov *Journal of Chemical Physics* **113**(2): 728 (2000).

[6] A.S. Shirinyan, and M. Wautelet *Nanotechnology* **15**: 1720 (2004).

[7] B. Hecht, B. Sick, U.P. Wild, V. Deckert, R. Zenobi, O.J.F. Martin, and D.W. Pohl *Journal of Chemical Physics* **112**(18): 7761 (2000).

[8] R.M. Stockle, N. Schaller, V. Deckert, C. Fokas, and R. Zenobi *Journal of Microscopy* **194**: 378 (1999).

[9] P. Petropoulos, H.S. Kim, D.J. Richardson, V.A. Fedotov, and N.I. Zheludev *Physical Review B* **64**(19): 193312 (2001).

[10] M. Bernasconi, G.L. Chiarotti, and E. Tosatti *Physical Review B*, **52**(14): 9988 (1995).

[11] V.A. Fedotov, V.I. Emel'yanov, K.F. MacDonald, and N.I. Zheludev *Journal of Optics A- Pure and Applied Optics* **6**(2): 155 (2004).

[12] K.F. Peters, Y.W. Chung, and J.B. Cohen *Applied Physics Letters* **71**(16): 2391 (1997).

[13] G.B. Parravicini, A.Stella, P. Tognini, P.G. Merli, A. Migliori, P. Cheyssac, and R. Kofman *Applied Physics Letters* **82**(9): 1461 (2003).

[14] M. Wautelet *Journal of Physics-Condensed Matter* **16**(12): 163 (2004).

[15] L. Bosio *Journal of Chemical Physics* **68**(3): 1221 (1978).

[16] A. Di Cicco *Physical Review Letters* **81**(14): 2942 (1998).

[17] A. Defrain *Journal De Chimie Physique Et De Physico-Chimie Biologique* **74**(7-8): 851 (1977).

[18] J.P. Borel *Surface Science* **106**(1-3): 1 (1981).

[19] V.M. Kuz'menko, V.I. Mel'nikov, and V.A. Rakhubovskii *Soviet Physics JETP* **59**: 612 (1984).

Chapter 4

Nanoparticles as all-optical memory elements

4.1 Synopsis

Nanoparticles undergoing light-induced transformations between two structural phases with different optical properties show a bistability that can be used to create a resonator-free optical memory element, operating at very low power levels. Furthermore, polymorphic systems exhibiting more than one phase transition make memory elements with logic bases higher than two possible.

In Section 4.3 the general concept of using phase changes in nanoparticles to create nanoscale memory elements is introduced. Section 4.4 shows how this type of memory functionality was demonstrated experimentally using a film of gallium nanoparticles and presents a method for differentially accessing the logic state of the memory using a modulated optical probe beam. Section 4.5 then describes the results of experiments that show how a single gallium nanoparticle can be used as a quaternary-logical optical memory element by encoding the information in the different structural phases with optical pulses of very low energy.

4.2 Introduction

In a society driven by information, the need for smaller devices with larger storage capacity and quicker write and access times compared to existing technologies continues to grow quickly. Many different solutions to the problem

of data storage have been proposed over the years. Moving on from the initial use of punch cards, magnetic tape started to be employed to store data around 1950 [1]. The next big step forward occurred in 1957 with the introduction of IBM's 305 RAMAC system which included the first magnetic disk [2]. Magnetic disks have moved a long way from this initial 5 MB disk, which had a recording density of about 2 Kb/in^2. Today's commercially available hard disks already have more than 500 GB capacity, with densities in the order of 0.1 Tb/in^2, and perpendicular recording technologies promise even higher densities [3]. Other technologies not based on magnetic recording also play an important role in the data storage market. Flash memories, for example, store information in an array of floating gate transistors, each storing one bit of information. They were first described in 1984 [4] and, as they don't suffer from the mechanical limitations of hard disks, are a candidate for their replacement in a range of applications. Storage capacities of about 64 GB in a single chip have recently been demonstrated by Samsung, using a bit cell with a size of about 40 nm [5]. Another recent development in terms of alternative technologies has been the development of holographic storage products, with disks capacities of up to 300 GB already commercially available [6].

The idea of achieving binary or even higher base logics in optical resonators was proposed and studied extensively in the 1980's, in optically bi- and multistable configurations, where optical nonlinearities were employed together with feedback to lock devices into stable states [7]. However, in all these solutions their minimum spatial size was limited to around one optical wavelength. In contrast, phase change memories [8-10], which store information in the phase of a material, are not subject to this constraint. This makes them strong candidates for addressing challenges in the size and power consumption of electronic memories [11]. In such materials, for example those used in today's DVD/DVR disks, data recording is achieved by switching between amorphous and crystalline phases. Blu-ray DVD/DVR disks have a data storage density of 0.015 Tb/in^2 and a record of 0.23 Tb/in^2 has recently been achieved in hard disks employing perpendicular recording technology [3]. With interest in phase-change materials intensifying a density as high as 3.3 Tb/in^2 was recently reported in a binary phase-change material addressed by means of a heated atomic force tip [10].

The use of nanoparticles for data storage is particularly promising. Not only do

they provide intrinsic mechanisms of phase meta-stability, they also require a very small amount of energy per logic state to write, and offer outstanding information storage density. As shown in Chapters 2 and 3, experiments on reversible light-induced structural transformations in gallium nanoparticles, in particular the observation of solid-to-solid light-induced phase transitions in a single gallium nanoparticle, illustrated that a nanoparticle with a diameter of a few tens of nanometers exhibits equilibrium coexistences between a number of solid and disordered structural phases with different dielectric properties. These can be controlled by optical excitation in a reversible and reproducible fashion. The energy required to exercise such control is only a few picojoules, which is extremely promising for low-energy photonic devices.

This Chapter describes the experimental demonstration of bistable memory functionality in gallium nanoparticle films, achieved by engaging transformations between structural phases with different dielectric properties. The state of the nanoparticles is read by a weak optical probe beam and it is shown that a single optical pulse can irreversibly switch nanoparticles from a low reflectivity phase into a high reflectivity phase, thus providing memory write functionality.

The first experimental demonstration of all-optical four-level memory functionality, in a single 80 nm nanoparticle grown at the end of a scanning nearfield optical microscope probe is also presented. The switching between the nanoparticle's four different structural states is achieved by excitation with single laser pulses, while the reading is performed by detecting changes in the nanoparticle's reflectivity with a pump-probe arrangement.

4.3 Phase-change memory functionality in nanoparticles

In Chapters 2 and 3 it was shown that nanoparticles can exist in a number of different structural phases. It was also explained that with these phases having different dielectric properties, a structural transformation is accompanied by a change in the optical properties of the nanoparticle. Furthermore, the fact that in nanoparticles phase transformations occur through a dynamic coexistence of the phases involved, and that the balance of this coexistence can be controlled

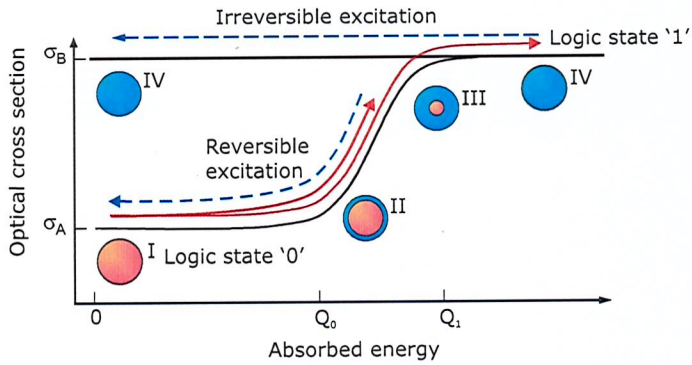

Figure 4.1: Binary memory functionality in a nanoparticle. Core-shell structures *II* and *III* are transitional mixed phase states occurring in the reversible excitation induced transition range between levels Q_0 and Q_1. If the excitation exceeds the upper level Q_1 for full transformation from state *I* into state *IV*, the particle remains in this upper phase even when the excitation is withdrawn. Information can be coded in the phases of the particle, for example by labeling the low level as logic state '0' and the upper level as logic state '1'.

by external stimulation to effectively achieve an optical nonlinearity were explained. This behavior is presented schematically in Figure 4.1 for a nanoparticle undergoing a phase transition from a low energy phase to a higher energy phase.

Consider a particle in the low energy phase (stage *I*). If one keeps the background temperature of the particle constant and increases the level of external excitation, this will initially convert the nanoparticle from stage *I*, through *II* and *III*. If the excitation is withdrawn before stage *IV* is achieved, the nanoparticle will return to its initial state, *I*. That is, if the excitation energy is in the range between $Q_0$and Q_1, reversible changes occur in the state of the particle as described in detail in the previous chapters.

When the excitation level exceeds Q_1 the reversibility breaks and upon withdrawal of the excitation, the particle will remain in the fully converted state *IV* until substantial overcooling is applied to the system. This type of hysteresis means that the nanoparticle can be seen as a bistable object, and this resonator free optical bistability can be exploited to obtain a binary optical memory element, wherein the two phases represent different logic levels, '0' and '1'.

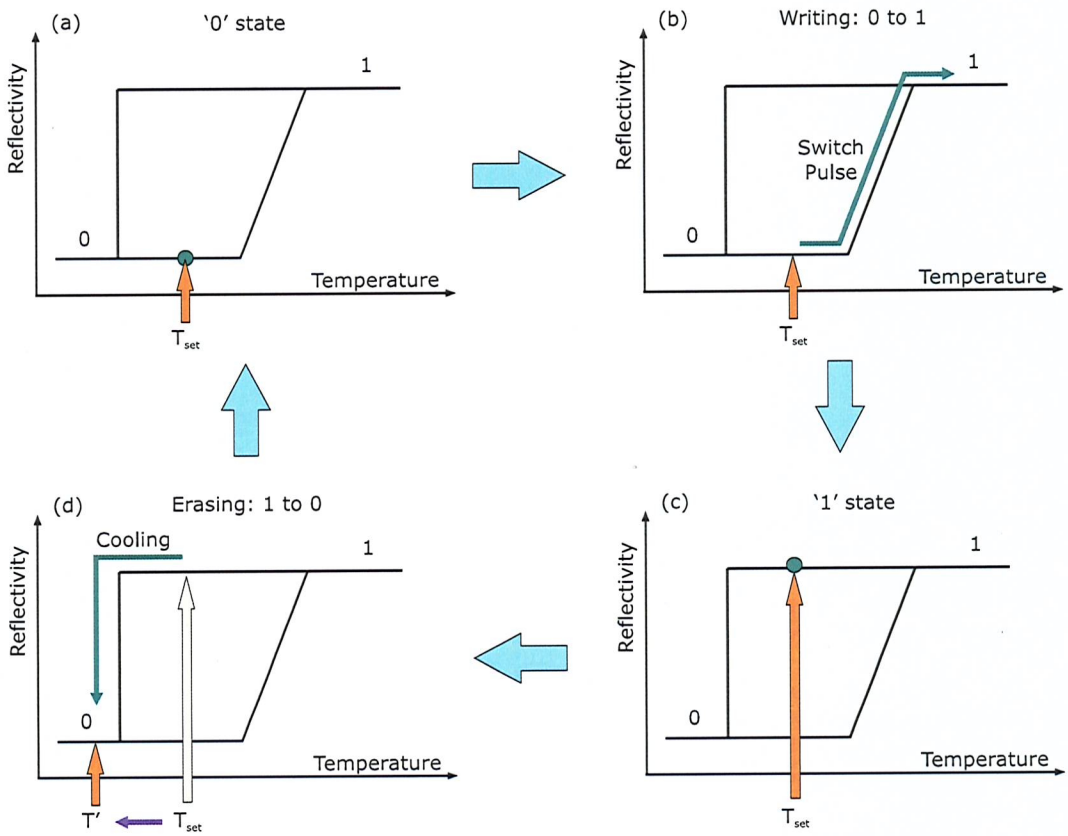

Figure 4.2: Operational scheme for nanoparticle memory functionality. Information can be written to a nanoparticle in the low reflectivity state '0', at a fixed temperature T_{set} inside the hysteresis loop (a), by exciting it with an appropriate switching pulse as shown in (b). The memory can be erased by cooling the nanoparticle to convert it from state '1' (c) back to state '0' as shown in (d).

Reading the memory is performed simply by monitoring the nanoparticle's optical properties, for example by measuring its reflectivity (see Figure 4.2). Then, beginning in the ground state, '0', a '1' can be written to the memory by using an optical pulse with a total energy larger than Q_1 to fully convert the particle to the higher state. The memory can be erased, that is returned to state '0', by cooling the nanoparticle temperature to a point below the hysteresis loop and the entire cycle can be repeated as needed .

If the nanoparticle can exist in more that two different structural phases, these extra phases can be used to increase the memory capacity. Once more, the phases with different optical properties are simply associated with successive logic levels. In Figure 4.3 this is schematically presented for a nanoparticle with

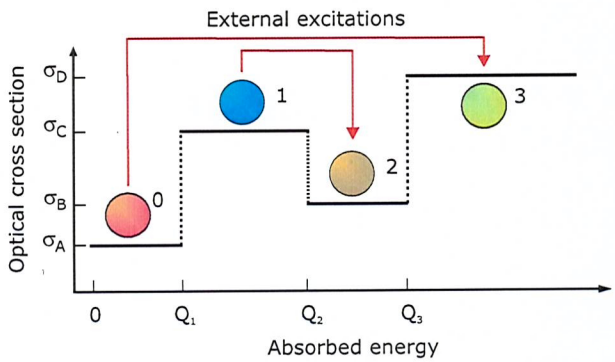

Figure 4.3: Quaternary memory functionality in a nanoparticle. This simplified generic diagram illustrates how high-logic memory can be obtained by employing four different phases, each representing a unique logical state. The different logic states can be accessed using external excitations of various energies. The mixed phase states that occur between different phases are not shown.

four different phases. The different phases can be accessed by using optical pulses with different total energies and the logical state can still be read by monitoring the optical properties of the particle. Thus, such a particle constitutes an optical quaternary logical element. One should note that in addition to the increased storage capacity of a quaternary logical element, a higher logic memory element also permits entirely new algorithms in computation where complex number arithmetic is considerably simplified and error accumulation reduced [12].

Gallium nanoparticles exhibit all the properties necessary to achieve this type of memory functionality and are therefore ideal candidates for the experimental demonstration of the concepts described above.

4.4 Binary memory in a gallium nanoparticle film

The type of binary memory functionality described in the previous section has been demonstrated using a film of gallium nanoparticles deposited on the end of an optical fibre.

A film of nanoparticles was grown, using the light assisted atomic beam deposition technique described in detail in Section 2.3, on the end of an optical

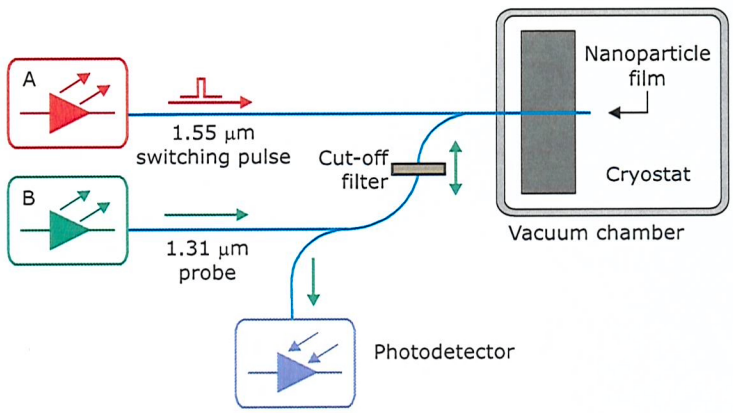

Figure 4.4: Experimental setup used to demonstrate the optical memory functionality of a film of gallium nanoparticles self-assembled on the end of an optical fibre. Laser A delivers on-demand single pulses, used for switching the nanoparticle to the higher energy state. The low power continuous wave laser B is used to monitor the nanoparticle logical state by measuring its reflectivity.

fibre attached to a liquid nitrogen cooled cryostat, such that the temperature of the film could be varied in the range from 80 to 300 K.

In order to demonstrate the memory functionality, two lasers were used as shown in the optical setup presented in Figure 4.4. The first laser, a 1 mW cw diode laser operating at a wavelength of 1310 nm, probed the state of the nanoparticles by monitoring the reflectivity of the film. The second, a 1550 nm pulsed diode laser, optically excited and switched the nanoparticles with on demand single optical pulses.

Initially, the reflectivity of the film was recorded in the absence of any pulsed optical excitation as function of temperature from 80 to 300 K (solid diamonds in Figure 4.5(a)). The corresponding reflectivity curve for a temperature scan in the reverse direction was then recorded - shown as open triangles in the same graph. These curves illustrate the thermal hysteresis of the optical reflectivity of the gallium nanoparticle film. At the starting temperature of $T = 80$ K, the film is initially in the low reflectivity state, which is labeled as logic state '0'. With increasing temperature, the reflectivity increases rapidly in the temperature domain of the phase transition ($T_1 < T < T_2$). As the temperature is increased even further ($T > T_2$), the film enters the high reflectivity state, labeled as logic '1'. The film remains in this state even as the ambient temperature is

decreased to the initial 80 K starting temperature. In order to switch the film back into the '0' logic low reflectivity state, the probe laser must be switched off. This allows the effective film temperature to drop below T_0. When the probe laser is switched on again, the film of nanoparticles has recovered to the original '0' level. As discussed in Section 2.4, following the phase diagram of gallium [13], state '0' can be identified with the β gallium phase, while state '1' is associated with liquid gallium.

Thus, a nanoparticle film displaying a temperature hysteresis between two phases can act as a bistable element encoding two logic levels. In order to demonstrate useful optical memory functionality in a gallium nanoparticle film, one must be able to switch the film into the high reflectivity (logic '1') state at a fixed temperature. Experimentally, this 'writing' was achieved using a manually triggered 1550 nm pulsed laser. The sample temperature was first increased from below to a temperature $T_{set} = 170$ K close to the phase transition. The sample was kept at this temperature, while a single optical pulse of peak power 13.1 mW and pulse duration 1 μs was used to excite the system and switch the film from the logic '0' to the logic '1'state. After exposure to this pulse, the film was indeed found to be locked into the high reflectivity '1' state and remained there after the pulse (see Figure 4.5(b)). Thus, the gallium nanoparticles can be switched by a single optical pulse from the low reflectivity state '0' to the high reflectivity state '1' at a fixed temperature below the lower transition temperature T_1, providing memory write functionality.

The written state '1' is maintained until the nanoparticle film is substantially cooled to a point below T_0 where the particles return to the logical '0' level. Such cooling thus provides memory erase functionality. At first glance, this procedure may appear to be a significant limitation, but a similar situation is found in the commercially widespread EPROM technology [14]. This type of memory is initially programmed with electric pulses, but can only be erased by exposure to strong ultra-violet light for a considerable period of time.

In the gallium system, there is an alternative possibility: The entire switching cycle may be controlled optically by setting the background temperature below the hysteresis loop and using the heating effect of the probe laser to obtain an effective set point within the loop (see Figure 4.6). In this case the '1' state can

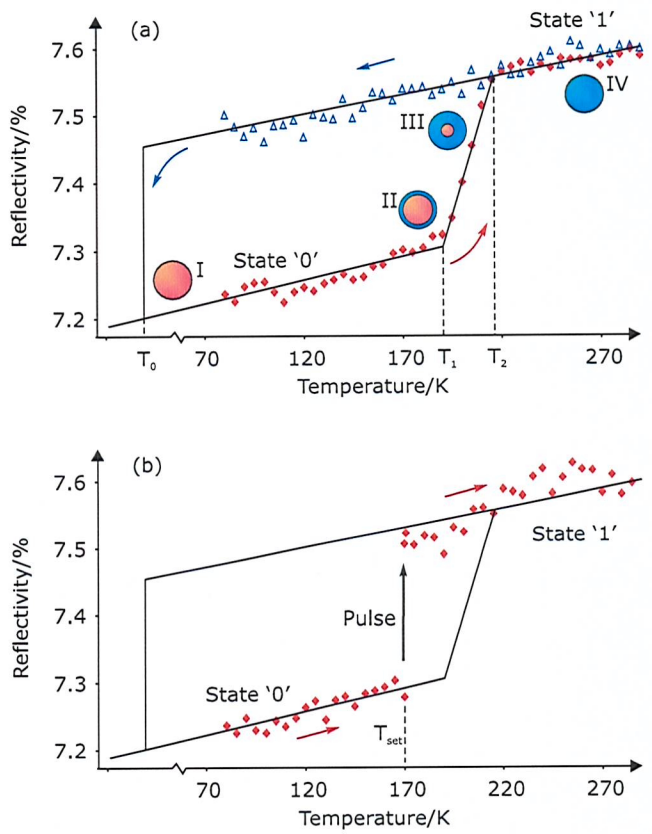

Figure 4.5: (a) Optical bistability in gallium nanoparticle films: The arrows show the hysteresis cycle followed during a complete temperature scan from below T_0 to above T_2 and back again. At low temperatures the film is in the low reflectivity '0' state. Between T_1 and T_2, there is a dynamic coexistence of structural forms in the gallium nanoparticle film. Above T_2 the film enters and remains in a high reflectivity '1' state. The film only returns to the low reflectivity '0' state after its temperature falls below the lower switching temperature T_0. (b) Demonstration of 'memory write' functionality: A single laser pulse is used to switch from the low reflectivity '0' state to the high reflectivity '1' state (pulse peak power = 13.1 mW, pulse width = 1 μs). After the pulse, the film remains in the high reflectivity '1' state.

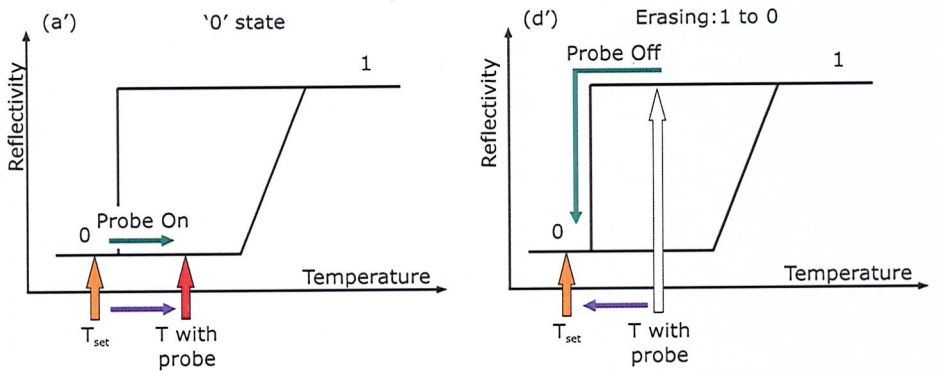

Figure 4.6: All-optical volatile memory functionality. These steps replace (a) and (d) in the full write-erase cycle shown in Figure 4.2: (a') The heating effect of the probe laser may be exploited to obtain an effective temperature point within the hysteresis loop. (d') The memory may then be erased by switching off the probe beam. In this scheme *all* information is lost when the power is switched off.

be erased simply by turning off the probe laser. The write, read and erase cycle of the nanoparticle memory can then be repeated time and time again without adjusting the background temperature. In this arrangement however, the '1' state is only maintained for as long as the probe laser light is present, making it a volatile memory, that is a memory which loses all the information stored when the power is switched off.

Finally, it should be noted that a third mechanism for recovering to the '0' logic state may exist. As described in Section 3.5, the extent of the hysteresis present can be reduced with short nanosecond pulses. This would constitute a very attractive way of optically switching to the lower level as there would be no need to act on the background temperature and the memory data would not be lost when the probe laser is switched off, thus creating an all-optical non-volatile memory element (see Figure 4.7). However, this has not yet been demonstrated experimentally and further research is needed to better understand the mechanisms involved.

An important issue is the reflectivity difference between the two logic states, which may at a first glance seem too small for any reliable application. However, instead of detecting the absolute reflectivity of the film, one can use a more effective scheme to determine the state of the nanoparticle memory, as you can monitor the kind of induced reflectivity change described in Section 2.4 and

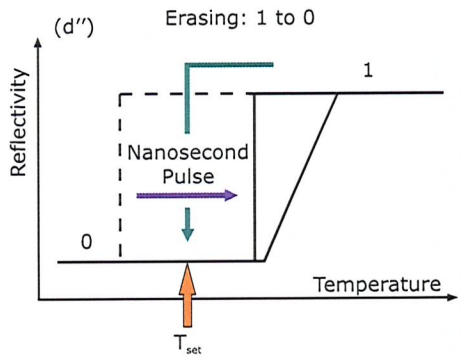

Figure 4.7: All-optical non-volatile memory. This step replaces (d) in the full write-erase cycle shown in Figure 4.2: Nanosecond pulsed excitation may be used to reduce the hysteresis shown by nanoparticles, thereby enabling information to be erased at a fixed temperature *inside* the hysteresis loop.

compare differences between the levels. To experimentally verify this principle of operation the previous setup was adapted to include a pulsed diode laser, operating at an intensity such that the energy supplied during each period was insufficient to induce a complete phase transition to the high reflective state, and at a repetition rate that allowed enough time for the system to recover between pulses. Figure 4.8(a) shows the actual 100 μs width , 2.5 kHz repetition rate, 3 mW peak power pulses used as the interrogation signal in the experiment. The induced reflectivity changes resulting from this excitation are shown in Figures 4.8(b) and 4.8(c), for the low '0' and high '1' states respectively. The memory can be written and erased using the same processes described above, but by extracting the sign of the induced reflectivity change, one can distinctly and reliably read the memory without affecting its state. In the low reflectivity state, the change induced by the pulses is positive, while in the high reflectivity state it is negative. The signal-to-noise ratios for these measurements were found to be 48 and 7.8 for the low and high reflectivity states respectively.

4.5 High-logic memory in a single nanoparticle

The previous section explained how a film of nanoparticles could be used as a memory element with functionality based on nanoscale effects. In contrast to optically bistable memory elements that rely on cavity resonances and optical feedback (which thus have a lower size limit of roughly a wavelength), this type

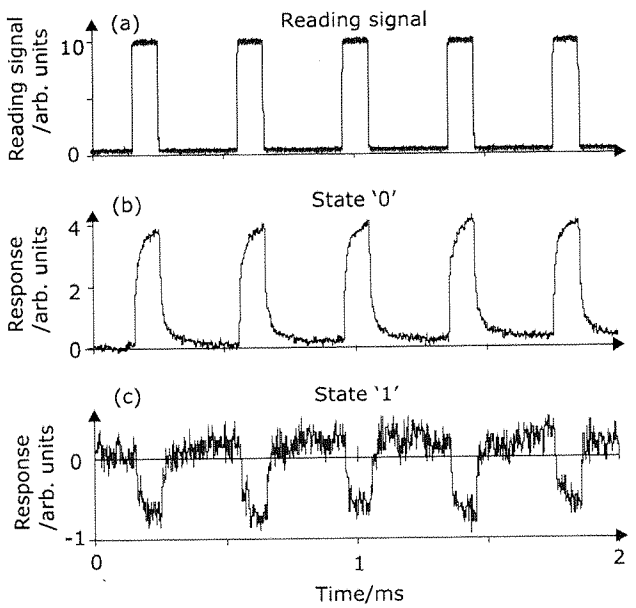

Figure 4.8: Differential change of reflectivity between the bias level and the induced change in the '0' and '1' level. As the pulses of the weak optical probe (peak power = 3 mW , frequency = 2.5 kHz) shown in (a) excite the nanoparticle film with an energy less than that of a full transition, the reflectivity of the low reflectivity state '0' is positively shifted as shown in (b). In (c) the shift for the high-reflectivity state '1' is seen to be negative. Switching between the two states is achieved with a single optical pulse of higher energy (peak power = 13.1 mW , pulse width = 1 μs).This type of measurement provides a more sensitive read-out of the nanoparticle memory state.

of memory functionality is based directly on differences in reflectivity between the structural phases and can in principle enable truly nanoscale memory elements. Nevertheless, in order to obtain such elements, one must be able to write and retrieve information to and from individual nanoparticles. This section describes the experimental demonstration of this type of single nanoparticle memory functionality.

The gallium nanoparticle used in this experiment was grown on the 30 nm aperture at the tip of a gold coated tapered fibre. The light-assisted deposition technique described in Section 3.3 was used to grow the nanoparticle (with a UHV pressure of 10^{-6} mbar and a deposition rate of ~ 3 nm/min for 30 minutes). The fibre was imaged with a SEM before and after the experiment and the images showed that a nanoparticle with a diameter of about 80 nm diameter was formed in the aperture (see Figure 3.4 of Section 3.3).

Having grown the nanoparticle in this position, the external fibre-optical setup illustrated in Figure 4.9 was used for its excitation and monitoring. To read out the structural phase of the nanoparticle induced reflectivity changes were monitored using a pump-probe technique: A cw diode laser of 1310 nm wavelength probed the particle's reflectivity, while another diode laser of 1550 nm wavelength modulated at a frequency $f = 2.5$ kHz acted as the pump. The reflected probe signal was measured by a photodetector, while a wavelength-division multiplexer (WDM) combined with a band-pass filter blocked reflected pump light. As described in Section 3.4, this type of pump-probe technique provides a reliable way of monitoring transitions between phases: The modulated pump gives a small periodic increase in the temperature of the particle, so the modulated component of the reflected probe signal is proportional to the temperature derivative of the particle's reflectivity. The detection of this modulated component of the reflected probe signal with a lock-in amplifier offers a substantially higher signal-no-noise ratio in monitoring the structural phase of the nanoparticle, than a direct measurement of small changes in the reflectivity of the particle.

As the temperature T is increased from 100 to 160 K, a sequence of narrow peaks in the induced reflectivity change is recorded, as shown in Figure 4.10(a).

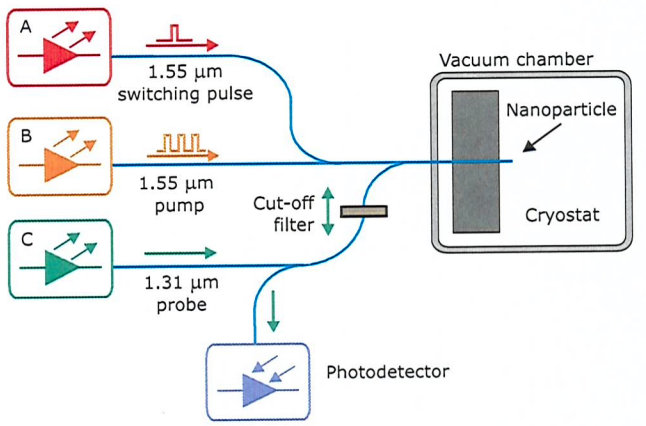

Figure 4.9: Experimental setup used to demonstrate the quaternary optical memory functionality of a single gallium nanoparticle grown on the end of a tapered optical fibre. Laser A delivers on-demand single pulses, used for switching the nanoparticle into each of the four different phases corresponding to the four levels of a quaternary logic memory element. The low-power modulated pump laser B and continuous wave laser C are used to monitor the logical state via induced reversible changes in the nanoparticle's reflectivity.

Each peak corresponds to a structural transformation between two phases of the nanoparticle, or equivalently between two logical states, with positive and negative peaks respectively corresponding to pump-induced increases and decreases in the nanoparticle's reflectivity. Starting from the base temperature of $T = 100\,\mathrm{K}$, the consecutive phases between the transition peaks are labeled '0', '1', '2' and '3' to represent the logical states of the memory element. Following the phase diagram of gallium [13], these states can tentatively be associated with the γ, ϵ, β and liquid phases. As the nanoparticle is cooled back to $T = 100\,\mathrm{K}$, the nanoparticle remains in state '3' until the pump and probe lasers are switched off, allowing the effective nanoparticle temperature to decrease sufficiently for the system to relax back to the initial '0'state.

In order to demonstrate the optical memory functionality of a single gallium nanoparticle, the switching between different logical states must be performed in a controlled way. Furthermore, for the nanoparticle to function as a higher-order logical element it is essential to demonstrate the possibility of switching the ground state into any targeted higher state by direct excitation. Experimentally this control was achieved by means of a third, manually triggered 1550 nm pulsed laser (laser A in Figure 4.9). While the pump

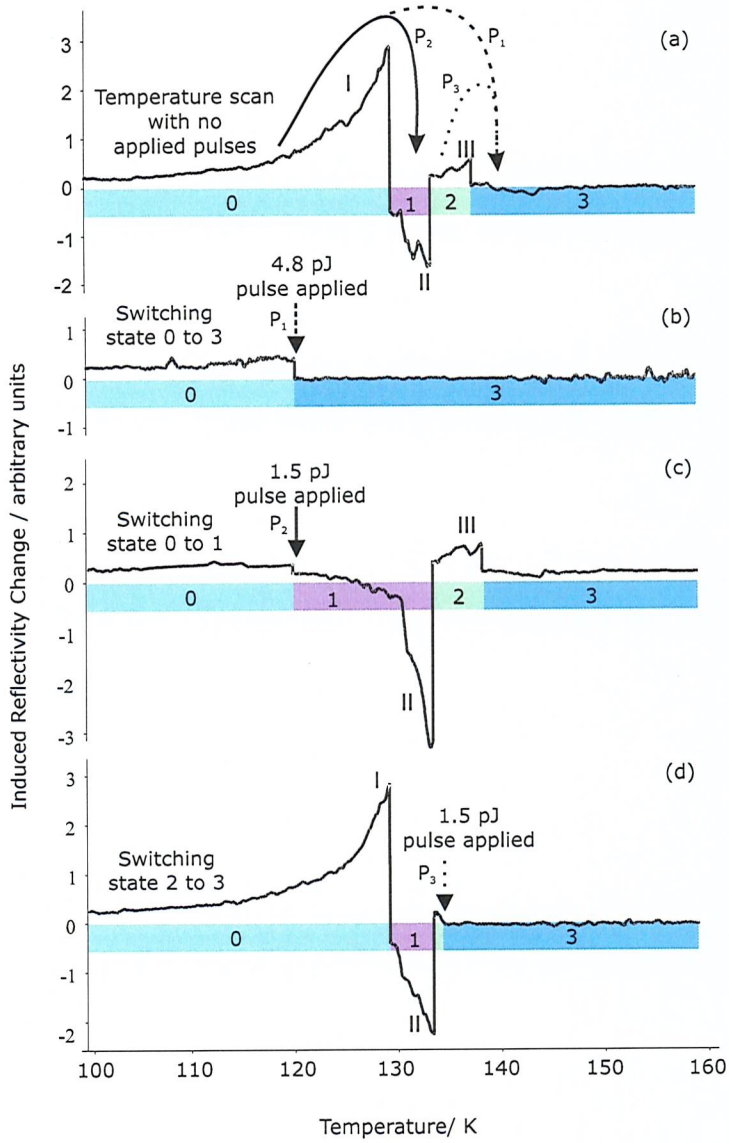

Figure 4.10: Quaternary memory functionality of a single gallium nanoparticle. A pump-probe technique is used to monitor the nanoparticle state. (a) Temperature dependence of the induced reflectivity change signal in the absence of writing pulses. (b) and (c) Temperature dependence of the induced reflectivity change signal with switching optical pulses of 1 μs duration and energies 4.8 pJ and 1.5 pJ respectively applied at $T = 120$ K. In (a), the particle undergoes a series of transitions between four states with different optical properties, while in (b) and (c) the particle is directly switched from state 0 into states 3 and 1, without passing through intermediate stages (these writing operations are indicated by labels P_1 and P_2 in (a)). Finally, in (d) a 1.5 pJ pulse is applied at $T = 135$ K, to switch the nanoparticle from state 2 to state 3 (indicated by label P_3).

laser (B) operated at an intensity such that the energy supplied was insufficient to induce a complete phase transition in the nanoparticle, the switching laser operated at higher powers, where complete transitions could be induced by a single optical pulse. Different nanoparticle states are then targeted by changing the total energy of the pulse.

Starting with the nanoparticle in the ground state '0', the temperature was increased to 120 K, and a single optical pulse of energy 4.8 pJ (at the particle) and duration 1 μs was applied to the system. This pulse changes the nanoparticle state from level '0' to level '3' as illustrated by the lack of further transitions peaks observed when the ambient temperature was further increased to 160 K (see Figure 4.10(b)). This absence of peaks in the remaining part of the scan is explained by the fact that the energy deposited in the nanoparticle by the switching pulse was large enough to fully transform it directly from state '0' to state '3'. After exposure to the optical pulse, the nanoparticle remained in this higher state even as the ambient temperature was reduced to the starting point temperature 100 K , due to the hysteresis present in the system.

In order to erase the nanoparticle memory, the temperature was reduced to 100 K and the lasers were switched off. The nanoparticle then returned to the ground state '0'. This fact was verified by an additional temperature scan that reproduced the graph shown in Figure 4.10(a).

The nanoparticle can be set into one of the intermediate memory states ('1' or '2') simply by using an optical pulse with less total energy than for the '0' to '3' transformation. For example, Figure 4.10(c) shows the result of increasing the temperature as before to 120 K and then applying a single optical pulse of energy 1.5 pJ and duration 1 μs for the excitation of the nanoparticle. In this case the absence of peak I and the presence of all the remaining peaks shows that the nanoparticle was transformed from state '0' to state '1'.

Finally, it is not necessary for the nanoparticle to begin in state '0'- switching between other states is also possible. Figure 4.10(d) shows precisely this for a transition between the states '2' and '3'. In this case the temperature was initially increased to 135 K, placing the nanoparticle in state '2', and at this point a 1.5 pJ pulse was applied. This time, the absence of peak III indicates that the particle was switched to state '3'.

In Section 4.4 it was explained that the entire write-erase cycle in nanoparticle films can be performed all-optically by keeping the cryostage temperature at a fixed value below the lower limit of the hysteresis, and by using the heating effect of the probe laser to obtain an effective set point within the hysteresis loop. In this scheme the erasing operation is executed simply by switching off the probe laser. The same technique can be applied to the single nanoparticle memory element, so that the writing, reading and erasing cycle of the nanoparticle memory can be repeated time and time again without any need to adjust the background temperature. However, for reasons of clarity, for this conceptual demonstration the results are presented in the temperature-erase format instead.

Using this type of quaternary logic, the potential data density achievable in a hexagonal close-packed lattice of 80 nm particles is about $0.2\,\mathrm{Tb/in^2}$. Obviously this requires the development of a mechanism to read and write information from an to individual particles when they are packed together in a film. One such possibility is the use of a tapered fibre head, in analogy to the way information is written in today's hard disks using a magnetic head. Technical issues aside, this value can be compared with the data densities for Blu-ray DVDs, $0.015\,\mathrm{Tb/in^2}$, and with the recent record of $0.23\,\mathrm{Tb/in^2}$ achieved in hard disks using perpendicular recording technology to go beyond the super-paramagnetic limit [3]. Additionally the energy required to write information to a nanoparticle, as little as 1.5 pJ, is at least an order of magnitude smaller than in today's state of the art devices [8]. Both of these values indicate that memory elements based on nanoparticles undergoing phase transitions certainly have the potential to compete with existing data storage technologies. However, the close spacing in terms of energy between the different phases involved probably mean that long term data storage capabilities will be far inferior than thoses of other phase change materials such as GST. In comparison to this type of materials, gallium also suffers of the obvious disavantage that in the nanoparticle form its phase transitions occur at very low temperatures. This means that although an excelent material for testing the proposed concepts, it is not suited for commercial applications. Research into materials that can form nanoparticles, have a range of phases available, and which transitions happen at more favorable temperatures, is, therefore, an important priority.

4.6 Summary and conclusions

The idea of using nanoparticles undergoing light-induced structural transformations as optical memory elements has been introduced. Furthermore, it has been experimentally demonstrated that a film of gallium nanoparticles can act as a two level rewritable all-optical memory, and that a single gallium nanoparticle alone can act as an all-optical quaternary logical memory element.

A nanoparticle presenting a number of different phases closely spaced in energy but with contrasting optical properties, in which phase changes can be optically excited, and which shows a significant hysteresis in optical properties with temperature may be used as a low power nanoscale all-optical memory element.

Using a gallium nanoparticle film grown at the end of a standard telecommunications fibre it was experimentally shown that single optical pulses of 13.1 mW peak power and 1 μs duration can write information to the nanoparticles by converting them from the β gallium phase to the liquid phase. It was also shown that despite the small reflectivity differences between the two phases, the contrast between them could be improved by using a modulated reading beam and looking at the induced change caused by this beam. Two operational schemes to erase the memory were experimentally demonstrated: One worked by directly reducing the particles' base temperature and the other by turning off the probe laser temporarily to achieve the necessary temperature reduction. It was also proposed that high intensity nanosecond pulses could be used to reduce the hysteresis present thereby facilitating another way to bring the particle back to the ground state.

Finally, the experiment was moved one step further to the use of a single a 80 nm gallium nanoparticle for the demonstration of a four level nanoscale optical memory element. In this case, writing was achieved using single optical pulses with as little as 1.5 pJ of energy at the particle, and it was possible to switch from the low temperature state to any of the higher energy states by changing the energy of the pulse. Switching from intermediate phases was also demonstrated. Assuming that individual particles like this could be individually addressed when closely packed together, a storage density of about 0.2 Tb/in^2 could be achieved, a value of the same order of recent records in labs developing hard disk technologies.

The results presented in this Chapter clearly show the potential for nanoparticles to provide memory functionality in future highly integrated nanophotonic devices, operating at very low power levels.

4.7 References

[1] L.D. Stevens *IBM Journal of Research and Development* **25**(5): 663 (1981).

[2] T. Noyes, and W. E. Dickinson *IBM Journal of Research and Development* **1**(1): 72 (1957).

[3] Reported by *Hitachi Global Storage Technologies*, see http://www.hitachigst.com/hdd/research/ (2005).

[4] F. Masuoka, M. Asano, H. Iwahashi, T. Komuro, and S. Tanaka *International Electron Devices Meeting* San Francisco, California (1984).

[5] Reported by *Samsung Electronics*, see http://www.samsung.com/he/presscenter/pressrelease/ (2006).

[6] Reported by *InPhase Technologies*, see http://www.inphase-technologies.com/news/ (2006).

[7] H. Gibbs *Optical bistability: controlling light with light* Academic Press, Orlando (1985).

[8] M. H. R. Lankhorst, B. W. S. M. M. Ketelaars, and R. A. M. Wolters *Nature Materials* **4**(4): 347 (2005).

[9] G. A. Gibson, A. Chaiken, K. Nauka, C. C. Yang, R. Davidson, A. Holden, R. Bicknell, B. S. Yeh, J. Chen, H. Liao, S. Subramanian, D. Schut, J. Jasinski, and Z. Liliental-Weber *Applied Physics Letters* **86**(5): 051902 (2005).

[10] H. F. Hamann, M. O'Boyle, Y. C. Martin, M. Rooks, and K. Wickramasinghe *Nature Materials* **5**(5): 383 (2006).

[11] *Nanoelectronics and Information Technology* Wiley-VCH, Weinheim (2005).

[12] D. E. Knuth *The Art of Computer Programming, Volume 2, Seminumerical Algorithms* Addison-Wesley, Reading (1998).

[13] A. Defrain *Journal De Chimie Physique Et De Physico-Chimie Biologique* **74**(7-8): 851 (1977).

[14] D. Frohman-Bentchkowsky *IEEE J. Solid-State Circuits* **6**(5): 301 (1971)

Chapter 5

Summary and future work

5.1 Summary

Two different types of nanoscale photonic functionality based on novel implementations of light-induced structural transitions in nanoparticles have been proposed and demonstrated. It has been shown that depending on the excitation regimes to which the nanoparticles are subjected they can act as low power nanoscale optical switches or as optical memory elements.

For the first time, optical switching has been observed simultaneously in reflection and transmission in a gallium nanoparticle film grown on the end of a standard single mode optical fibre by light-assisted deposition (see Chapter 2). The switching is related to a sequence of light-induced structural transitions that allow for reversible control of the optical properties of the nanoparticles: As the temperature is cycled between 80 and 300 K the nanoparticles show reflective and transmissive transition-based nonlinear responses to low-power near-infrared excitation. At least two of gallium's metastable crystalline phases and the liquid phase are involved and the response can be observed at pump frequencies as high as 1 MHz. These measurements of the megahertz dynamics of light-by-light control in a particle film have also provided new insight into the kinetics of solid-solid and solid-liquid structural transformations in nanoparticles. They indicate that solid-solid transitions are faster and more symmetrical than the solid-liquid transition, in agreement with the fact that the recrystallization time is longer than the melting time.

Furthermore, a femtosecond pulsed laser has been used for second harmonic generation in the nanoparticle film and it has been shown that the transmitted

nonlinear signal gives larger contrast between phases than the linear transmission at the same wavelength. The results of an effective medium model for the optical properties of closely packed nanoparticle films are consistent with the observed excitation-induced increases in the transmission and reflection of the gallium nanoparticle film.

A novel system to grow and study individual nanoparticles has been developed (see Chapter 3). An atomic beam has been used to grow single gallium nanoparticles in the nanoaperture at the tip of a tapered gold-coated optical fibre, and for the first time reversible light-induced reflectivity changes associated with a sequence of transformations between different structural forms, stimulated by optical excitation with powers as low as 10 nW, have been observed in such particles. With increasing temperature, the gallium nanoparticle is believed to go through the following sequence of transitions between different structural forms: $\gamma \rightarrow \epsilon \rightarrow \delta \rightarrow \beta \rightarrow$ liquid, each transition having a sharp peak in the induced reflectivity change signal associated with it. An extra peak with different characteristics may be evidence of a shape change in the particle.

Furthermore, it has been discovered that the extent of the overcooling hysteresis displayed by nanoparticles can be controlled by varying the optical pumping regime. If a modulated cw pump is used to excite the gallium nanoparticles, they show overcooling of up to 90 K, but if subjected to high intensity, low power nanosecond pulses, the hysteresis width falls to less than 5 K.

The idea of using nanoparticles undergoing light-induced structural transformations as optical memory elements has been introduced and the first proof of concept demonstration of such all-optical nanoscale memory functionality has been performed (see Chapter 4). It has been experimentally shown that single 1 μs optical pulses of 13.1 mW peak power can 'write' information to a gallium nanoparticle film by converting the particles from a lower energy phase (logic state 0) to a higher energy phase (logic state 1) with a different reflectivity. As the reflectivity difference between the two phases is small, an alternative high contrast method for 'reading' the state of the nanoparticle memory, based on measurements of reflectivity change induced by a modulated pump beam, has been developed. Both volatile and non-volatile modes of operation have been demonstrated: In the two alternative operation

schemes, the memory was erased either by directly reducing its base temperature or by turning off the probe laser temporarily to achieve the necessary cooling. It has also been suggested that erasure could be achieved using nanosecond high intensity pulses to narrow the hysteresis and return the particles to the ground state.

For the first time, a four-level nanoscale optical memory element has been demonstrated using a single 80 nm gallium nanoparticle. Information is encoded by switching the particle between the different phases with single optical pulses with energies as low as 1.5 pJ. By changing the total pulse energy different phases can be directly accessed from both ground and intermediate states. If a convenient way to access individual particles within a closely packed array is developed a storage density of about $0.2\,\mathrm{Tb/in^2}$ could be achieved.

The results presented in this thesis have helped to improve the understanding of nanoscale light-induced phase transitions, and have illustrated the potential of single nanoparticles for achieving low power nanoscale photonic functionality.

5.2 Future work

Numerous new research opportunities have opened up to the research group in Southampton with the recent acquisition of a scanning electron microscope (SEM). It has already been demonstrated that gallium nanoparticles can be grown, and subjected to the type of optical studies reported in this thesis inside the SEM chamber.

The SEM will help to shed new light on the details of the nanoparticle growth process. By looking at nanoparticles in real time as atomic beam deposition is happening, one will be able to understand exactly how different types of laser excitation affect the formation of the nanostructures. This will lead to better control of the size distribution of the particles and may perhaps allow films with a much smaller average gallium nanoparticle radius to be obtained. Very small nanoparticles, called clusters, raise another set of interesting questions, as their size means that quantum effects become significant and a number of unusual phenomena, such as quantum shell melting appear. In terms of the manufacturing process, another very interesting possibility is the use of the electron beam itself to control the growth of the particles or maybe even to create custom designed patterns of nanoparticles.

Another possibility is the use of electron backscatter diffraction (EBSD). This very useful technique allows crystallographic information to be obtained from samples inside the SEM. It has already been tested, and successfully identified different domains in an aluminium/gallium sample, but the greatest promise of this technique may lie in its use for the analysis of nanoparticle films. Among other possibilities, this would allow information about the particles' structure to be obtained directly alongside the complementary information acquired by optical probing.

In terms of the optical properties of the nanoparticles, a full analysis of their spectra in both transmission and reflection while they undergo phase transitions will soon be performed and the data obtained will allow more accurate numerical models to be developed. Very little information exists on the values of the dielectric constants for gallium's metastable phases and this study should change that. It should also give a better understanding of the shell model for nanoparticle phase transitions.

With the demonstration of nanoparticle memory functionality presented in this thesis a new area of research has been opened up. A more detailed study of this type of functionality could prove crucial to the development of future nanophotonic devices. Particular attention should be paid to the understanding of how high intensity nanosecond pulses appear to the break the thermal hysteresis shown by the particles, thus allowing the memory to be erased using light pulses. Another interesting research avenue would be the study of ways to address individual particles within a closely packed array.

Additionally, the work with single particles should be further developed. In particular, the low energies involved in the processes described in this thesis, mean that it may be possible to fully convert a nanoparticle with a diameter of a few nanometres into a new phase with the energy obtained by absorbing only a few or perhaps even just a single photon. This could make single-photon all-optical switching a reasonable possibility.

Yet another path that should be carefully analyzed is the search for ways to integrate nanoparticles into other types of promising nanophotonics materials. For example, nanoparticles could be used to switch light signals inside a three-dimensional photonic band-gap optical router, to control the output of miniature semiconductor lasers, or as active elements inside hollow fibres.

Another interesting emerging research field is the area of active plasmonic devices, i.e. devices capable of switching surface plasmon-polariton (SPP) signals. It has already been shown that the kind of nanoscale structural phase transitions described in this thesis can control SPP signals by reversibly altering the properties of a SPP waveguide (a metal/ dielectric interface). Ongoing experimental work in this field should yeild further developments.

Finally, one should note that although gallium nanoparticles are an excellent 'playground' in which to study and understand the physics involved in achieving nanoscale optical functionality through phase transformations, the low temperatures at which the transitions occur for pure gallium make them unlikely candidates for commercial applications. Thus, the search for materials that present a range of crystalline phases closely spaced in energy but with different optical properties and phase transitions that occur in nanoparticles closer to room temperature should be high in the research priorities. Applying the techniques discussed in this thesis to a material with such properties could lead to a wide range of commercially viable products based on nanoscale photonics.

Appendix A

Obtaining relaxation time information from the phase data of a lock-in amplifier

Lock-in amplifiers can detect and accurately measure small AC signals even when the noise is many thousands of times larger that the signal of interest. They work by extracting the component of the signal at a certain reference frequency and phase and are therefore extremely useful instruments when studying the response of systems excited with a periodic oscillation. This Appendix explains how the temporal phase data measured by a lock-in amplifier can provide some insight into the dynamics of excitation-induced transitions in nanoparticles.

It is useful to start by analyzing the simple case in which a square-wave signal of period T, is slightly altered so that the "on" part of the cycle is extended by a small amount of time ΔT (see Figure A.1).

The Fourier series expansion of a function $f(t)$ with period T is given by:

$$f(t) = \frac{a_0}{2} + \sum_{n=1}^{\infty} [a_n \cos(w_n t) + b_n \sin(w_n t)]$$

Where

$$w_n = n\frac{2\pi}{T}$$

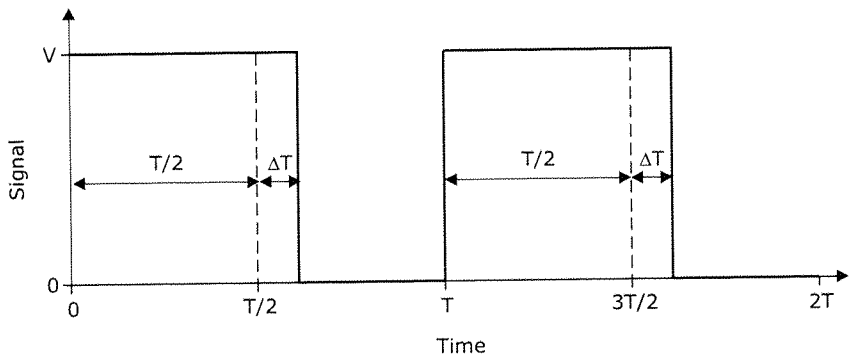

Figure A.1: Representation of a square-wave signal with period T and 'on'-cycle width of $T/2 + \Delta T$.

$$a_n = \frac{2}{T}\int_{t_0}^{t_0+T} f(t)\cos(w_n t)dt$$

$$b_n = \frac{2}{T}\int_{t_0}^{t_0+T} f(t)\sin(w_n t)dt$$

Thus, for the signal shown in Figure A.1:

$$\begin{aligned} f(t) &= \frac{T/2+\Delta T}{T}V + \\ &+ \sum_{n=1}^{\infty}\frac{V}{n\pi}(-1)^n \sin(w_n\Delta T)\cos(w_n t) + \\ &+ \sum_{n=1}^{\infty}\frac{V}{\pi n}[1-(-1)^n\cos(w_n\Delta T)]\sin(w_n t) \end{aligned}$$

The lock-in amplifies this signal and then multiplies it by the lock-in reference signal using a phase-sensitive detector or multiplier (PSD). In a two channel instrument there are two PSDs, working with a $\pi/2$ phase shift between them. That is, if the reference signal for channel X is taken to be $\sin(w_{ref}t + \theta_{ref})$ then for the Y channel it would be $\sin(w_{ref}t + \theta_{ref} + \pi/2) = \cos(w_{ref}t + \theta_{ref})$. The reference phase θ_{ref} can be chosen arbitrarily, but to simplify calculations here it will be taken to be 0. Thus, for each channel the signal after the PSD is given by:

$$V_X^{PSD}(t) = f(t)sin(w_{ref}t)$$

$$V_Y^{PSD}(t) = f(t)cos(w_{ref}t)$$

These signals are then passed through low pass filters to remove any AC component. For the present case the signals after the filters will be:

$$V_X^{filter} = \frac{V}{2\pi}[1 + \cos(w_{ref}\Delta T)]$$

$$V_Y^{filter} = -\frac{V}{2\pi}\sin(w_{ref}\Delta T)$$

The phase θ recorded by the lock-in is related to the ratio of these signals:

$$\tan(\theta) = \frac{V_Y}{V_X} = -\frac{\sin(w_{ref}\Delta T)}{1 + \cos(w_{ref}\Delta T)} = \tan(-\frac{w_{ref}\Delta T}{2})$$

From this expression one obtains the following relationship between ΔT , the period T and the measured phase θ:

$$\Delta T = -\frac{\theta}{\pi}T$$

Note, that the minus sign in this expression appears because the phase difference measured by a lock-in amplifier in this way is negative. This expression shows that information about the temporal characteristics of the signal can indeed be obtained from the lock-in phase data. In the case of the light-induced phase transitions in nanoparticles reported in this thesis, the initial response to pump excitation is much faster than the recovery when the excitation is removed. Thus, the response of the system can be approximated by the signal shown in Figure A.2.

It can be shown that for this signal shape, the above relation holds provided that ΔT is taken to be the width of the decay part of the signal at half the maximum voltage level. From the figure it should also be evident that this relation is only meaningful if ΔT is less than $T/4$, that is if the measured phase

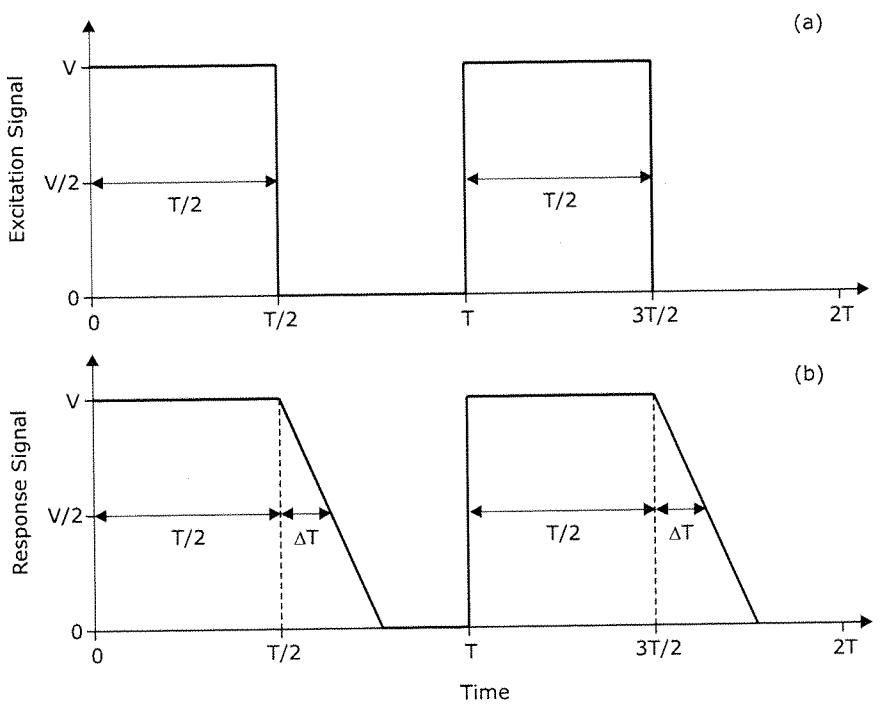

Figure A.2: Approximation of nanoparticle response (b) to a square-wave excitation signal with period T (a). The rising part of the response curve is much faster than the decay part, so the signal can be approximated by a square signal with an extra triangular decay section with a half maximum width equal to ΔT.

is less than $\pi/4$. Finally, it should be noted that this method doesn't allow for exact relaxation times to be obtained (only their approximate magnitude) but it is nevertheless very useful, particularly when it comes to comparing the relaxation times of different transitions in the same sequence.

Appendix B

Sample List

The table belows presents a list of all samples produced during the period of time in which the work described in this thesis was executed. Brief summaries of the experiments performed, the main properties and any important notes are given for each sample. Note that a sample described to be 'ok' showed similar measurement characteristics to typical results presented in this thesis. A list of abbreviations used is given at the end of this appendix.

SN	*Date*	*F*	*Experiments performed and sample properties*	*Notes*
1	2002/10/16	S	*Dep.:* slow changes. *TS:* OP ok; no SF; LR ok	Bad fibre alignment
2	2002/11/13	S	*Dep.:* ok. *TS:* OP ok; LR ok; no LT; no SF	
3	2002/11/26	S	*Dep.:* slow changes; very small increase in LR	Too small hole in integration sphere makes alignment difficult: size increased.
4	2002/11/28	S	*Dep.:* ok. *TS:* OP ok; LR ok; LT noisy; no SF; NLR ok	
5	2002/12/06	S	*Dep.:* ok; *TS:* OP ok; LR noisy; SF noisy; NLR ok;	
6	2002/12/13	T	*Dep.:* LT and LR down; SFR changed; *TS:* no repeatable changes in either signal	

SN	*Date*	*F*	*Experiments performed and sample properties*	*Notes*
7	2003/01/21	T	*Dep.:* LT jump; LR no change; *TS:* SFT noisy but some sort of peaks in real slow scan; no NLR	Too much power used
8	2003/04/03	S	*Dep.:* OP ok; LR noisy; LT changed *TS:* LR noisy; LT jumps but noisy; SFT no signal	Transmission detector moved into chamber
9	2003/05/16	S	*Dep.:* T signal saturates when shutter open: too much light from effusion cell	T. detector temp. stabilized; power levels decreased.
10	2003/05/28	S	*Dep.:* Op ok; LR ok; *TS:* LR ok; LT change but no hyst. seen	Changed holder to obtain better thermal contact.
11	2003/06/02	S	*Dep.:* OP ok; LR ok; *TS:* LT bad; SFT changed but noise;	LT changes as before even with no gallium; rest ok; abandoned SF exps and opted for NL type only as noisy level too high.
12	2003/06/05	S	Tried to put drop of Se and see any changes in signals: no success; also tried spectral difference: not successful.	
13	2003/06/11	S	Further Se experiments: not successful.	
14	2003/07/21	S	*Dep.:* LR ok; OP ok; *TS:* LR; NLR and NLT initially noisy, then after adjustments NLR and NLT ok;	First experiments with NL setup. Introduced mechanical shutter to reduce leakage in T.
15	2003/07/28	S	*Dep.:* LR ok; OP ok; *TS:* NLR; NLT ok; PD ok; HF ok;	Extensive PD and HF study
16	2003/09/05	PT	*Dep.:* no change	
17	2003/09/09	PT	*Dep.:* LT small change; *TS:* all signals noisy	
18	2003/09/12	PT	*Dep.:* no change	
19	2003/09/17	S	*Dep.:* no change	Put more gallium in effusion cell

SN	*Date*	*F*	*Experiments performed and sample properties*	*Notes*
20	2003/10/15	S	*Dep.:* measurement settings error	
21	2003/10/16	S	*Dep.:* LR ok; OP ok *TS:* LR;NLR and NLT ok	
22	2003/10/24	PT	*Dep.:* no signal changes; *TS:* no NL signals	Detected laser problem
23	2003/10/28	T	*Dep.:* NLT and LR noisy; NLR decreasing; *TS:* NLR detected	
24	2003/10/31	T	*Dep.:* NLR change; *TS:* NLR ok	Tested cleaning gallium with high power and depositing again: works.
25	2003/11/04	T	*Dep.:* ok; *TS:* NLR no change	
26	2003/11/06	T	*Dep.:* ok; *TS:* NLR ok; PD ok	
27	2003/11/27	T	Dep.: ok; *TS:* NLR ok; PD ok; multiple peaks first seen; signals remain even after 5 weeks	Extensive tests to optimize signal and reduce noise
28	2004/01/07	T	*Dep.:* ok; *TS:* NLR ok- multiple peaks again present; NLT still noisy	Introduced shades in chamber windows to try improve T signals; new T detector
29	2004/02/11	T	*Dep.:* ok; *TS:* NLR ok- now confident with reproducibility ; no NLT; attempts at nanosecond excitation	Extensive tests to measure nanosecond excitation
30	2004/03/16	T	Dep.: ok; TS: NLR ok; nanosecond signal ok	
31	2004/04/15	T	Dep.: ok; TS: NLR ok; LR: noisy	Extensive test to improve LR measurements: no success
32	2004/04/26	T	Dep.: ok; NLR ok; PD ok;	Extensive characterization
33	2004/07/13	SL	Testing SHG setup outside chamber	Gallium slabs from previous work; until stated Nd:YLF laser used as SH pump

SN	*Date*	*F*	*Experiments performed and sample properties*	*Notes*
34	2004/07/20	S	*Dep.:* ok; *TS:* NLR ok; SHGT signal detected	Laser problems: stops mode-locking and power fluctuations; also leakage from pump
35	2004/07/29	S	*Dep.:* ok; *TS:* NLR ok; SHGT noisy	Cut leakage with extra filters; laser still fluctuating
36	2004/08/19	S	*Dep.:* ok: *TS:* NLR ok; SHGT outside chamber to try improving measurements: noisy	Introduced SHG crystal to normalize power; also introduced isolator in laser path: helps stability
37	2004/10/05	SL	SHGT outside chamber: signal finally stable	
38	2004/10/06	T	*Dep.:* no signal change; *TS:* NLR noisy	
39	2004/10/07	T	*Dep.:* noisy signal; *TS:* NLR noisy	After extensive testing, realized fibre was broken near feedthrough: replaced
40	2004/10/25	T	*Dep.:* Ok; *TS:* NLR ok; PD ok; LR noisy	Extensive optimization attempt in preparation for time-resolved experiments
41	2004/11/02	S	SHG outside chamber: noisy	First attempts at SHG from Ga in fibre
42	2004/11/04	S	*Dep.:* error-see note; *TS:* no NLR; OP: there but no change in temp.	Pulsed laser only on half-way through deposition by mistake.
43	2004/11/19	S	*Dep.:* ok; *TS:* NLR ok; SHG outside chamber detected; SHG PD initially ok, but too much power changed signal	Extensive testing outside chamber to understand SHG detection

SN	*Date*	*F*	*Experiments performed and sample properties*	*Notes*
44	2004/11/22	S	*Dep.:* slower change (1h30m); *TS:* no NLR	New holder to allow SHGT measurements in chamber introduced;
45	2004/11/23	S	*Dep.:* small change(1h40m); *TS*: no NLR	Deposition temperature slightly higher than usual, so cleaned up cooling system
46	2004/11/25	S	*Dep.:* slower change but deposited 1h; *TS:* no NLR	Extensive testing for problem; possible misalignment of new holder
47	2004/11/26	S	*Dep.:* very slow change;*TS:* no NLR	Tried better alignment, but it got worse
48	2004/11/30	S	*Dep.:* slow change; OP signal always negative; *TS:* no NLR;	Replaced new holder with old sphere; still problems; realized temperature in effusion cell- higher by 40K than usual
49	2004/12/02	S	*Dep.:* ok; *TS:* NLR ok;	Reduced effusion cell temperature
50	2004/12/04	S	*Dep.:* faster;*TS:* no NLR	Increased effusion cell temperature; so problems were from bad alignment of new holder and increased temperature in cell
51	2004/12/05	S	*Dep.:* ok; *TS:* LR ok; NLR OK:HF ok;	NLR on scope: frequency from 200Hz up to 200kHz
52	2004/12/11	T	*Dep.:* ok; NLR noisy;	
53	2004/12/15	T	*Dep.:* ok; NLR ok;	Noise level characterization, testing with and without cell on
54	2005/01/28	S	*Dep.:* ok; NLR noisy	Effusion cell rebuilt after heating element broke

SN	*Date*	*F*	*Experiments performed and sample properties*	*Notes*
55	2005/02/02	S	*Dep.:* ok; LR noisy; *TS:* NLR ok;	Fibre then transferred to new holder and first attempts at T in photon counter; chamber viewport broken
56	2005/02/11	S	*Dep.:* slow (3h); *TS:* no NLR	New viewport; deposition now with new holder; adjusted effusion cell T to compensate for different holder
57	2005/02/15	S	*Dep.:* ok; *TS:* NLR ok; very small change in LT at 660nm; SHG signal detected but laser stability makes it hard to do T scan.	In this and following samples all SHG and LT measurements are performed by rotating sample mount by 90 degrees and using photon counter; decided to hold SHG exp. until laser problems solved.
58	2005/03/10	S	*Dep.:* ok; *TS:* NLR ok	First attempts at spectral measurements; but fibre damaged when moving to vertical
59	2005/03/17	S	*Dep.:* ok; *TS:* NLR measurement problems	Problems traced to faulty cable
60	2005/03/18	S	*Dep.:* ok; *TS:* LR ok; NLR initially noisy but then ok- see note; SM: not successful	Noise improves by cleaning all fibre connections in system each day
61	2005/04/07	S	*Dep.:* ok; *TS:* NLR initially ok; SM: no change detected; and subsequent NLR tests also not showing changes	Mirror placed in shutter to try SM without moving fibre.

SN	*Date*	*F*	*Experiments performed and sample properties*	*Notes*
62	2005/04/08	S	*Dep.:* ok; *TS:* NLR ok; extensive SM attempts but noise levels always too high; new attempts at SHG with laser slightly more stable, but still not good enough.	A better spectrometer and a different experimental setup could have made this SM possible, but as the new SEM system was already being built it was decided to leave this work for a later time.
63	2005/05/19	S	*Dep.:* small LR change; *TS:* no NLR	Chamber was cleaned and all gaskets changed
64	2005/06/06	S	*Dep.:* ok; NLR ok; *Memory:* switching seen when manually turning on lasers and cooling by removing all power; single pulse switching successful monitoring first NLR and then also LR;	Film memory experiments
65	2005/07/04	S	*Dep.:* ok; *TS:* NLR ok; *Memory:* single pulse NLR and LR switching ok; time resolved experiments attempted of rise and decay times: not successful	
66	2005/08/04	S	*Dep.:* ok; *TS:* NLR ok; SHG difference between hot and cold observed; temp. cans not successful as lab temperature still drifting too much and laser changing.	Returned to SHG attempts: this time with Fianium Fibre Supercontinuum Femtosecond Source SC1060-1 as a pump.

SN	*Date*	*F*	*Experiments performed and sample properties*	*Notes*
67	2005/09/26	H	*Dep.:* ok; *TS:* NLT ok but transition at lower temperature than usual making it hard to use higher power; attempted to deposit on top to increase transition point but not successful	The entire setup was moved into a new lab; 1060nm fibre introduced to improve on pump propagation for SHG experiments.
68	2005/09/27	H	*Dep.:* effusion cell temperature increased to try and improve transition point: not successful: NLR still low	Attempt to increase transition point by change effusion cell temperature.
69	2005/09/28	H	*Dep.:* decreased cell temperature to improve transition point; not successful: transition still low.	Attempt to decrease transition point by change effusion cell temperature.
70	2005/10/10	H	*Dep.:* ok ; *TS:* NLR ok; LR ok; sample moved to vertical position and signals lost: might have touched it	Trimmed down holder to try and improve temperature in sample.
71	2005/10/20	H	*Dep.:* very small LR change; then on heating huge increase: 50x, and drop at hot to 20x starting level; *TS:* NLR present but no change in temperature	
72	2005/10/26	H	*Dep.:* same problems as sample 71.	As a result: cleaned chamber and changed all gaskets.
73	2005/10/29	H	*Dep.:* ok; *TS:*NLR ok; SHG: laser stability increased but changes with temperature aren?t reproducible	Heating resistor broke so opened chamber after deposition to repair.
74	2005/11/10	H	*Dep.:* LR change higher than usual (final level 20%); *TS:*NLR no change;	Improved power normalization; trimmed holder further to increase transmission to detector further.

SN	*Date*	*F*	*Experiments performed and sample properties*	*Notes*
75	2005/11/12	H	*Dep.:* stopped when usual LR reached; *TS:* NLR transition at lower T than usual: only occurs if left cold and with lasers off.	Decreased effusion cell temperature by 20K
76	2005/11/13	H	*Dep.:* ok; *TS:* NLR ok; SHG signal change detected; SHG PD at hot and cold; noisy area appeared in signals between 170-220K	Effusion cell temperature increased by 10K. Problems with laser instability if people enter and exit lab.
77	2005/11/24	H	*Dep.:* ok; *TS:* NLR ok; SHG temp. scans successful; LT at 523nm shows no change; PD at hot and cold ok;	New fibre feedthrough in system as old fibres seemed to be broken.
78	2005/12/13	H	*Dep.:* large drop in LR on heating;	
79	2005/12/14	H	*Dep.:* large drop in LR on heating;	Cleaned everything and changed all gaskets.
80	2005/12/15	H	*Dep.:* ok; *TS:* NLR ok; SHG ok; simultaneous pump-probe NLR and SHG successful, but high noise.	
81	2005/12/16	H	*Dep.:* ok; *TS:* NLR ok; SHG ok; noise level measurements	Problems with cooling system prevented some scans to be completed;
82	2006/01/10	H	*Dep.:* change in LR detected before shutter open; *TS:* NLR noisy	Decided to clean chamber, replaced gaskets and service pumps
83	2006/01/11	H	*Dep.:* error in optical setup detected half-way through deposition	
84	2006/01/12	H	*Dep.:* ok; *TS:* NLR: ok; SHG ok; PD SHG ok; fibre images taken in SEM	New upgraded version of Fianium laser introduced with great improvement in stability.
85	2006/01/18	SL	EBSD trial measurements in SEM on bulk gallium: alpha phase identified at low temperature	A EBSD system was on trial for 1 month on the SEM system.

SN	*Date*	*F*	*Experiments performed and sample properties*	*Notes*
86	2006/01/24	SL	EBSD trial measurements in SEM on gallium aluminium structure: distinguished between areas with possible different phases and aluminium only regions	
87	2006/01/26	SL	Deposited Ga on Al in slab; EBSD patterns detected but and possible beta phase match but low signals from most areas	
88	2006/01/30	SL	Gallium drop on fresh Al; SEM shows arms forming of Ga spreading through aluminium; mapping is extremely hard to obtain	
89	2006/03/07	T	*Dep.:* Ok; *TS:* NLR ok; PD to try to identify switching levels: not successful	First attempts at single particle memory experiments
90	2006/03/14	T	*Dep.:* Ok; *TS:* NLR ok; PD to try to identify switching: successful; single pulse switching between different phases; SEM images taken of fibre before and after deposition showing single particle in aperture	
91	2006/03/29	T	*Dep.:* OK; *TS:* NLR ok; single pulse switching ok; attempting erase with pulse: not successful	
92	2006/03/30	T	*Dep.:* OK; *TS:* NLR ok; single pulse switching ok; erase with pulse not successful	
93	2006/04/01	T	*Dep.:* OK; *TS:* NLR ok; single pulse switching ok; PD of switching study; erase with pulse not successful	
94	2006/04/17	S	*Dep.:* Ok; *TS:* NLR ok; tried to see hysteresis reduction in nanoparticle film: not successful	

Abbreviations used:

SN: sample number

F: fibre type

S: standard telecommunications optical fibre single mode at 1310 nmand 1550 nm

T: gold-coated silica single-mode tapered fibres produced by Jasco Corporation

PT: tapered fibre pulled from single-mode standard telecommunications fibre

H: single mode fibre at 1060 nm

SL: microscope slab

Dep.: deposition

Temp.: temperature

T: transmission

R: reflection

LT: linear transmission

LR: linear reflection

NLR: nonlinear reflection, i.e., induced reflectivity change measured in lock-in amplifier

NLT: nonlinear transmission, i.e., induced transmission change measured in lock-in amplifier

OP: oscilloscope pulse, i.e., induced reflectivity change signal measured in oscilloscope.

SF: pump-probe sum frequency signal

SHG: second harmonic generation

PD: power dependence measurements

HF: high-frequency measurements

EBSD: electron backscattered difraction

Appendix C

Refereed publications

[1] **Resetting single nanoparticle structural phase with nanosecond pulses**
B.F. Soares, K. F. MacDonald, and N.I. Zheludev *Applied Physics Letters* **91**: 043115 (2007).

[2] **All-optical phase-change memory in a single gallium nanoparticle**
B.F. Soares, F. Jonsson, and N.I. Zheludev *Physical Review Letters* **98**: 153905(2007).

[3] **Polymorphic nanoparticles as all-optical memory elements**
B. F. Soares, M. V. Bashevoy, F. Jonsson, K. F. MacDonald, and N. I. Zheludev *Optics Express* **14**(22): 10652 (2006).

[4] **Controlling light with light via structural transformations in metallic nanoparticles**
K. F. MacDonald, B. F. Soares, M. V. Bashevoy, and N. I. Zheludev *IEEE J. Sel. Top. Quant.* **12**(3):371 (2006).

[5] **Light-induced structural transformations in a single gallium nanoparticulate**
B. F. Soares, K. F. MacDonald, V. A. Fedotov, and N. I. Zheludev *Nano Lett.* **5**: 2104 (2005).

[6] **Oscillating bubbles at the tips of optical fibers in liquid nitrogen**
K. F. MacDonald, V. A. Fedotov, S. Pochon, B. F. Soares, and N. I. Zheludev C. Guignard, A. Mihaescu, and P. Besnard *Physical Review E* **68**: 027301 (2003).

[7] **All-optical switch and memory element based on a single nanoparticle**
B. F. Soares, F. Jonsson, and N. I. Zheludev in *9th International Conference on Near-field Optic, Nanophotonics and Related Techniques*, paper Tu2-3 (2006).

[8] **A nanoparticle as a bit of optical memory**
B. F. Soares, M. V. Bashevoy, K. F. MacDonald, F. Jonsson, and N. I. Zheludev in *Quantum Electronics and Photonics-17 at Photon06* (2006).

[9] **Nonlinear plasmonics in a gallium/aluminium nano-composite**
K. F. MacDonald, A. V. Krasavin, B. F. Soares, M. V. Bashevoy, F. Jonsson, and N. I. Zheludev in *Quantum Electronics and Photonics-17 at Photon06* (2006).

[10] **Dynamic structural equilibrium in self-assembled nanoparticles at the fiber tip: probing with second harmonic generation**
B. F. Soares, F. Jonsson, K. F. MacDonald, A. I. Denisyuk, and N. I. Zheludev in *Quantum Electronics and Photonics-17 at Photon06* (2006).

[11] **Nonlinear optical interactions in mixed-state metal nanoparticles undergoing a structural transformation**
B. F. Soares, F. Jonsson, K. F. MacDonald, A. I. Denisyuk, and N. I. Zheludev in *SPIE Optics and Photonics*, paper 6323-71 (2006).

[12] **(invited) Nanophotonics under a scanning electron microscope: studying resonator-less all-optical switching and memory functionality in Gallium nanoparticles**
K. F. MacDonald, M. V. Bashevoy, A. I. Denisyuk, F. Jonsson, B. F. Soares, and N. I. Zheludev in *Conference on Lasers and Electro-Optics Quantum Electronics and Laser Science Conference Conference on Photonic Applications, Systems and Technologies*, paper QTuJ2 (2006).

[13] **Nanoparticle optical memory function**
B. F. Soares, M. V. Bashevoy, K. F. MacDonald, F. Jonsson, and N. I. Zheludev in *Nanotech/ Conference on Nano Electronics & Photonics* (2006).

[14] **Resonator-less optical memory in nanoparticles**
B. F. Soares, M. Bashevoy, K. F. MacDonald, F. Jonsson, and N. I. Zhe-

ludev in *Nanophotonics Topical Meeting (NANO) at IPRA/NANO OSA Collocated Topical Meetings*, paper NThB3 (2006).

[15] **(invited) Nanowatt nanosecond nanophotonics**
N. I. Zheludev, B. F. Soares, K. F. MacDonald, and V. A. Fedotov in *SPIE Optics and Photonics*, paper 5927-02 (2005).

[16] **(invited) Nanowatt photonics of structural transformations in a single nanoparticle**
K. F. MacDonald, B. F. Soares, V. A. Fedotov, M. V. Bashevoy, and N. I. Zheludev in *International Quantum Electronics Conference and the Pacific Rim Conference on Lasers and Electro-Optics*, paper QWG1-4-INV (2005).

[17] **(invited) A single nanoparticle as a femtojoule photonic switch and optical memory element**
B. F. Soares, K. F. MacDonald, M. Bashevoy, V. A. Fedotov, and N. I. Zheludev in *Surface Plasmon Photonics 2*, paper T-39 (2005).

[18] **(invited) 3N: Nanowatt nanosecond nanophotonics**
B. Soares, K. MacDonald, V. Fedotov , A. Krasavin, M. Bashevoi, and N. Zheludev in *International Conference on Coherent and Nonlinear Optics*, paper IThK2 (2005).

[19] **(invited) Nano3photonics**
N. I. Zheludev, K. MacDonald, A. Krasavin, and B. Soares in *Microtechnologies for the New Millennium* Technical Programme, paper 5840-58 (2005).

[20] **Single nanoparticle as photonic switch and optical memory element**
B. F. Soares, K. F. MacDonald, V. A. Fedotov, M. Bashevoy, and N. I. Zheludev in *Nanophotonics for Information Systems Topical Meeting* Technical Digest, paper NWA3 (2005).

[21] **Nanowatt photonics of structural transformations in a single nanoparticle**
K. F. MacDonald, B. F. Soares, and N. I. Zheludev in *Quantum Electronics and Photonics-16 at Photon04* (2004).

[22] **Controlling the optical properties of a single nanoparticle at nanowatt power levels**
B. F. Soares, K. F. MacDonald, and N. I. Zheludev in *Conference on Lasers and Electro-Optics Quantum Electronics and Laser Science Conference Conference on Photonic Applications, Systems and Technologies*, paper IThM5 (2004).

The following published papers were included in the bound thesis. These have not been digitised due to copyright restrictions, but their doi or reference are provided.

Soares, B.F., MacDonald, K.F. & Zheludev, N.I., 2007. Resetting single nanoparticle structural phase with nanosecond pulses. Applied Physics Letters, 91(4), p.043115. Available at: http://dx.doi.org/10.1063/1.2760174

Soares, B.F., Jonsson, F. & Zheludev, N.I., 2007. All-Optical Phase-Change Memory in a Single Gallium Nanoparticle. Physical Review Letters, 98(15). Available at: http://dx.doi.org/10.1103/physrevlett.98.153905

MacDonald, K. F., Soares, B. F., Bashevoy, M. V., & Zheludev, N. I. (2006). Controlling light with light via structural transformations in metallic nanoparticles. IEEE Journal of Selected Topics in Quantum Electronics, 12(3), 371–376. Available at: http://dx.doi.org/10.1109/jstqe.2006.872052

Soares, B. F., MacDonald, K. F., Fedotov, V. A., & Zheludev, N. I. (2005). Light-Induced Switching between Structural Forms with Different Optical Properties in a Single Gallium Nanoparticulate. Nano Letters, 5(10), 2104–2107. Available at: http://dx.doi.org/10.1021/nl0515652

MacDonald, K. F., V. A. Fedotov, S. Pochon, B. F. Soares, N. I. Zheludev, C. Guignard, A. Mihaescu, and P. Besnard. (2003). Oscillating bubbles at the tips of optical fibers in liquid nitrogen. Physical Review E, 68(2). Available at: http://dx.doi.org/10.1103/physreve.68.027301

Soares, B.F., Jonsson, F., Bashevoy M. V., MacDonald, K.F., Zheludev, N.I (2006) Memory Functionality of a Single Nanoparticle. At 9th International Conference on Near-field Optics, Nanophotonics & Related Techniques, Switzerland, 10-15 September 2006.

Soares, B.F., Bashevoy, M.V., MacDonald, K.F., Jonsson, F. and Zheludev, N.I. (2006) A nanoparticle as a bit of optical memory. At *QEP-17 at Photon06 QEP-17 at Photon06. 04 - 07 Sep 2006.*

Soares, B.F., Jonsson, F., MacDonald, K.F., Denisyuk, A.I. and Zheludev, N.I. (2006) Nonlinear optical interactions in mixed-state metal nanoparticles undergoing a structural transformation. At Society of Photo-Optical Instrumentation Engineers Optics and Photonics 2006 Society of Photo-Optical Instrumentation Engineers Optics and Photonics 2006, United States. 13 - 17 Aug 2006.

MacDonald, Kevin F., Bashevoy, Max V., Denisyuk, Audrey I., Jonsson, Fredrik, Soares, Bruno F. and Zheludev, Nikolay I. (2006) Nanophotonics under a scanning electron microscope: studying resonator-less all-optical switching and memory functionality in Gallium nanoparticles. In Quantum Electronics and Laser Science Conference 2006. Optical Society of America. QTuJ2.

Soares, B.F., Bashevoy, M.V., MacDonald, K.F., Jonsson, F. and Zheludev, N.I. (2006) Nanoparticle optical memory function. At Nano Science and Technology Institute Nanotech - Conference on Nano Electronics & Photonics Nano Science and Technology Institute Nanotech - Conference on Nano Electronics & Photonics, United States. 07 - 11 May 2006.

Soares, Bruno F., Bashevoy, Maxim, MacDonald, Kevin F., Jonsson, Fredrik and Zheludev, Nikolay I. (2006) Resonator-less optical memory in nanoparticles. Integrated Photonics Research and Applications/Nanophotonics, Connecticut, 24-26 April 2006.

Zheludev, N.I., Soares, B.F., MacDonald, K.F. and Fedotov, V.A. (2005) Nanowatt nanosecond nanophotonics. At Plasmonics: Metallic Nanostructures and their Optical Properties III at Photonics 2005 Plasmonics: Metallic Nanostructures and their Optical Properties III at Photonics 2005, United States. 31 Jul - 04 Aug 2005

MacDonald, K.F., Soares, B.F., Fedotov, V.A., Bashevoy, M.V. and Zheludev, N.I. (2005) Nanowatt photonics of structural transformations in a single nanoparticle. At International Conference on Quantum Electronics 2005 and the Pacific Rim Conference on Lasers and Electro-Optics 2005 (IQEC/CLEO-PR 2005) International Conference on Quantum Electronics 2005 and the Pacific Rim Conference on Lasers and Electro-Optics 2005 (IQEC/CLEO-PR 2005). 11 - 15 Jul 2005

Soares, B.F., MacDonald, K.F., Bashevoy, M., Fedotov, V.A. and Zheludev, N.I. (2005) A single nanoparticle as a femtojoule photonic switch and optical memory element. At Surface Plasmon Photonics 2 Surface Plasmon Photonics 2, Austria. 21 - 26 May 2005

Soares, B.F., MacDonald, K.F., Fedotov, V., Krasavin, A., Bashevoy, M. and Zheludev, N.I. (2005) 3N: Nanowatt nanosecond nanophotonics. At *International Conference on Coherent and Nonlinear Optics (ICONO/LAT 2005) International Conference on Coherent and Nonlinear Optics (ICONO/LAT 2005). 11 - 15 May 2005.*

Zheludev, N.I., MacDonald, K.F., Krasavin, A. and Soares, B.F. (2005) Nano3photonics. At Microtechnologies for the New Millennium Microtechnologies for the New Millennium, Spain. 09 - 11 May 2005.

Soares, B.F., MacDonald, K.F., Fedotov, V.A., Bashevoy, M. and Zheludev, N.I. (2005) Single nanoparticle as photonic switch and optical memory element. At Nanophotonics for Information Systems Topical Meeting (NPIS) Nanophotonics for Information Systems Topical Meeting (NPIS), United States. 13 - 15 Apr 2005

MacDonald, K.F., Soares, B.F. and Zheludev, N.I. (2004) Nanowatt photonics of structural transformations in a single nanoparticle. At Photon '04 / QEP-16 Photon '04 / QEP-16. 06 - 09 Sep 2004.

Soares, B.F., MacDonald, K.F. and Zheludev, N.I. (2004) Controlling the optical properties of a single nanoparticle at nanowatt power levels. At International Quantum Electronics

Conference (IQEC) International Quantum Electronics Conference (IQEC), United States. 16 - 21 May 2004.